

Acknowledgements

The authors would like to thank the following people, for their help and guidance, without whom the project would not have been possible:

Dr David Brown	Portsmouth University
Dr Richard Crowder	University of Southampton
Martin Goodall	R&M Electrical Group Ltd.
Timothy Brody	University of Southampton
Damian Brierley	BAE Systems
Danny Russell	University of Southampton
The Engineering Design and Manufacture Centre (EDMC)	University of Southampton
Physics Mechanical Workshop	University of Southampton
Graham Hill	LVM Ltd.
Dr. R Wood	University of Southampton
Mr S Lockyer and Mr. Phil Jones	Penske Cars Ltd
Department of Ship Science	University of Southampton
GF Jones Ltd	
Christophe Pastchas	

Particular thanks go to our supervisor and second examiner for their guidance through the project:

Dr. Suleiman Abu-Sharkh	University of Southampton
Dr S Turnock	University of Southampton

Contents

ACKNOWLEDGEMENTS	1
CONTENTS	2
LIST OF FIGURES	7
1 INTRODUCTION	11
2 OBJECTIVES	13
3 METHODOLOGY	13
4 WATER JET ROV SPECIFICATION	14
5 PROPULSION SYSTEM	15
5.1 NUMBER OF DEGREES OF FREEDOM	15
5.2 ANALYSIS OF THE PREVIOUS ROV'S PROPULSION SYSTEM	16
5.3 VALVES VERSUS MULTIPLE PUMPS	17
5.4 NOZZLES	17
6 BI-DIRECTIONAL PUMPS	19
7 UNIDIRECTIONAL PUMP OPTIONS	22
8 ANALYSIS OF PREVIOUS PROJECT'S PROPULSION SYSTEM	
MODELLING	22
9 PROPULSION SYSTEM MODELLING	23
9.1 STRAIGHT PIPE LOSSES	25
9.2 ENTRY LOSSES	25
9.2.1 <i>With Inlet Diffuser</i>	26
9.2.2 <i>Without Inlet Diffuser</i>	26
9.3 COMBINING/DIVIDING FLOW CONNECTORS	26
9.4 NON-RETURN VALVE LOSSES	26
9.5 NOZZLE LOSSES	26
9.6 EXIT TUBE LOSSES	27
9.6.1 <i>Abrupt contraction losses</i>	27
9.6.2 <i>Pipe losses</i>	27
9.6.3 <i>Exit losses</i>	27
10 INITIAL PIPE NETWORK COMPARISONS	28
11 RESULTS OF PUMP SEARCHES	29
12 SENSITIVITY TO INLET DIFFUSER	31
13 PIPE NETWORK OPTIMISATION	32
13.1 PUMP SELECTION.....	33
13.2 MULTIPLE PUMPS PER NOZZLE	36
13.3 NOZZLE DESIGN AND DIAMETER SELECTION	36
14 EXPERIMENTAL RESULTS	40
15 PRELIMINARY EXPERIMENTAL RESULTS	41
15.1 EXIT TUBE EXPERIMENTS	43
15.1.1 <i>Two Pumps in Parallel</i>	43
15.1.2 <i>Two Pumps in Series</i>	44
15.2 NOZZLE EXPERIMENTS.....	45
16 JET ORIENTATION AND CONFIGURATION	46
16.1 MOVABLE BALLAST	47
16.2 FORCE VECTORING	48
16.3 REQUIREMENTS	49
16.3.1 <i>Materials</i>	49
16.3.2 <i>Initial Designs</i>	52

16.4	OCTAGONAL FRAME FOR CYLINDRICAL BODY	52
16.5	STRUCTURE FOR NACA AEROFOIL SECTION.....	54
16.6	STRUCTURE FOR WIDE BODIED ROV	56
16.7	FINAL DESIGN OF INTERNAL STRUCTURE.....	60
16.8	INTERNAL SHELF	62
16.9	COMPONENT ATTACHMENT	64
16.10	FRAME DESIGN RECOMMENDATIONS AND IMPROVEMENTS	65
16.11	NOZZLE DESIGN AND ATTACHMENT.....	66
16.11.1	<i>Nozzle Requirements</i>	66
16.11.2	<i>Simple Nozzles</i>	67
16.11.3	<i>More Efficient Nozzles</i>	68
16.11.4	<i>Nozzle Attachment</i>	70
16.11.5	<i>The Final Nozzle</i>	70
16.12	RECOMMENDATIONS FOR NOZZLE DESIGN	73
17	INITIAL DESIGN PERFORMANCE.....	74
18	INITIAL DRAG ESTIMATE	74
18.1	THRUST REQUIREMENTS.....	74
18.2	ROV DRAG:.....	75
18.3	TETHER DRAG.....	75
19	DETAILED RESEARCH INTO COMPONENTS OF TETHER DRAG... 76	
20	PERFORMANCE OF BARE HULL FORM.....	78
21	EFFECT OF FAIRING ON THE HYDRODYNAMIC PERFORMANCE OF A BODY IMMersed IN A FLUID.....	79
21.1	FACTORS AFFECTING THE DRAG OF A BODY	79
21.2	CALCULATION OF ROV REYNOLDS NUMBER.....	81
21.3	OPTIMISATION FOR LEAST DRAG.....	82
22	ESTIMATION OF DRAG COEFFICIENT OF MODIFIED NACA SECTIONS.....	84
22.1	COMPUTATIONAL METHODS AVAILABLE.....	84
22.2	USE OF PANEL METHODS	85
22.3	COUPLED BOUNDARY LAYER AND POTENTIAL FLOW PANEL CODES.....	85
22.4	GEOMETRY DEFINITION	86
22.5	PREVIOUS WORK.....	86
22.6	WIND TUNNEL VALIDATION OF COMPUTATIONAL PANEL TECHNIQUE.....	87
22.7	CHOICE OF SHAPE DUE TO TIME RESTRICTIONS.....	88
22.8	VARIABLES DEFINED FOR THE PROGRAMS.....	88
22.9	LIMITATIONS OF THE PROGRAMME	89
22.10	FAMILIES OF GEOMETRIES TESTED	91
22.11	SENSITIVITY STUDY FOR PANEL ASPECT RATIO AND MINIMUM CP.....	91
22.12	OUTPUTS FROM THE PROGRAMME.....	94
22.13	RESULTS.....	94
22.14	TRANSITION AND SEPARATION	98
22.15	PRESSURE AND VELOCITY DISTRIBUTION	98
22.16	DRAG PENALTIES NOT ACCOUNTED FOR.....	99
22.17	ALTERNATIVE CHOICE OF SECTION, IF ANY	99
22.18	UNIDIRECTIONAL OPTIMISATION.....	99
23	GENERAL ARRANGEMENT AND 3D MODELLING OF ROV COMPONENTS	100
24	SHELL DESIGN MANUFACTURE AND CONSTRUCTION	101
24.1	POSSIBLE MATERIALS AND METHODS OF MANUFACTURE	102

24.1.1	<i>Wood construction</i>	102
24.1.2	<i>Metal construction</i>	102
24.1.3	<i>Glass Fibre Composite Design</i>	103
25	BUOYANCY	103
26	WEIGHTS AND CENTRES	105
27	STABILITY	108
27.1	STATIC STABILITY	108
27.2	DIRECTIONAL STABILITY	109
28	FULL-SCALE TESTS	110
28.1	IMMERSION AND FLOATATION	110
28.2	ROV AND STRUT DRAG TESTS	110
28.3	TETHER DRAG TESTS	112
29	COMPARISON OF DRAG TEST AND PANEL CODE RESULTS	113
30	ROV OPERATIONAL CAPACITY	113
30.1	ROV THRUST AND DRAG	114
30.2	TETHER LENGTH SUSTAINED	114
30.3	PERFORMANCE AND MANOEUVRABILITY	115
30.4	INTAKE SLOTS AND THEIR IMPLICATION ON THE ROV OPERATIONAL PERFORMANCE	115
31	ELECTRONICS SECTION	117
31.1	REQUIREMENTS	117
31.2	MICROPROCESSOR SELECTION	117
31.2.1	<i>CANbus</i>	117
31.2.2	<i>PIC micro-controller</i>	119
31.2.3	<i>Chosen control device – the PIC microcontroller</i>	120
31.3	SENSOR SELECTION	120
31.4	CAMERA SELECTION	121
31.4.1	<i>Requirements</i>	121
31.4.2	<i>Previous ROV camera</i>	122
31.4.3	<i>Choice and specification of new camera</i>	122
31.5	INITIAL CIRCUIT DESIGN	123
31.5.1	<i>Pump Interface</i>	123
31.5.2	<i>Sensor Interface</i>	125
31.5.3	<i>PC Interface</i>	126
31.5.4	<i>Power Supply</i>	126
31.5.5	<i>Tether</i>	127
31.6	FINAL CIRCUIT DESIGN AND PCB FABRICATION	127
31.7	ENCLOSURES	130
31.7.1	<i>Requirements</i>	130
31.7.2	<i>Enclosures considered and chosen</i>	132
31.7.3	<i>Special notes</i>	133
31.8	CONNECTORS	134
31.8.1	<i>Requirements</i>	134
31.8.2	<i>Specifications for circuit</i>	135
31.8.3	<i>Options available and chosen solution</i>	136
31.9	LOOM CONFIGURATION	140
31.9.1	<i>Tether</i>	140
31.9.2	<i>Cable combination and splitting</i>	141
31.9.3	<i>Loom layout in ROV</i>	142
31.10	THE FUTURE	144

32	PC CONTROL SOFTWARE	144
32.1	FUNCTIONAL REQUIREMENTS OF THE SOFTWARE.....	144
32.1.1	<i>Initial Main Problems</i>	<i>144</i>
32.1.2	<i>Main Requirements Of The Application.....</i>	<i>145</i>
32.1.3	<i>Internal Processing of the System.....</i>	<i>146</i>
32.1.4	<i>Logical Design of Windows Within The System</i>	<i>147</i>
32.1.5	<i>Integration / Communication with Other Systems.....</i>	<i>149</i>
32.1.6	<i>Users Of The System</i>	<i>149</i>
32.2	NON-FUNCTIONAL REQUIREMENTS OF THE SOFTWARE.....	150
32.2.1	<i>Hardware Configuration.....</i>	<i>150</i>
32.2.2	<i>Hardware And Environmental Constraints On The System.....</i>	<i>150</i>
32.2.3	<i>Alternative Technical Environments For The System.....</i>	<i>151</i>
32.2.4	<i>Other Considerations of the System.....</i>	<i>151</i>
32.3	DEVELOPMENT	151
32.3.1	<i>Gantt Chart of Progress of Software Development</i>	<i>151</i>
32.3.2	<i>Constraints.....</i>	<i>151</i>
32.4	DIRECTX – AN OVERVIEW	152
32.4.1	<i>Goals</i>	<i>152</i>
32.4.2	<i>DirectInput.....</i>	<i>152</i>
32.4.3	<i>Architectural Overview of DirectInput</i>	<i>153</i>
32.4.4	<i>The DirectInput Object.....</i>	<i>153</i>
32.4.5	<i>The DirectInputDevice Object.....</i>	<i>153</i>
32.4.6	<i>DirectInputDevice Object Instances</i>	<i>154</i>
32.4.7	<i>The DirectInputEffect Object.....</i>	<i>154</i>
32.4.8	<i>Integration with Windows.....</i>	<i>154</i>
32.4.9	<i>Use of DirectInput.....</i>	<i>155</i>
32.5	ACTIVE X – AN OVERVIEW	155
32.5.1	<i>Goals</i>	<i>155</i>
32.5.2	<i>Common ActiveX Controls</i>	<i>155</i>
32.5.3	<i>Specialised ActiveX Controls.....</i>	<i>155</i>
32.6	PC SOFTWARE OVERVIEW	156
32.6.1	<i>Introduction</i>	<i>156</i>
32.6.2	<i>System Requirements.....</i>	<i>156</i>
32.6.3	<i>Installation.....</i>	<i>157</i>
32.6.4	<i>Running the Software</i>	<i>157</i>
32.6.5	<i>Set-up Menu Window</i>	<i>159</i>
32.6.6	<i>Control</i>	<i>159</i>
32.6.7	<i>Calibrating the Sensors.....</i>	<i>161</i>
32.6.8	<i>Simulating The ROV Or Controlling The ROV</i>	<i>161</i>
32.6.9	<i>Camera Window.....</i>	<i>162</i>
32.6.10	<i>The Application’s Menus.....</i>	<i>163</i>
32.6.11	<i>Testing</i>	<i>164</i>
32.6.12	<i>Communication</i>	<i>164</i>
32.6.13	<i>Simulated Pulse Width Modulation.....</i>	<i>168</i>
32.6.14	<i>Summary.....</i>	<i>169</i>
32.6.15	<i>Source Code.....</i>	<i>169</i>
32.7	FUTURE DEVELOPMENTS OF THE SOFTWARE	169
32.8	PIC SOFTWARE	170
32.8.1	<i>Requirements</i>	<i>170</i>
32.8.2	<i>Sensor communications.....</i>	<i>170</i>

32.8.3	<i>PC communications</i>	172
32.8.4	<i>Commands and actions</i>	172
32.8.5	<i>Possible future modifications</i>	180
33	CONSTRUCTION PHASE	182
33.1	MANUFACTURE AND CONSTRUCTION OF THE SHELL	183
33.1.1	<i>Stage One</i>	183
33.1.2	<i>Stage Two</i>	184
33.1.3	<i>Stage Three</i>	184
33.1.4	<i>Stage Four</i>	185
34	ROV TESTING	186
34.1	TEST PROGRAMME	188
34.1.1	<i>PC Control Software Testing</i>	188
34.1.2	<i>Control System Testing</i>	188
34.1.3	<i>Camera Testing</i>	191
34.1.4	<i>Enclosure Testing</i>	191
34.1.5	<i>Acceptance Testing</i>	193
35	BUDGET	195
36	CONCLUSIONS	195
37	RECOMMENDATIONS FOR FURTHER WORK	196
38	REFERENCES	199
38.1	BIBLIOGRAPHY	199
38.2	WEB SITE REFERENCES	200

List of Figures

FIGURE 1 - THE HYDRO-VISION HYBALL.....	12
FIGURE 2 - SIX DEGREES OF FREEDOM USING BI-DIRECTIONAL PUMPS.....	16
FIGURE 3 - EXIT TUBE DESIGN, 4MM DIAMETER.....	18
FIGURE 4 - FREE DISCHARGE NOZZLES [INTERNAL FLOW <i>D.S.MILLER P.270</i> FIG.14.16A]	18
FIGURE 5 - FLUID FLOW LINES THROUGH A GOOD PERFORMANCE NOZZLE.....	19
FIGURE 6 - BI-DIRECTIONAL PUMP PIPE NETWORK 1.....	20
FIGURE 7 - BI-DIRECTIONAL PUMP PIPE NETWORK 2.....	20
FIGURE 8 - UNI-DIRECTIONAL PUMP PIPE NETWORK 1.....	22
FIGURE 9 - COMPARISON OF INITIAL PIPE NETWORKS.....	28
FIGURE 10 - INLET DIFFUSER SENSITIVITY.....	31
FIGURE 11 - SENSITIVITY TO INLET DIFFUSER.....	32
FIGURE 12 - PUMP SELECTION PIPE NETWORK.....	33
FIGURE 13 - 6MM NOZZLE; FORCE, FLOW RATE, PRESSURE LOSS RELATIONSHIP.....	33
FIGURE 14 - FORCE, FLOW RATE, PRESSURE LOSS RELATIONSHIP FOR NOZZLE SIZES 1 TO 19MM DIAMETER.....	34
FIGURE 15 - INITIAL PUMP COMPARISONS.....	34
FIGURE 16 - NOZZLE OPTIMISATION PIPE NETWORKS.....	37
FIGURE 17 - OPTION 1, FREE DISCHARGE NOZZLE WITH LVM CONGO PUMP.....	37
FIGURE 18 - PREDICTED FORCES, LVM CONGO PUMP, FREE DISCHARGE NOZZLE (OPTION 1, FIGURE 16).....	38
FIGURE 19 - OPTION2, EXIT PIPES WITH LVM CONGO PUMPS.....	39
FIGURE 20 - PREDICTED FORCES, LVM CONGO PUMP, EXIT PIPES (OPTION 2, FIGURE 16).....	39
FIGURE 21 - EXPERIMENTAL SET UP.....	40
FIGURE 22 - SINGLE LVM CONGO PUMP, EXPERIMENTAL RESULTS.....	41
FIGURE 23 - TWO PARALLEL LVM CONGO PUMPS, EXPERIMENTAL RESULTS.....	43
FIGURE 24 - TWO SERIES LVM CONGO PUMPS, EXPERIMENTAL RESULTS.....	44
FIGURE 25 - 10MM FREE DISCHARGE NOZZLE, EXPERIMENTAL RESULTS.....	45
FIGURE 26 - 16 WATER JET OPTION.....	46
FIGURE 27 - 12 WATER JET OPTION.....	47
FIGURE 28 - 8 WATER JET OPTION.....	47

FIGURE 29 - PUMP FORCE VECTORING.....	48
FIGURE 30 – THEORETICAL 2MM GAUGE	51
FIGURE 31 – READILY AVAILABLE 3.2MM GAUGE.....	51
FIGURE 32 - CYLINDRICAL BODY	52
FIGURE 33 - OCTAGONAL FRAME	53
FIGURE 34 - EXAMPLE OF PROTRUSION TO SECURE COMPONENTS IN POSITION.....	54
FIGURE 35 - INTERNAL FRAME	54
FIGURE 36 - INITIAL MODEL OF WIDE-BODIED ROV	56
FIGURE 37 - FLAT PLATE STRUCTURE.....	56
FIGURE 38 - EXAMPLE OF PERFORATED PLATE	57
FIGURE 39 - PLASTIC FRAME.....	57
FIGURE 40 - ALUMINIUM FRAME.....	58
FIGURE 41 - WEIGHT BALANCE.....	59
FIGURE 42 - SIMPLIFIED WEIGHT BALANCE.....	59
FIGURE 43 - I_{xx} DIAGRAM.....	60
FIGURE 44 - LONGER FRAME WITH CENTRAL SUPPORT.....	60
FIGURE 45 - FINAL FRAME DESIGN.....	61
FIGURE 46 - Y-CONNECTOR	63
FIGURE 47 - SUPPORTING SHELF.....	63
FIGURE 48 - SIMPLE TUBE NOZZLE.....	67
FIGURE 49 - NOZZLE POSITIONING BLOCK	67
FIGURE 50 - AN EXAMPLE OF A MORE EFFICIENT NOZZLE	68
FIGURE 51 – FINAL NOZZLE DESIGN.....	70
FIGURE 52 - FINAL NOZZLE.....	71
FIGURE 53 - INITIAL DESIGN OF NOZZLE ATTACHMENT TAB	72
FIGURE 54 - TETHER GEOMETRY	77
FIGURE 55 ~ LAMINAR-TURBULENT TRANSITION	80
FIGURE 56 - NACA0020 SECTION	84
FIGURE 57 - MIRRORED NACA0020 SECTION WITH SOME PARALLEL MID BODY	84
FIGURE 58 - PANEL DISTRIBUTION 120X15	93
FIGURE 59 - CLOSE UP OF PANEL DISTRIBUTION AT ENDS	94
FIGURE 60 - OPTIMISED UNIDIRECTIONAL AUV DESIGN SOURCE: THIBAUT JACQUET- LAGREZE, MSC THESIS UNIVERSITY OF SOUTHAMPTON	100
FIGURE 61	105

FIGURE 62	105
FIGURE 63 ~ CENTRELINES AND SIGN CONVENTION	106
FIGURE 64 - ACTUAL LOCATION OF PUMPS	108
FIGURE 65 - FLOATATION TEST	110
FIGURE 66 - DRAG TESTING ROV	111
FIGURE 67 - TETHER AND STRUT DRAG ARRANGEMENT	112
FIGURE 68 - RS485 STANDARD USING HALF-DUPLEX TRANSMISSION, AS FOUND IN CANBUS.....	118
FIGURE 69- A POTENTIAL CANBUS SETUP FOR THE ROV	119
FIGURE 70 - THE CHOSEN BLACK AND WHITE BOARD CAMERA WITH INFRA RED LEDs.	123
FIGURE 71 - BLOCK DIAGRAM OF THE PWM CHIP CONTROL SCHEME.....	124
FIGURE 72 - BLOCK DIAGRAM OF LIMIT SPEED SELECTION	124
FIGURE 73 - COMPLETE CIRCUIT SCHEMATIC	128
FIGURE 74 - COMPLETED CIRCUIT	129
FIGURE 75 - THE KESTREL IP68 RATED ENCLOSURE USED FOR THE CAMERA AND SENSOR.	133
FIGURE 76 - THE KESTREL IP68 RATED ENCLOSURE USED FOR THE MAIN CIRCUIT.....	134
FIGURE 77 - DIAGRAM OF ALL OF THE SIGNAL AND POWER LINES IN THE ROV SYSTEM..	136
FIGURE 78 - EXAMPLES OF THE MINI BUCCANEER CONNECTORS BY BULGIN	136
FIGURE 79 - TECHNICAL DIMENSIONS OF THE MINI BUCCANEER CONNECTORS.....	137
FIGURE 80 - EXAMPLES OF THE 900 SERIES BUCCANEER CONNECTOR RANGE BY BULGIN.....	137
FIGURE 81 - TECHNICAL DIMENSIONS OF THE 900 SERIES CONNECTORS.....	138
FIGURE 82 - THE LOCATION OF THE CONNECTORS ON THE MAIN CIRCUIT ENCLOSURE.....	140
FIGURE 83 - DIAGRAM OF THE SPLIT OF CABLES ON THE TETHER.....	142
FIGURE 84 - DIAGRAM OF THE COMBINATION OF THE PUMP CABLES INTO ONE SINGLE CABLE.....	142
FIGURE 85 - DIAGRAM OF LOOM LAYOUT.....	143
FIGURE 86- AVERAGE CURRENT 50%	145
FIGURE 87 - AVERAGE CURRENT AT 20%	145
FIGURE 88 - SOFTWARE OVERVIEW	147
FIGURE 89 - LOGICAL DESIGN OF WINDOWS.....	148
FIGURE 90 - HARDWARE CONFIGURATION.....	150
FIGURE 91 – THE USER SETUP INTERFACE.....	159

FIGURE 92 - CONFIGURE JOYSTICK.....	160
FIGURE 93 – THE ROV USER INTERFACE	162
FIGURE 94 - RECEIVE PITCH FLOW CHART	171
FIGURE 95 - COMMAND WORD BITS REPRESENTING DIFFERENT ROV WATER JET POSITIONS	173
FIGURE 96 - COMMAND ANALYSIS FLOWCHART	175
FIGURE 97 – SET WAIT COMMAND FLOWCHART.....	177
FIGURE 98 - HOVER COMMAND FLOWCHART.....	179

1 Introduction

Remotely Operated underwater Vehicles or ROVs are widely used in industry. Their main use is for operations either in environments hazardous to humans or at depths that pressurised vehicles carrying humans become impractical or uneconomical. The majority of ROVs in service are used by the oil industry for maintaining oil rigs and pipelines. ROVs, as their name indicates, are controlled remotely. Usually they are controlled and powered by a tether that connects them to the surface and a controller. A tether is required if real time control of an ROV is desired.

ROVs fall into two main categories: observation and work classes. The Work class subdivides into light and heavy, which specifies their maximum working depth. Heavy work class ROVs are capable of reaching depths of greater than 3,000m. These require very large propulsion systems to generate the forces required to tow the length to tether required.

This project, however, is a technology-prover and is intended to assess the viability of water jets as a form of propulsion for ROVs. All commercially available ROVs use thrusters to provide propulsion. These are propellers attached to either electrical or hydraulic motors. Commercially available ROVs use thrusters because of the efficiency difference between propellers and water jets at low speeds. Water jets work by increasing the velocity of a relatively small mass of fluid by a relatively large amount. Conversely, propellers work by increasing the velocity of a relatively large mass of fluid by a relatively small amount. As a result, propellers are more efficient at low speeds and water jets at higher speeds (in excess of 40knots). For this reason, water jets are usually used, for example, in high-speed catamarans and propellers in low speed ships.

This indicates that an ROV built using water jets will have an inherently inefficient design. As a result, all other factors within a water jet powered ROV will require significant optimisation in order to overcome this problem.

Through the use of water jets, it is hoped to reduce the size and cost of manufacturing small, observation class ROVs. An example of an observation class ROV is the Hydro-Vision Hyball shown in Figure 1. It is also hoped that through the use of water

jets, bulky thrusters can be removed and a greater number of degrees of freedom can be achieved for a similar size.



Figure 1 - The Hydro-Vision Hyball

This is a continuation project from two years previously. When it was run then, an ROV was produced using a central pump to provide water pressure to a set of solenoid actuated valves. One valve was used to produce each water jet. Each valve was positioned such that the vectored forces would produce six degrees of freedom. This project succeeded in building the ROV but did not complete the wet testing. This was due to sealing problems with the electronics boxes. As a result, the electronics were flooded with water, causing delays. Some limited testing did occur, however very little speed was achieved. It is intended that this project overcomes this problem.

It is an advantageous position that this is a continuation project, the basic design concepts having already been discussed and this assessed, and therefore, increases the speed with which the project can progress. The information provided, along with the tests conducted, allow more accurate assumptions and estimates to be made.

2 Objectives

The objectives of the project were defined as follows:

“To design, build and test a small, low cost ROV, powered by water jets with a comparable performance to other ROV’s in its target market.”

This objective clearly outlines the aims of the project. The target market has already been defined in the introduction as an observation class ROV.

Through this objective, the group will assess the capability of such an ROV and establish if water jets are a viable solution for ROV propulsion.

3 Methodology

As this is a continuation project, the initial task was to analyse the previous project. With this information, the objectives and a specification for the new ROV were produced. With the knowledge of the previous ROV and this specification, a ‘rich diagram’ was produced. This identified the systems within the ROV and allowed the project to be divided into areas for the team members to focus on. This diagram is included in Appendix A. It allowed the interconnections between the different areas of the project to be established, and therefore allowed the team to visualise the overall system and the required flow of information. From this diagram, the following key areas were identified and the methodology for each is as follows:

- Propulsion System. Assess the previous projects propulsion system. Analyse different propulsion system options. Model and test possible propulsion systems and select the most effective. Integrate this into the ROV design.
- Hydrodynamics. Optimise and assess the ROV hydrodynamics computational fluid dynamics will be used. Various methods of computational modelling available will be investigated and one chosen to evaluate the ROV hull drag. Various body shapes are to be investigated and an optimum ROV body for minimal drag in the forward and backward direction will be sought. The computational modelling is then to be validated by full-scale tests.

- PC Software Control. Functional and Non-Functional Requirements were to be determined. Use 3D modelling, independent threads, and serial communication to allow the software to function. Display the camera output on computer screen.
- Electronics and Power. Consider options to reduce the size of the ROV control electronics looking at component selection of sensors, control and power electronics. The electronics must allow the control of the propulsion system from a remote PC.
- Structure. Design a structure that is load bearing and lightweight. Designed to be a stable platform on to which to mount the nozzles and attach the internal components.

This allowed a Gantt chart to be produced (see Appendix B). This established the project critical path and the tasks that could be run simultaneously.

4 Water Jet ROV Specification

- The ROV is to be powered by water jets
- Maximum Operating Depth of 10m
- Minimise complexity
- Minimise costs
- Minimise size
- A minimum forward speed of 0.5m/s is required. This is comparable to other ROVs in the target market [Given D, *ROV Review*]
- A minimum lateral and vertical speed of 0.3m/s is required
- Maximise manoeuvrability achievable with the available budget.
- Low drag hull
- Static stability (BG+)
- Level trim
- Neutrally buoyant
- Structure should be load-bearing, lightweight and corrosion resistant

- The structure must allow access to the ROV's internal components.
- Minimise the electronics so as to have a small as possible overall control system.
- The control system must sense the ROV's surrounding environment by use of positional sensors and a camera and feed this information back to the user.
- The electronics must act on sensor information and user requests to switch on the correct water jets and move the ROV as desired.
- To allow control of the ROV by the use of a joystick.
- The enclosures must provide the electronics with an watertight environment for extended periods of time.

5 Propulsion System

5.1 Number of Degrees of Freedom

There are six independent degrees of freedom, three translational and three rotational. The number of required degrees of freedom dictates the manoeuvrability of the ROV and affects the configuration of the water jets on it. The aim as stated in the specification, is to maximise the manoeuvrability of the ROV. The previous project discussed different options for water jet configuration. These effectively divided into two classes of vehicle: those with control surfaces and those without. Control surfaces reduce manoeuvrability, as they require forward speed. The addition of control surfaces or adjustable direction nozzles required mechanically moving components. These require sealing and increased complexity, both of which would dramatically increase the cost of the ROV and is therefore in conflict with the specification. For these reasons it was decided to try to avoid control surfaces. It is probable that, for these reasons, the commercially available ROVs do not contain control surfaces and only the largest have thrusters with adjustable direction. It is an aim of the ROV industry to minimise the number of moving components within the ROVs to minimise costs and maximise reliability. Using bi-directional pumps for example, six degrees of freedom can be achieved using six pumps in a configuration as follows:

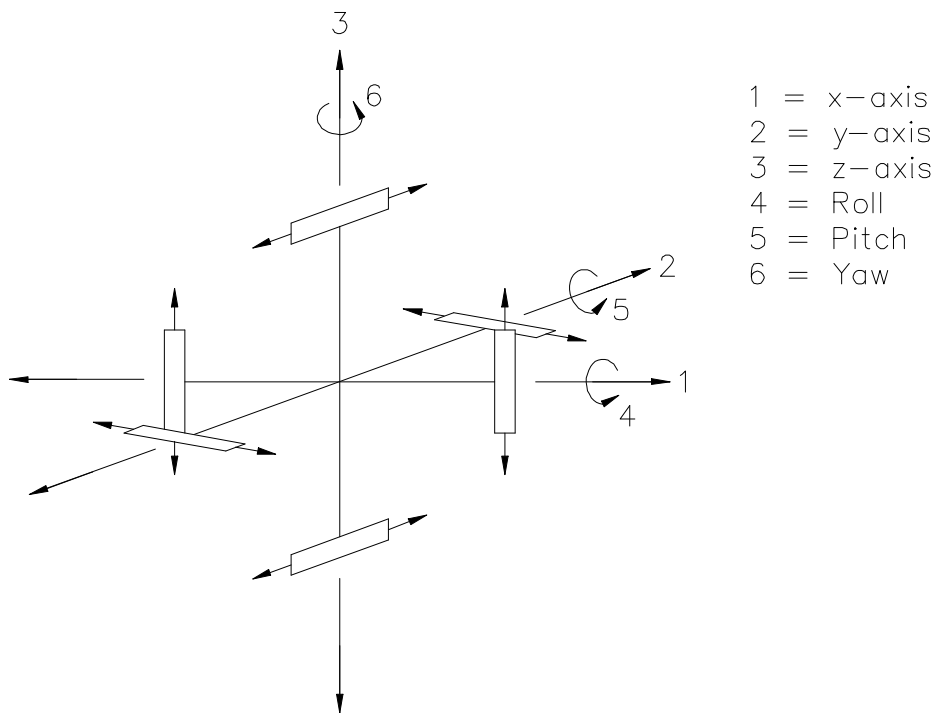


Figure 2 - Six Degrees of Freedom Using Bi-Directional Pumps

This allows translational movement by turning on pumps in pairs in the same direction, and rotational movement by turning on pumps in pairs in opposite directions.

5.2 Analysis of the previous ROV's propulsion system

The main failing of the previous ROV was that it achieved virtually no velocity. Analysis showed that there were a combination of reasons for this. The idea of using individual valves to control the water jets is, in theory, good in that accurate control of the water jets can be achieved and multiple jets can be operated simultaneously. There are, however shortfalls with this design. The valves used in this design were globe valves. This type of valve on its own is not a bad choice but the actual valves used had a very convoluted route within them, dramatically increasing the pressure loss across them, and therefore the force generated. By having one central pump, the forces generated will vary according to different valve combinations used. By opening different numbers of valves, the pressure head presented to the pump changes. This causes a change in the operating position on the pump performance curve and therefore the flow rate produced by the pump. This creates a less predictable system for the operator.

The previous ROV had the valves venting directly to the environment. This provided a very turbulent exit flow that did not pass through a nozzle. As a result, the exit diameter was dictated by the valve port size. This did not allow for the exit diameter to be optimised for the pumps used.

5.3 Valves versus Multiple Pumps

A decision needed to be made as to whether to continue down same line as the previous project by using a central pump with valves, or to replace the valves with multiple pumps, as had been suggested as a possible alternative.

Research was conducted into possible replacements for the valves. Valves with lower pressure losses that would cope with the underwater environment were searched for, however very few options were available that were any better than those used in the previous project. This led on to a more in-depth analysis of the multiple pump solution. Purely on a size and weight basis the multiple pump option looked very favourable. The size and weight of the valves used in the previous project exceeded that of the pumps used. This is favourable for replacing the valves by individual pumps.

As already stated in the introduction, water jets are an inefficient method of propulsion and therefore all factors need to be optimised to achieve the maximum possible vehicle speed. On a mass basis, replacing each valve by a pump would be a better solution, as the major system loss will then be only the exit loss. If this is then extended to replacing two valves by a bi-directional pump then both mass and volume decreases could be achieved. This would enable a smaller ROV to be built, and therefore a higher speed to be achieved due to lower drag forces. As a result, the valve option was rejected in favour of a multiple pump solution.

5.4 Nozzles

One of the identified failings of the previous project's design was the lack of optimisation of nozzle design with regards to the pumps. The nozzle diameter significantly affects the force generated and therefore, the performance of the ROV. For these reasons, it was decided to investigate nozzle designs. Initially for simplicity, ease of manufacture and cost reduction, exit tubes were suggested as a suitable alternative for complex shaped nozzles. This consisted of a solid bar with a

hole of the required diameter drilled through the length. A diagram of such an exit tube is given below:

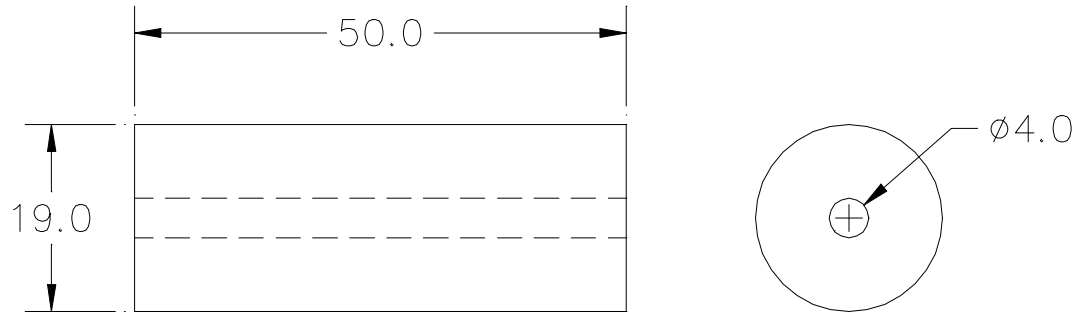


Figure 3 - Exit Tube Design, 4mm Diameter

The cost reduction benefits of this option needed to be compared with the performance increases of getting nozzles machined properly. It was expected that the exit tubes would have a significant associated pressure loss due to the sudden contraction and then the length of small diameter pipe. Research was also conducted into possible design options for high efficiency nozzles. Two possible options for nozzle designs were found in [Internal Flow *D.S. Miller*] and used in the subsequent modelling. The two designs are given below:

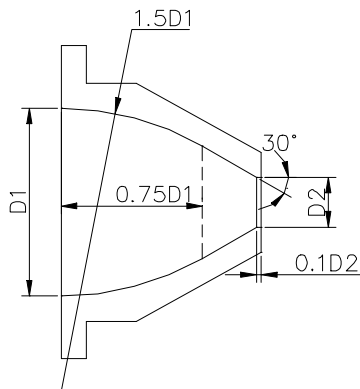


Fig. 14.16a

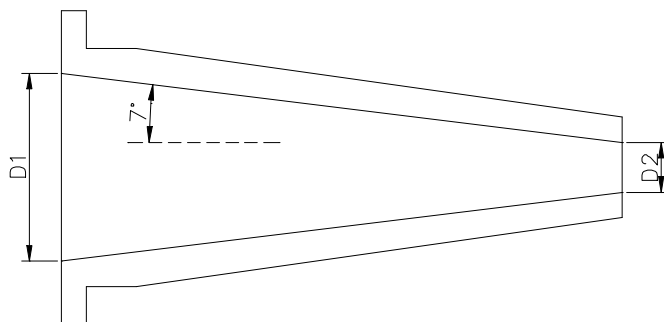


Fig. 14.16b

Figure 4 - Free Discharge Nozzles [Internal Flow *D.S. Miller* p.270 Fig.14.16a]

The benefits of such nozzles are that they do not have as large a sudden contraction loss as their shape follows the fluid flow lines. In addition, they do not have a parallel pipe section before the exit as do the exit tubes. Because the contraction is occurring just before the fluid exits, the fluid is still accelerating as it leaves the nozzle and continues to reduce in cross sectional area outside the nozzle. This increases the force generated, as it is proportional to the velocity squared as shown later in Equation 3. This occurs without the pressure loss associated with using a smaller diameter nozzle that would achieve the same force without this effect. A representation of this effect showing the fluid flow lines is given in Figure 5.

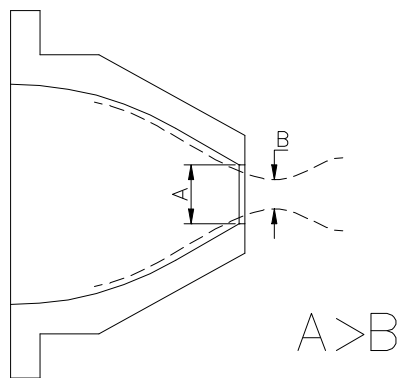


Figure 5 - Fluid Flow Lines Through a Good Performance Nozzle

It was thought that the 7° nozzles would have too long a length for the envisaged ROV size due to the bending radii of the pipes. Therefore, the more complex shaped nozzle was concentrated on during the pipe network modelling due to its shorter overall length. This was a compromise as this nozzle design has a larger pressure loss coefficient and therefore, will reduce the force that a given pump can generate.

6 Bi-directional Pumps

Initially, bi-directional pumps were favoured on the grounds of reduced pump numbers for the same number of water jets, and therefore reduced ROV mass and size. For the bi-directional pump option, the following possible pipe networks were designed:

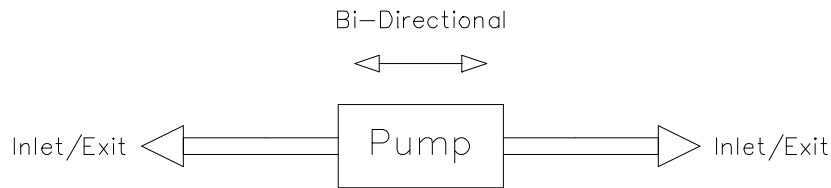


Figure 6 - Bi-Directional Pump Pipe Network 1

This was the first bi-directional pump option designed. It sucks the water in through one of the nozzles and then ejects it through the other. The concern with this design was that there would be a very high pressure loss from sucking the water in through a nozzle. For this reason, the following design was developed to incorporate non-return valves in a more complicated pipe network, so that the water would not have to be drawn in through the nozzles:

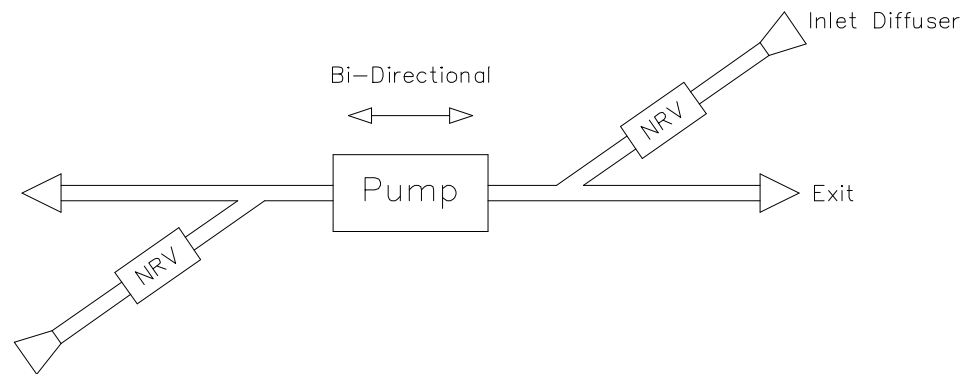


Figure 7 - Bi-Directional Pump Pipe Network 2

Simultaneously to developing these pipe networks, a pump search was conducted for bi-directional pumps. For this to be effective, a pump specification was drawn up. The required attributes of a suitable pump were as follows:

- Bi-directional water pump
- Continuously submersible; sealing pumps within a casing would be expensive.
- 12/24V DC, preferably 24V due to reduced currents.
- In-line, so that pipes can be attached to either end.
- Small, to minimise the ROV size.
- Appendix C contains the complete list of all companies contacted during all the pump searches. Initial feedback from the companies contacted indicated that the

specification was too tight, in particular requiring the pump to be both bi-directional and submersible. As a contingency, unidirectional pump options were developed.

7 Unidirectional pump options

Unidirectional pumps were the second choice for the propulsion system. This is because using unidirectional pumps to achieve the same number of water jets as a bi-directional pump system requires twice the number of pumps. However, different optimal solutions, for specific numbers of degrees of freedom, exist for the uni and bi-directional pumps.

As one pump is required for each nozzle, the pipe network in this situation is very simple. This can be seen below:

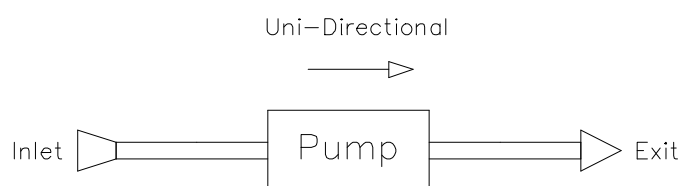


Figure 8 - Uni-Directional Pump Pipe Network 1

As one pump is used for each nozzle, it is possible that different power pumps could be used to achieve forward to reverse and sideways movements. This is because of the different speed requirements stated in the specification. This would possibly be cheaper and a more efficient use of power.

As for the bi-directional pump option, a pump search for suitable uni-directional pumps was conducted. The specification became less stringent as in this situation the pumps were not required to be in-line, allowing sump pumps to be considered. The other components of the specification remained the same.

8 Analysis of Previous Project's Propulsion System Modelling

The previous project modelled some of the propulsion system. They analysed the proposed pipe network and produced a required flow rate and pressure head. This approach produced only one possible solution for the system. It did not take into account that pumps have a flow-head curve (the pump performance curve) along which they operate. For any given pump there is a performance curve which shows that the flow rate decreases as the head increases. These pump performance curves are available from the pump manufacturers. The system used in the previous project,

by just producing one point, only allowed pumps to be either accepted or rejected, and not to be compared. In addition, their calculation of the required pump power is not put to any use, nor indeed is it any real use in specifying a commercially available pump.

The only propulsion system tests conducted by the previous project were the final ROV tests, when it was discovered that that it did not achieve the specified velocity, at which point it was too late to adjust the design. This problem arose due to there being no predictions of the force generated by the ROV.

It was decided that in order to accurately predict the performance of the ROV, it was necessary to be able to calculate the force different pumps could generate. This would allow accurate specification of the propulsion system components.

9 Propulsion System Modelling

In order to accurately specify the pumps, a regressive modelling process was required. For a given ROV a drag coefficient will exist. For different vehicle speeds with this drag coefficient, different propulsion forces are required. This means that for a given propulsion system, a specific flow rate and pressure head are required to overcome these drag forces. This is as far as the previous project took the modelling. The force developed by the propulsion system is equal to the momentum transfer. The momentum of the exiting water jet is given by:

$$\text{Momentum} = \dot{m}\bar{v}$$

Equation 1

Where \bar{v} is the mean fluid velocity and \dot{m} is the mass flow rate of the exiting flow, this is given by:

$$\dot{m} = \rho A \bar{v}$$

Equation 2

Where ρ is the density of the fluid and A is the area of the nozzle.

Combining these two equations, the force developed by a water jet is:

$$F = \rho A \bar{v}^2 \text{ (N)}$$

Equation 3

This shows that the force developed is proportional to the nozzle area as well as the fluid exit velocity. The fluid exit velocity is determined by the nozzle area and the mass flow rate as shown in Equation 2. Therefore combining Equation 2 and Equation 3, the following relationship can be developed:

$$F = \frac{\dot{m}^2}{\rho A}$$

Equation 4

This shows that, for a given mass flow rate, as the nozzle size is decreased, the force increases. This implies that the nozzle size should be minimised. However, as the nozzle size is decreased, the pressure head to maintain this flow rate increases. Positive displacement pumps could maintain the flow rate at the increased pressure head, but they tend to be large, heavy and not submersible, so are not suitable for this application. This leaves centrifugal, diaphragm and axle pumps. For these pumps, this increase in the required pressure head shifts the operating position on the pump performance curve. It decreases the flow rate, and therefore, the force developed as shown by Equation 4.

This introduces the concept of a 'balance point'. This is the point on the pump performance curve where the pressure losses in the pipe network balance with the maximum flow rate a given pump can generate for that situation. This therefore shows the point at which the pump will operate. As a result, for any given pipe network, there is a maximum flow rate and therefore a maximum force that can be generated. Therefore, the pipe network can be optimised to find the maximum force a pump can generate. By knowing how individual pumps will perform, comparisons can be made between different pumps and the most suitable selected.

In order to optimise the pipe network, and, more specifically, the nozzle type and diameter, a relationship between force, flow rate and pressure loss needs to be established. The relationship between force and flow rate is already defined by Equation 4. Therefore, a relationship between flow rate and pressure loss needs to be developed.

The pressure losses in a pipe network are dictated by the flow rate and the component loss coefficients. Therefore, the pipe network needs to be broken down into its

constituent components. For each component, the pressure loss can be expressed in the following form:

$$\Delta P = \frac{1}{2} r \bar{v}^2 k$$

Equation 5

This defines the component pressure losses in terms of the fluid density, r , and mean fluid velocity, \bar{v} , and the component pressure loss coefficient, k . The component pressure loss coefficients are defined as follows.

9.1 Straight Pipe Losses

$$k = 4f \frac{l}{d}$$

Equation 6

Where f is the friction factor, l is the pipe length and d is the hydraulic diameter. As the pipes considered are round, d is the pipe diameter. The friction factor, f , is found from a Moody Chart [Engineering Data Book *Munday and Farrar*] through the Reynolds number. Reynolds number is defined by:

$$\text{Re} = \frac{r \bar{v} d}{m}$$

Equation 7

Where d is again the hydraulic diameter and m is the fluid dynamic viscosity. In order to simplify the calculations, the smooth pipe curve on the Moody chart was modelled to allow replication of calculations within the spreadsheets. This plot is included in Appendix D and gave the following equation:

$$f = 0.0465 \text{Re}^{-0.2004}$$

Equation 8

For the purpose of these calculations, the pipes were grouped together and a total length of 15cm was used. This is an estimate based on the initial design. The pipe diameter was taken as 3/4" as this was the most common pump exit diameter found during the initial pump searches.

9.2 Entry Losses

This divided into two types, with and without inlet diffuser.

9.2.1 With Inlet Diffuser

The inlet diffuser modelled was assumed to have a 45° inlet angle with a t/d ratio of greater than 0.2, where t is half the difference between the inlet and outlet diameters and d is the outlet diameter taken as ¾". This gave a constant loss coefficient of 0.2. [Internal Flow *DS Miller* p.269 Fig.14.12]

9.2.2 Without Inlet Diffuser

This situation effectively models fluid entry into a pipe. Again, the t/d ratio is used where in this situation t is the pipe thickness and d the pipe internal diameter. In this situation the loss coefficient equals 0.54 for all ratios greater than 0.075. This covers all situations that are likely to be experienced in this project, so the loss coefficient of 0.54 was taken. [Internal Flow *DS Miller* p.269 Fig.14.12]

9.3 Combining/Dividing Flow Connectors

For simplicity, these were all assumed to be equal y-connectors with an internal diameter equal to the ¾" pipe diameter. In all cases, 100% of the flow was assumed to pass from one arm to a second. This is a reasonable assumption as these connectors are only used in the bi-directional pump calculations where very little flow will pass in through the nozzle. In the combining flow case, the loss coefficient is taken as 0.34 [Internal Flow *DS Miller* p.230 Fig.13.18]. In the dividing flow case the loss coefficient is taken as 0.31 [Internal Flow *DS Miller* p.238 Fig.13.29]

9.4 Non-Return Valve Losses

Very little data was available for losses associated with Non-Return Valves (NRVs). Manufacturers data sheets were obtained for possible NRVs, however the only ratings given were the maximum pressure rating and the valve opening pressure. It was decided to use the valve opening pressure as the pressure loss across the valve. This was considered to be a reasonable assumption, as the spring inside the valve provides a restriction which in order to be overcome requires this level of pressure which is probably then lost. As a result, a pressure loss of 25mbar was used which is the opening pressure for a potentially suitable NRV, available from RS (part number 325-412).

9.5 Nozzle Losses

The nozzle design modelled is shown in Figure 4. It is the first of the two with the more complex but shorter shape. The loss coefficient K_n is given by:

$$K_n = \left(\frac{A_1}{A_2 C_d} \right)^2$$

Equation 9

Where A_1 and A_2 are the inlet and outlet areas respectively and C_d is the discharge coefficient. The discharge coefficient varies linearly from 0.805 to 0.825 as the nozzle area ratio is varied from 0.1 to 0.25 [Internal Flow *DS Miller* p.270].

9.6 Exit Tube Losses

The exit tubes shown in Figure 3 divide into three separate component losses: the abrupt contraction losses, the pipe losses and the exit losses.

9.6.1 Abrupt contraction losses

The abrupt contraction losses occur as the fluid enters the exit tube. The loss coefficient depends on the ratio of inlet and exit pipe areas. For this section of the modelling, the range of nozzle sizes considered was 1mm to 19mm diameter. Over this range of diameters, the loss coefficient varies from 0.61 to 0. For each of the different ratios, a loss coefficient value was returned from the graph in [Internal Flow *DS Miller* p.269 Fig.14.14].

9.6.2 Pipe losses

The pipe losses in the exit tubes are calculated in the same way as for the other pipe losses. In this situation, due to the smaller pipe diameter and by conservation of mass, the Reynolds numbers are considerably higher. As a result the friction factor is higher and therefore the pressure loss across this length of pipe.

9.6.3 Exit losses

Exit losses in this situation consist of an abrupt expansion loss. As the pipe discharges effectively to a reservoir the area ratio is zero. Therefore, the loss coefficient equals 1. [Internal Flow *DS Miller* p.269 Fig.14.15]

With all the pressure loss coefficients found, Equation 5 can then be used to calculate the pressure loss across each component. When the individual component pressure losses have been calculated, they can then be summed to give the total pipe network losses for that flow rate. This gives a single point that indicates a flow rate, pressure loss and therefore, the force generated at that flow rate for that nozzle size.

10 Initial Pipe Network Comparisons

The first comparison to be made was between the three pipe networks described above in Figure 6 to Figure 8. For this, a common situation was developed where all components were identical so that the only difference was the pipe network configuration. Appendix E shows the calculations used for this comparison. In these calculations, a generated force of 6N from two jets was modelled; this was to mimic a possible ROV. Figure 9 below, shows the results of these calculations.

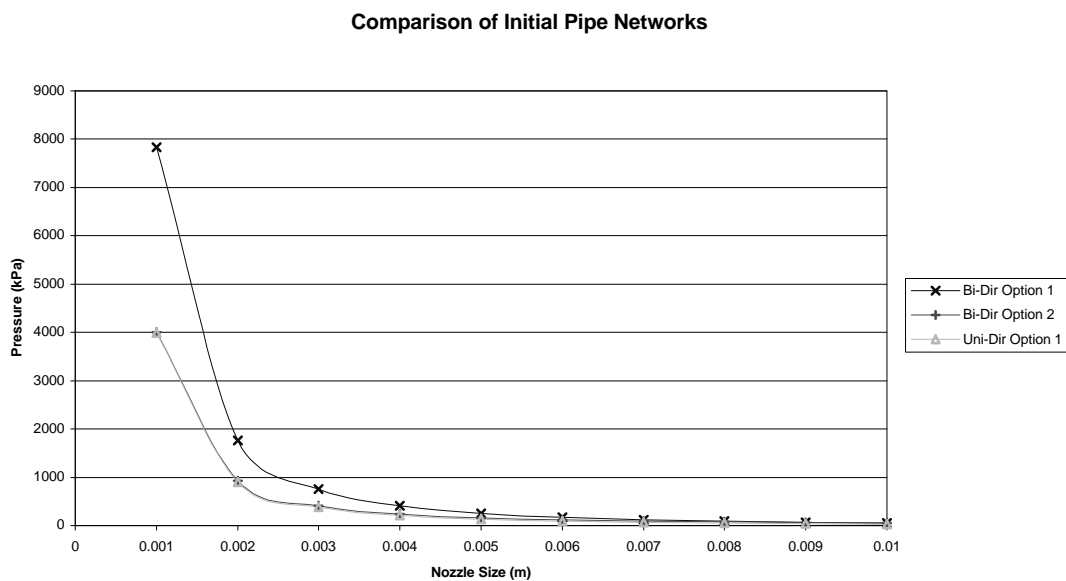


Figure 9 - Comparison of Initial Pipe Networks

This indicated that bi-directional Option 1 is the least efficient of the systems as it has the highest pump pressure requirement. This is the situation where water is sucked in through a nozzle. These results allow this option to be rejected. This leaves bi-directional Option 2 and uni-directional Option 1. These two lines are almost identical with bi-directional Option 2 slightly higher. As a result either would be a suitable system.

11 Results of Pump Searches

Due to the potential ROV size reduction through the use of bi-directional pumps, this was the favoured option. However, at this point it was apparent that a suitable bi-directional pump with the required specification could not be found. For this reason the uni-directional pump option had to be adopted.

However, the uni-directional pumps found through the pump search were still very limited. They mainly consisted of marine application pumps with some for bait tank circulation and sump pumps. The requirement for DC pumps limited the manufacturers considerably and those contacted all suggested either ITT Industries or LVM Ltd. LVM Ltd. provided the pumps for the previous project and were very helpful in providing information. ITT Industries divided into ITT Jabsco and ITT Rule. Jabsco produce more general pumps where as Rule produce marine specific pumps. A lot of overlap was discovered in their product lines. Rule, however, provided pump performance curves and technical data for their pumps more freely. In addition a possibly suitable pump, manufactured by Flo-Jet was found.

The following pumps were found that complied with the pump specification and suitable information obtained for comparisons:

- LVM Congo
- LVM Amazon
- Rule 3700
- Rule 2000
- Rule 1500
- Rule 1100
- Rule 500
- Flo-Jet 4125-314

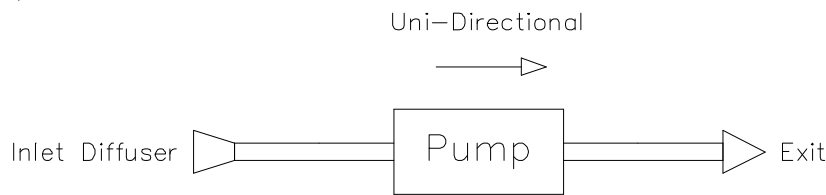
There were no pumps found that complied with the specification, that had a significantly higher pressure capability than the pumps used in the previous project. This was a problem encountered by the previous project that enforces the decision to move away from valves and their associated high pressure losses. The only pumps

found of a small enough size, that had higher pressure capabilities, were flexible impeller pumps, which incidentally are also bi-directional. These, however, were almost exclusively supplied separately to a drive motor due to their usual application of being mechanically driven by an engine. Due to time constraints, it was decided not to pursue this path, as suitable a waterproof motor would need to be found and then matched to a suitable pump.

12 Sensitivity to Inlet Diffuser

In the first pipe networks, an inlet diffuser was included in the design. This improves the flow of water into the pipe and therefore, reduces the pressure loss associated with fluid entry. However, inlet diffusers require a large volume. Therefore, their benefit needs to be compared to the increase in volume of the ROV required for their presence. Therefore, a comparison between the following two pipe networks was made.

Option 1



Option 2

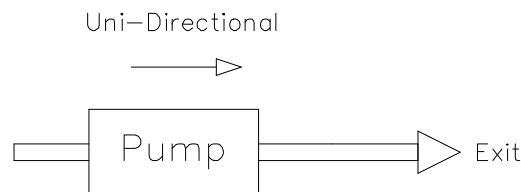


Figure 10 - Inlet Diffuser Sensitivity

Both options have exit tubes (see Figure 3) and 15cm of smooth PVC piping, and Option 1 has an inlet diffuser before the pump.

Again, a common situation was created where all factors were kept constant, except the presence of the inlet diffuser. These calculations (included in Appendix F) produced the following graph:

Sensitivity to Inlet Diffuser

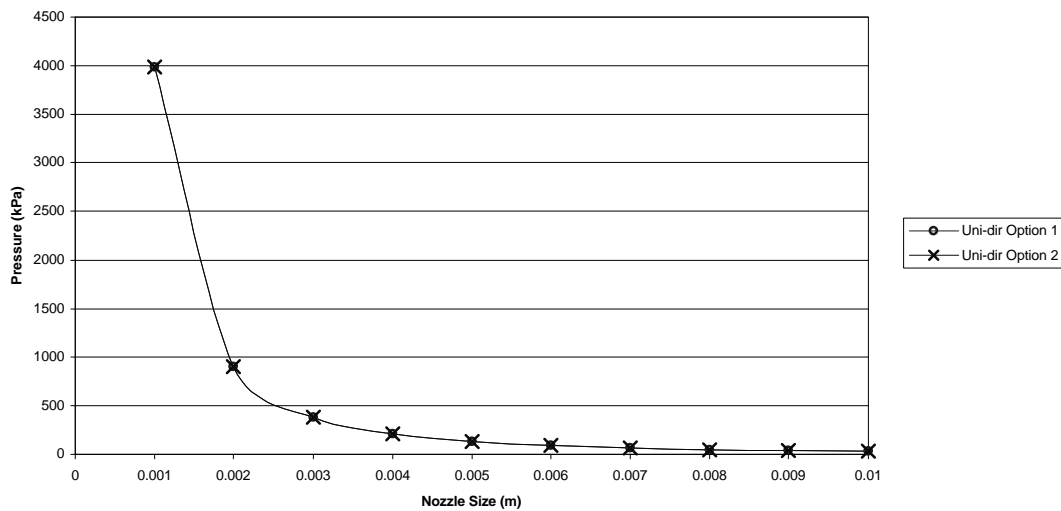


Figure 11 - Sensitivity to Inlet Diffuser

Though there only appears to be one line on this graph, there are two. They are so close to each other they appear as one. This shows that the pump pressure requirement reduction, as a result of adding an inlet diffuser, is negligible. For this reason, inlet diffusers shall not be used, as their associated volume far outweighs the benefit gained through their presence.

13 Pipe Network Optimisation

The approach adopted for optimising the pipe networks was to calculate the required flow rate to achieve a range of forces in one Newton increments between one and fifteen Newtons. With these flow rates known, the component pressure losses could then be calculated and a curve generated. It is this line that will cross a pump performance curve indicating the balance point. In order to optimise the nozzle type, size and other pipe network components, a range of these curves were required. Therefore, for each pipe network permutation, a set of curves need to be produced, consisting of one curve for each nozzle diameter. With these curves, and a pump performance curve, a set of balance points can be found which will indicate the optimum nozzle diameter and maximum force for that pump.

13.1 Pump Selection

In order to select the most suitable pump, comparisons between the different pumps need to be made. In order to do this a common situation needs to be modelled and the forces generated by different pumps calculated. For this purpose, the following pipe network was modelled:

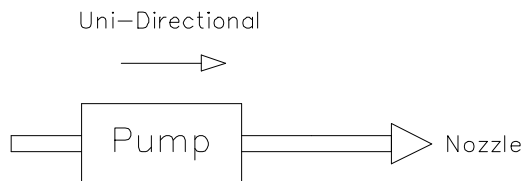


Figure 12 - Pump Selection Pipe Network

This pipe network has a free discharge nozzle (Figure 4 - *D.S. Miller Fig 14.16a*) attached to the pump via 15cm of smooth PVC piping.

Using this pipe network, a spreadsheet was created for each nozzle size, from 1 to 19 mm. 19mm was taken as the upper limit for the nozzle size as, during the pump search, the most common pump exit diameter was $\frac{3}{4}$ " (19.05mm). For example, a nozzle diameter of 6mm produces the graph below:

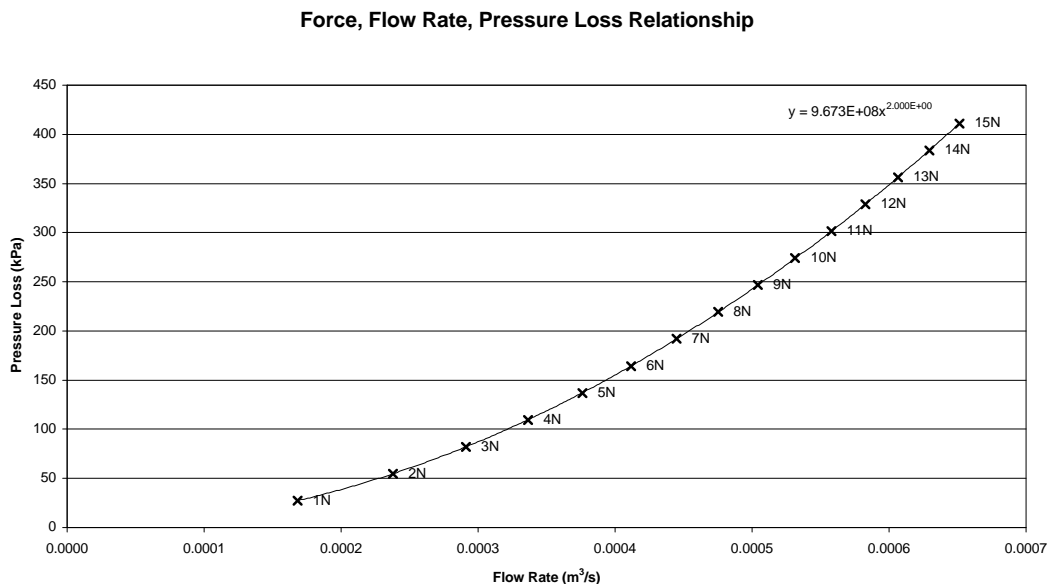


Figure 13 - 6mm Nozzle; Force, Flow Rate, Pressure Loss Relationship

With the curves for each nozzle size generated, they were all compiled in to one graph. This produced the graph shown below in Figure 14.

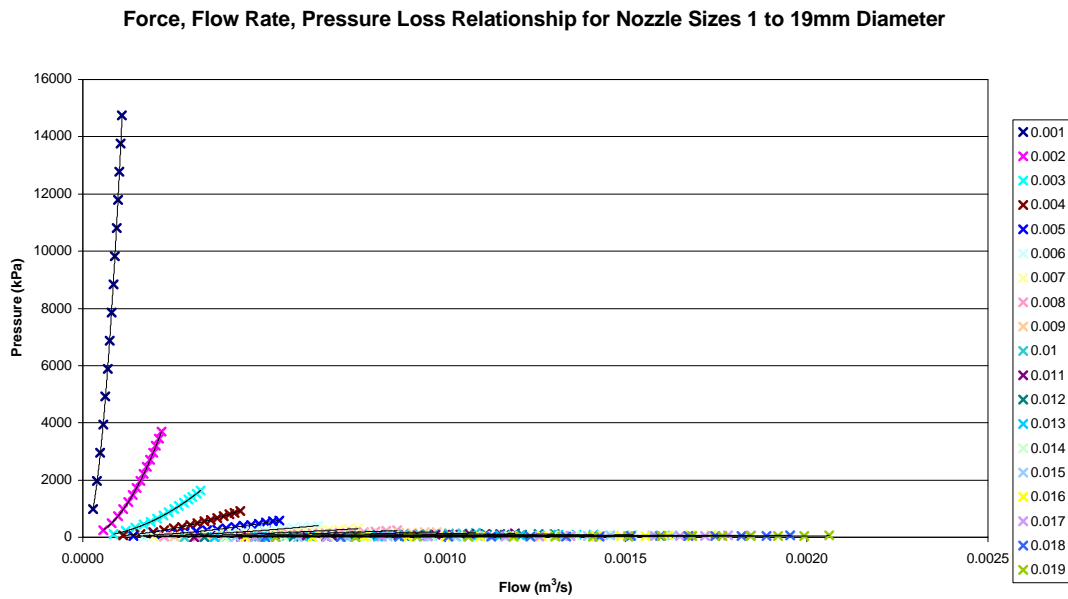


Figure 14 - Force, Flow Rate, Pressure Loss Relationship for Nozzle Sizes 1 to 19mm Diameter

This is now in a position where it can be combined with pump performance curves and solved to find the balance points for the different nozzle sizes. The performance curves for the pumps found from the pump search were superimposed on to Figure 14. These curves fell into a small section of Figure 14. This area was enlarged, giving the following graph:

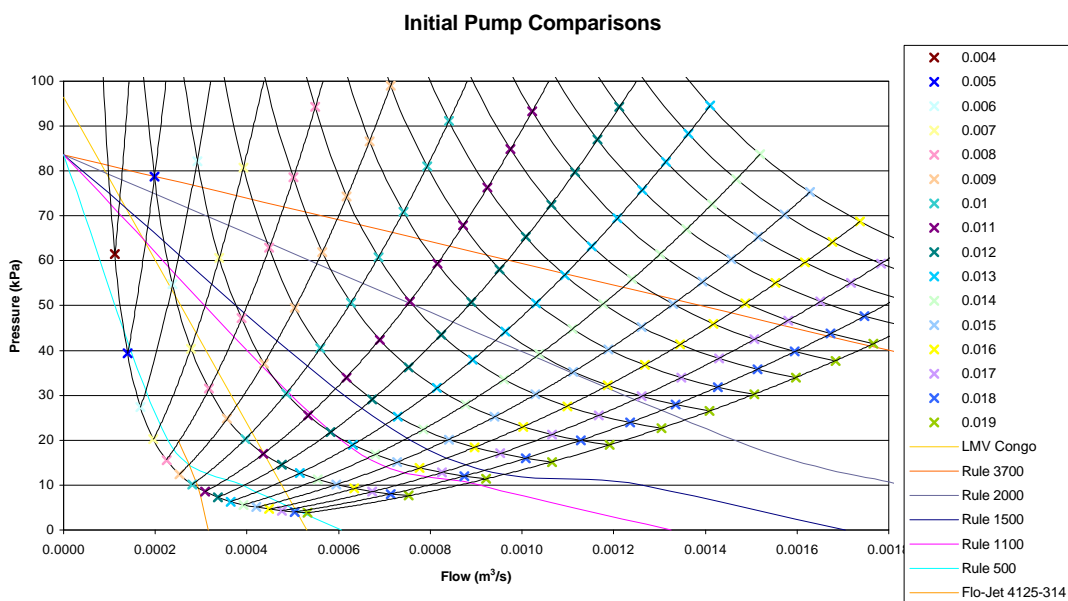


Figure 15 - Initial Pump Comparisons

On this graph, the lines with the positive gradient in the matrix are lines of constant nozzle size; there is one line per nozzle diameter modelled. The lines with the negative gradient in the matrix are lines of constant force, starting with one Newton closest to the axis and increasing in one Newton increments to fifteen Newtons, furthest from the axis. These allow the force generated at the different balance points to be visualised more accurately.

The complete set of spread sheets used to produce Figure 15 and all the other force prediction curves are included on the CD provided with this report. An example set are present in Appendix G. This contains a single nozzle diameter's spread sheets for free discharge nozzles and the summary spread sheets used to produce the force, flow rate and pressure relationship graphs (Figure 15 and Figure 17) and the calculation sheet used to solve the curves.

Figure 15 allows the Flo-Jet pump and the Rule 500 to be immediately rejected as they produce too little force. Further investigation into the Rule pumps revealed that the Rule 3700 and 2000 were physically very much larger than the other pumps. This explains the considerably higher flow rates and therefore force predictions. These much larger pumps would increase the size of the ROV considerably, which would take the design away from the project objective of producing a small low cost ROV. For this reason, these two were rejected. This left the LVM Congo and the Rule 1100 and 1500. Though the Rule 1500 produces, at its maximum, twice as much force as the LMV Congo, however, it needs to be considered in context of its size. The Rule 1500 has 7.5 times the volume of the LVM Congo. For only double the force, this is an uneconomical use of space. In comparison between the Rule 1100 and the LVM Congo, the Rule 1100 has 4 times the volume. Again, the LVM Congo displays the best (lowest) volume to force ratio. The table below shows these results and the data used for their calculation.

Pump	Diameter	Height	Volume (in ³)	Max Force (N)	Vol:Force
Rule 1100	2-3/8"	4-1/4"	46.9	3.1	15.1
Rule 1500	4-1/4"	6"	85.1	3.8	22.4
LVM Congo	1-1/2"	6-1/2"	11.5	2.2	5.2

Table 1 - Pump Characteristics Comparisons

In addition to this, the ability to compactly stack the pumps needs to be taken into consideration. The Rule pumps, like most centrifugal pumps, have the entry and exit at 90° to each other. This is not favourable for stacking a number of pumps next to each other. The LVM Congo has the entry and exit inline at the top and bottom of the pump. This allows the pumps to be stacked together very compactly enabling the size of the ROV to be reduced. For these reasons, it was decided to use LVM Congo pumps.

13.2 Multiple Pumps Per Nozzle

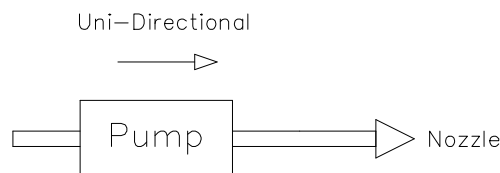
As a result of the marked difference between the volume to force ratio of the LVM Congo, it was decided to investigate the possibility of using multiple pumps for each water jet. By using two pumps, in either series or parallel, the force generated per water jet can be increased. For this reason, the graphs in the following section, Nozzle Design and Diameter Selection, include multiple pump performance curves. There is one for each of the following situations: single pump, two pumps in parallel and two pumps in series. Through the following analysis, it is possible to ascertain the benefit of using multiple pumps and find an optimal solution.

For the purposes of the modelling, two pumps in series is assumed to produce twice the pressure for the same flow rate as a single pump. For two pumps in parallel, it is assumed that twice the flow rate for the same pressure is produced.

13.3 Nozzle Design and Diameter Selection

In order to optimise the nozzle design and size, the force, flow rate and pressure relationship calculation process was repeated for the following pipe networks:

Option 1



Option 2

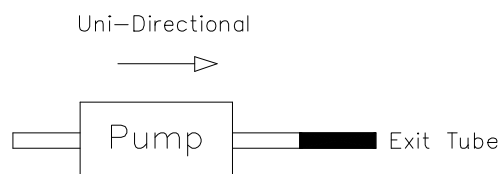


Figure 16 - Nozzle Optimisation Pipe Networks

Option 1 has a free discharge nozzle (Figure 4 - *D.S. Miller Fig 14.16a*) where as Option 2 has an exit tube (Figure 3).

This allows the difference between the types of nozzle to be assessed in terms of the maximum force generated. Option 1 is the same as previously used in the pump selection process. This situation gives the following relationship between the pump performance curves and the force produced for the different nozzle sizes.

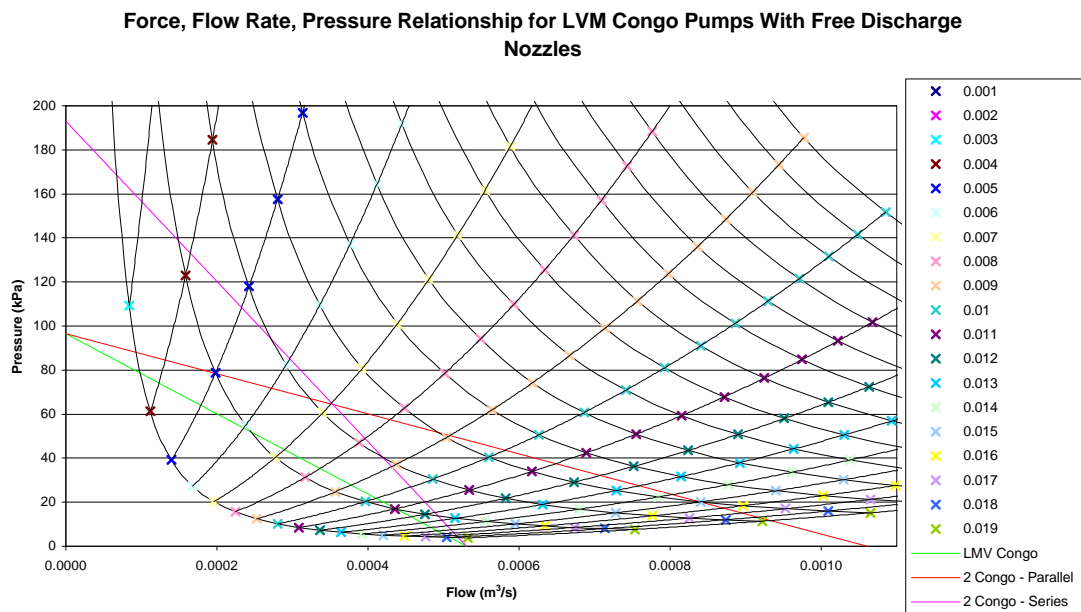


Figure 17 - Option 1, Free Discharge Nozzle With LVM Congo Pump

From this graph, the maximum force generated for each pump configuration can roughly be seen. To find this value more accurately, the equations for the pump performance curves and the nozzle lines need to be solved. The equations for the nozzle lines approximately follow an ‘x-squared’ relationship to within three decimal places. Therefore, in order to use the quadratic equation to solve these equations, it was assumed that they were all ‘x-squared’.

For example, solving the single Congo pump and the 6mm nozzle diameter line:

The single Congo pump performance curve has the following equation:

$$y = -181935x + 96.484$$

Equation 10

The 6mm nozzle diameter line has the following equation:

$$y = 9.673 \times 10^8 x^{1.9998} \approx 9.673 \times 10^8 x^2$$

Equation 11

By combining these two equations the following equation can be produced:

$$9.673 \times 10^8 x^2 + 181935x - 96.484 = 0$$

Solving this equation using the quadratic equation and taking the positive solution, gives a flow rate of $2.36 \times 10^{-4} \text{m}^3/\text{s}$. Applying this to Equation 4, mass flow rate to force relationship, this gives the following predicted force for this situation:

$$F=1.96\text{N}$$

This calculation can then be conducted for the three pump performance curves to give the following predicted forces for the different nozzle sizes.

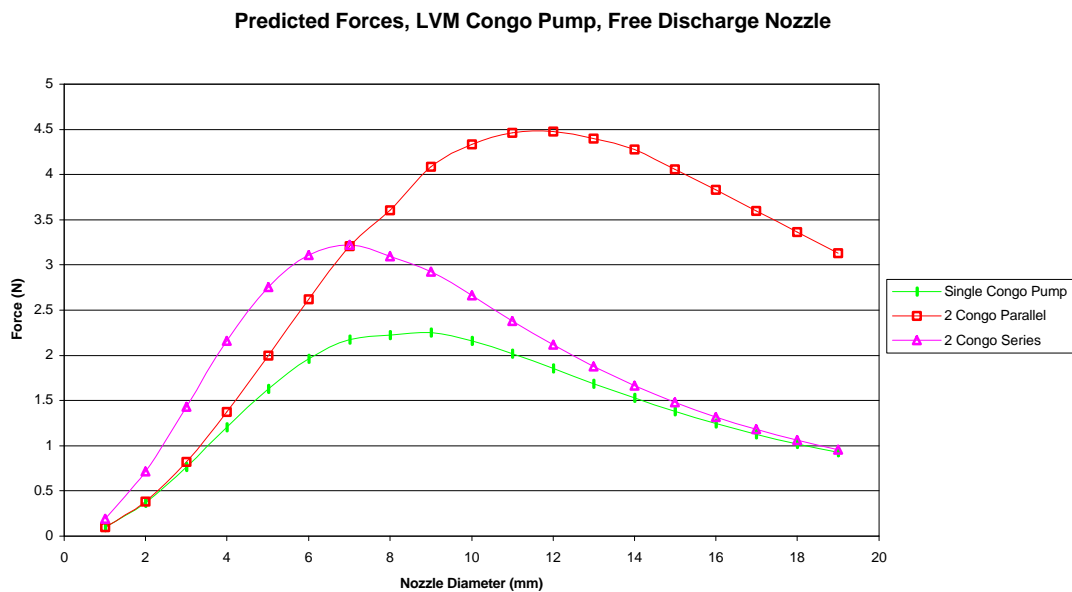


Figure 18 - Predicted Forces, LVM Congo Pump, Free Discharge Nozzle (Option 1, Figure 16)

This shows that the different pump configurations produce a different skew on the graph and therefore, the maximum force at different nozzle sizes. As would be expected, the double pump combinations produce more force with the parallel option producing almost twice the force.

This process can be repeated for Figure 16, Option 2 – exit pipes. Again, the following graph is produced.

Force, Flow Rate, Pressure Relationship for LVM Congo Pumps With Exit Pipes

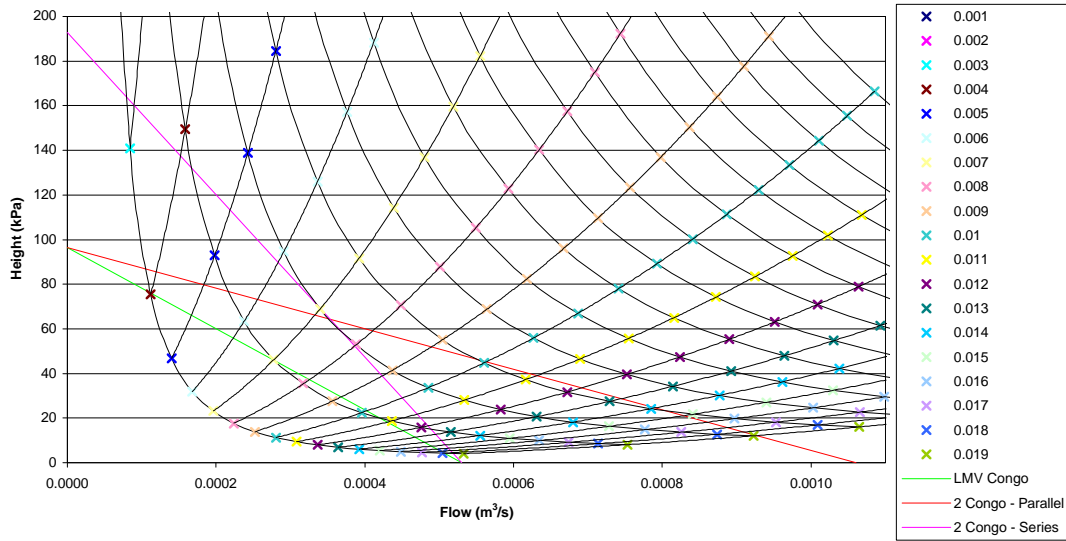


Figure 19 - Option2, Exit Pipes with LVM Congo Pumps

This appears very similar to the previous graph for free discharge nozzles, but the forces generated are smaller as shown below:

Predicted Forces LVM Congo Pump, Exit Tubes

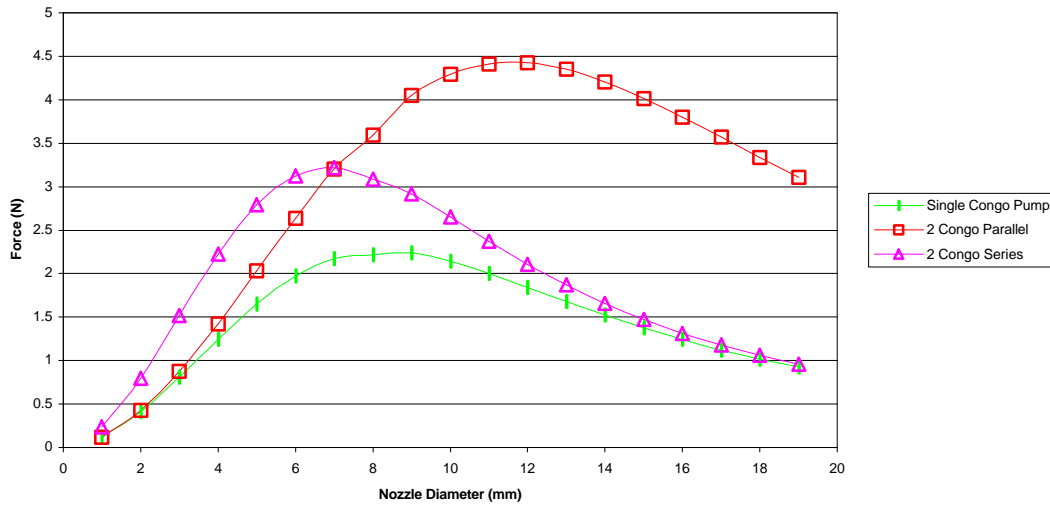


Figure 20 - Predicted Forces, LVM Congo Pump, Exit Pipes (Option 2, Figure 16)

In summary the comparisons between the two Options are as follows:

	Free Discharge Nozzles (Diameter)	Exit Tubes (Diameter)	Percentage Difference
Single Pump	2.25N (9mm)	2.23N (9mm)	0.9
Parallel	4.48N (12mm)	4.42N (12mm)	1.3
Series	3.22 (7mm)	3.21N (7mm)	0.3

Table 2 - Analytical Force Comparisons

This shows a surprisingly small difference between the exit tubes and the free discharge nozzles. It was expected that there would be a larger difference due to the inefficiency of the sudden contraction and the length of small diameter and therefore high loss piping in the exit tube.

14 Experimental Results

To confirm the theoretical predictions and therefore the correct nozzle diameter experiments were conducted. It was decided to measure the static force generated by the pipe networks. To do this, the following experimental set up was used.

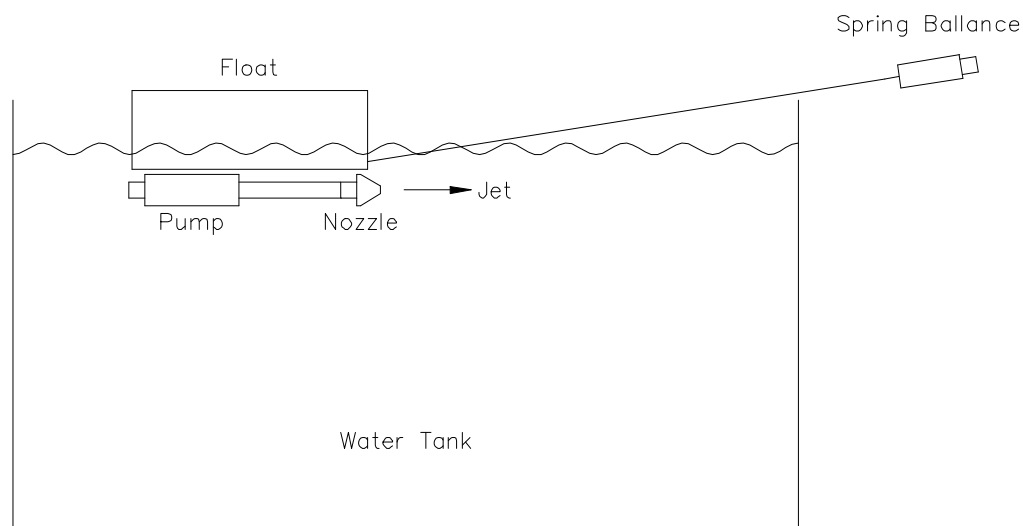


Figure 21 - Experimental Set up

The pump was attached to the nozzle or exit pipe via a length of 15cm PVC hose, to comply with assumptions used in the analytical predictions. The pump and nozzle were then attached to a float such that they were suspended below the water line, deep enough that the water jet did not have a surface effect. A length of fishing wire

attached the nozzle and to a spring balance to measure the force developed. The length of fishing wire used was long enough such that the angle between the jet and the wire was minimised. This was to ensure that the force was vectored as little as possible to gain the most accurate results.

15 Preliminary Experimental Results

Once it had been decided to use LVM Congo pumps, LVM was contacted and sent a pump to us for evaluation purposes. This allowed pipe network tests to be conducted before purchasing all the pumps required. For this a set of exit tubes (Figure 3) were manufactured. These ranged in diameter from 2mm to 7mm. This range was chosen, because at the time of manufacture the analysis predicted the maximum force to lie within this range. As a result of these tests, the model was corrected giving the results given in the analysis above. Using no nozzle and having the water exiting directly from the pipe achieved the 19mm result. The forces were measure experimentally, as described above, and achieved the following results.

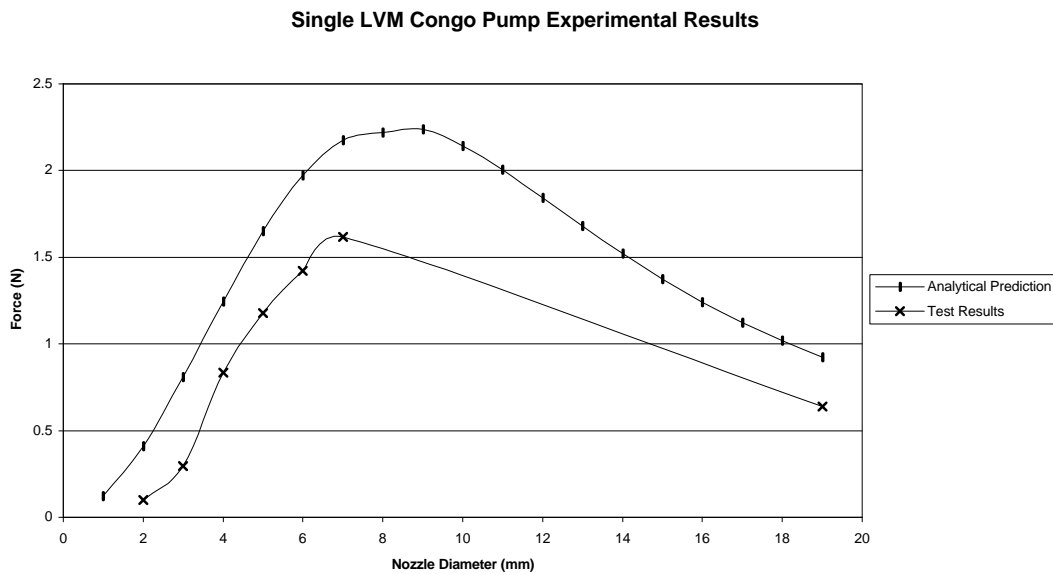


Figure 22 - Single LVM Congo Pump, Experimental Results

These results showed actual values significantly lower than the analytical predictions, however, the curve shape is relatively similar. The table below shows the actual results.

Exit Tube Dia. (mm)	Test Results (N)	Analytical Results (N)	% Difference
2	0.10	0.41	76.1
3	0.29	0.81	63.6
4	0.83	1.24	32.9
5	1.18	1.65	28.7
6	1.42	1.97	27.8
7	1.62	2.17	25.6
19	0.64	0.92	31.0

Table 3 - Single LVM Congo Pump Experimental Data

Though the percentage difference between the analytical and the experimental results are reducing as the diameter is reducing, the difference is still significant.

If the test results in Figure 22 are extended over the remaining nozzle sizes, and the shape of the graph is assumed to continue following the predicted curve, then the maximum force generated will be 1.75N. This was considered too small a value for the ROV. As a result, it was decided to use the multiple pump option. The two pumps in parallel are predicted to produce the largest force. It was therefore decided to use this solution.

As a result of these poor test results, combined with an offer from Penske Cars to manufacture nozzles free of charge, it was decided to have free discharge nozzles built. The shorter of the two nozzles designs was chosen (Figure 4 *D.S.Miller Fig.14.15a*) on the grounds that it would save space within the ROV. The initial test results showed a reasonable correlation between the shapes of the curves. Therefore analytical predictions suggested 12mm as being the optimum size nozzle. However it was requested that 10mm be used to simplify manufacture. This smaller nozzle diameter will result in a reduction of 0.14N or 3.1 % per jet, which is an acceptable level of reduction.

15.1 Exit Tube Experiments

To confirm the benefits shown analytically of using two pumps, parallel and series combinations were tested using the same exit pipes as before. The same experimental set up shown in Figure 21 was used with two pumps instead of one.

15.1.1 Two Pumps in Parallel

The parallel pump combination produced the following results:

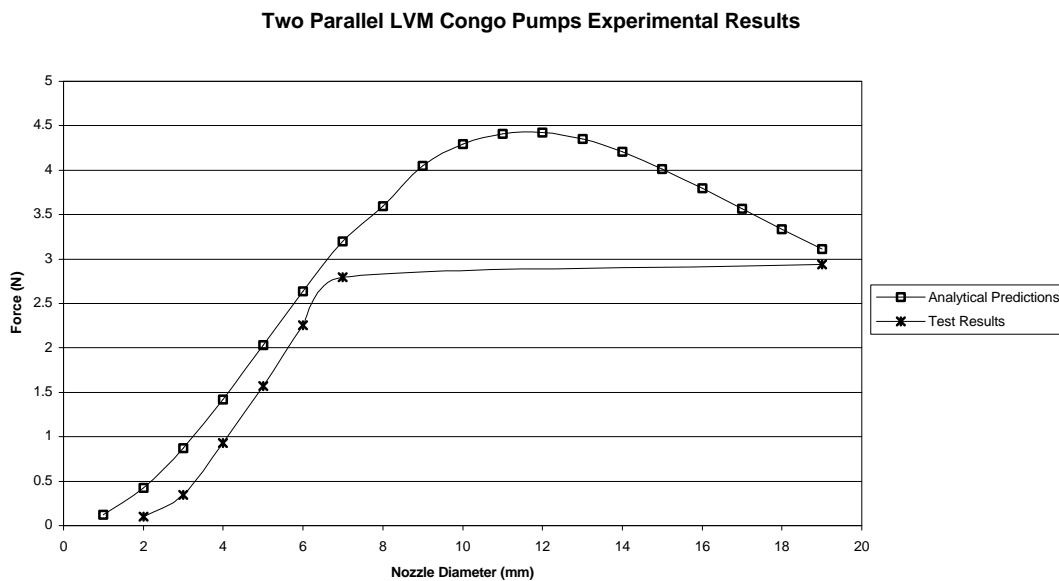


Figure 23 - Two Parallel LVM Congo Pumps, Experimental Results

The experimental data for this and all the experiments is given in Appendix H. This data shows that the percentage difference between the analytical and experimental results is less than for the single pump, at 7mm. The difference is 12.7%, which is still a reasonable amount. The percentage difference should be even smaller as the parallel pumps situation assumes that there is only one pump producing twice the flow rate. This is not the case as there are two pumps attached through a ‘y-connector’ that would provide a further loss, reducing the force generated. Again, as in the single pump case, the experimental curve has a similar shape to the analytical curve, however to prove the location of the maximum, further tests using larger diameters are required.

15.1.2 Two Pumps in Series

The series pump combination produced the following results:

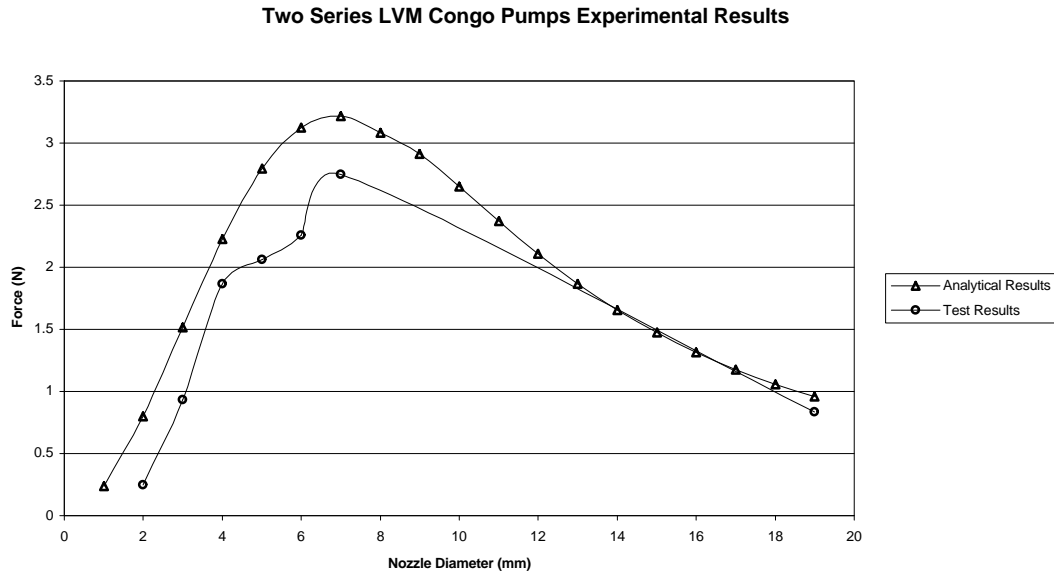


Figure 24 - Two Series LVM Congo Pumps, Experimental Results

In this situation, the experimental results at 5mm and 6mm diameter appear to be too small. They do not follow the expected path. These are probably anomalous results and need to be repeated.

It can be seen from the experimental test data that the percentage difference between the analytical and test results, for all pump combinations, decreases as the nozzle diameter increases. As all component losses allow for the change in nozzle diameter, it can be assumed that this is the result of an interaction effect. This is probably the result of the interaction between the sudden contraction and exit losses. The more severe the sudden contraction, the longer the fluid flow takes to settle down. Therefore, it is likely that as the nozzle diameter increases the sudden contraction effect recedes back down the pipe reducing the interaction effect. The fact that at 19mm there is still a difference indicates that there are other inaccuracies in the modelling producing an offset. One such difference would be due the pipe joint losses between components, for example where the pipes leave the pumps. In addition, the roughness coefficient used for the exit pipe is likely to be too low. They were assumed to be smooth, which is not the case as they have been drilled and not finished accurately.

15.2 Nozzle Experiments

When the nozzles had been manufactured, it was then possible to compare these to the analytical predictions. As there is only one nozzle size, only one point on each of the force prediction curves can be compared. These experiments were conducted in the same manner as before and produced the following results:

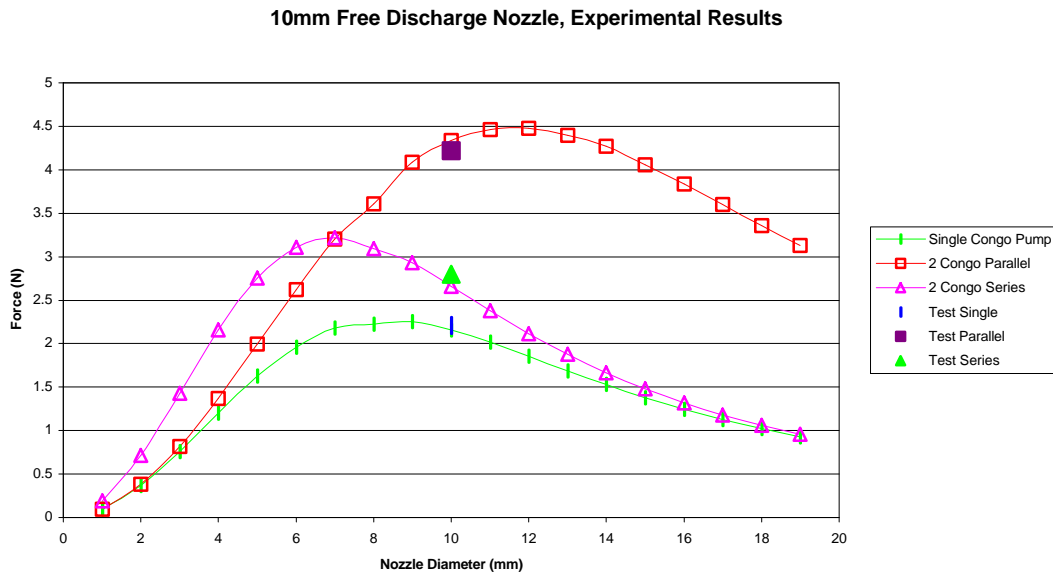


Figure 25 - 10mm Free Discharge Nozzle, Experimental Results

These results are very close to the analytical predictions, and, surprisingly for the single pump and the series pumps, the experimental results are higher than the analytical predictions. The following table shows the percentage differences:

	Test Results (N)	Analytical Results (N)	% Difference
Single Pump	2.21	2.15	2.30
2 Pumps Parallel	4.22	4.34	-2.73
2 Pumps Series	2.80	2.66	5.07

Table 4 - 10mm Free Discharge Nozzle Experimental Data

These show a particularly good correlation to the analytical predictions. It is probable that the adjusted nozzle design has a higher discharge coefficient (see Equation 9) and therefore a lower loss coefficient, producing test results higher than the analytical predictions.

16 Jet Orientation and Configuration

If the number of degrees of freedom required is reduced, then the, the number of water jets required also reduces. Commercially available ROVs frequently do not have the six degrees of freedom. They substitute some of the degrees of freedom of the ROV by incorporating cameras that can be moved within the ROV. For example, the Hydro-Vision Hyball (see Figure 1) has only four degrees of freedom: three translational, and yaw. The camera has adjustable pitch within its dome. In order to achieve this, the Hyball has to be very statically stable; have a large distance between the centre of buoyancy and the centre of mass. This is the same as having a keel, which rights the ROV should any roll or pitch be experienced. To simulate this situation a minimum of six water jets would be required and a mechanism to move the camera. This mechanism was considered to be too expensive a solution and was not taken any further.

As this project is intended to prove water jets as a viable propulsion system for ROVs, it was decided to produce a vehicle that had all six degrees of freedom. There are many different methods of producing six degrees of freedom for example the solution used by the previous project. This involved twelve water jets: four vertically up, four vertically down, two vectored at 30° forwards and two vectored at 30° backwards.

By using vectored water jets, it is possible to reduce the number of jets required. Reducing the number of jets required is of a significant benefit, as it reduces the number of pumps required. If no jets are vectored then 16 jets are required to achieve all six degrees of freedom. This can be seen below:

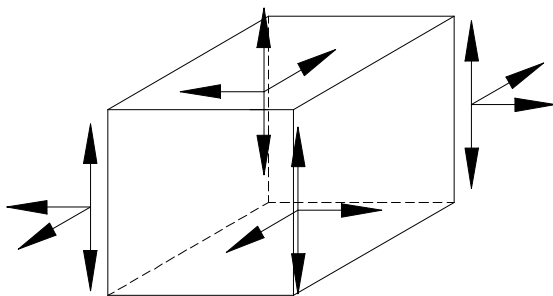


Figure 26 - 16 Water Jet Option

By vectoring the eight water jets in the x-y plane, these can be reduced to four while still maintaining the six degrees of freedom. This gives a total of 12 water jets and is the solution used by the previous project. This can be seen below:

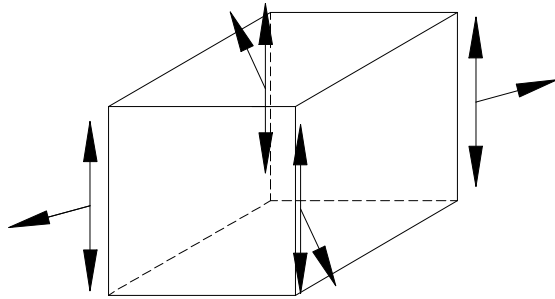


Figure 27 - 12 Water Jet Option

This can then be taken to the next stage by vectoring all of the remaining water jets. This allows a further four to be removed while still maintaining six degrees of freedom. This gives a total of 8 water jets and can be seen below:

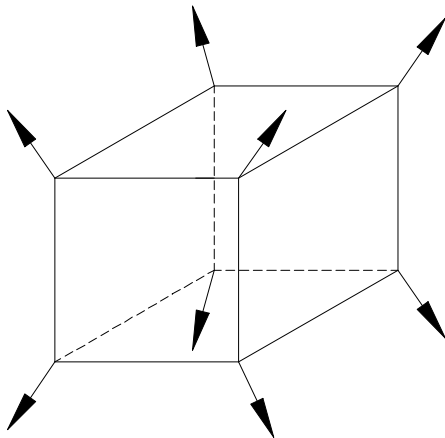


Figure 28 - 8 Water Jet Option

This achieves the minimum number of water jets possible to achieve six degrees of freedom. It therefore minimises the number of pumps needed. For this reason it was decided to use this solution. It has already been stated that two pumps will be used per water jet. This gives a total of 16 LVM Congo pumps required.

16.1 Movable Ballast

During the water jet orientation and configuration design process, the idea of movable ballast was investigated. By having either a movable ballast or movable buoyancy, it would be possible to achieve a constant pitch for the ROV. This would reduce the number of water jets required. Six water jets could be used to achieve six degrees of freedom along with the movable ballast. The movable ballast could also be used to

compensate for the tether drag and weight. In this situation the tether would produce a moment on the ROV causing a pitch. The movable ballast could then be used to compensate for this moment.

Despite these benefits, it was decided to abandon this idea for the same reasons control surfaces were; it would require moving parts within the ROV and therefore expensive sealing.

16.2 Force Vectoring

Each jet can be broken down into components along the primary axes. By resolving these forces, the total force generated for movement in a single direction can be found. This can then be used with the ROV and tether drag coefficient to find the maximum speed in any direction. The forces along the primary axis are shown below.

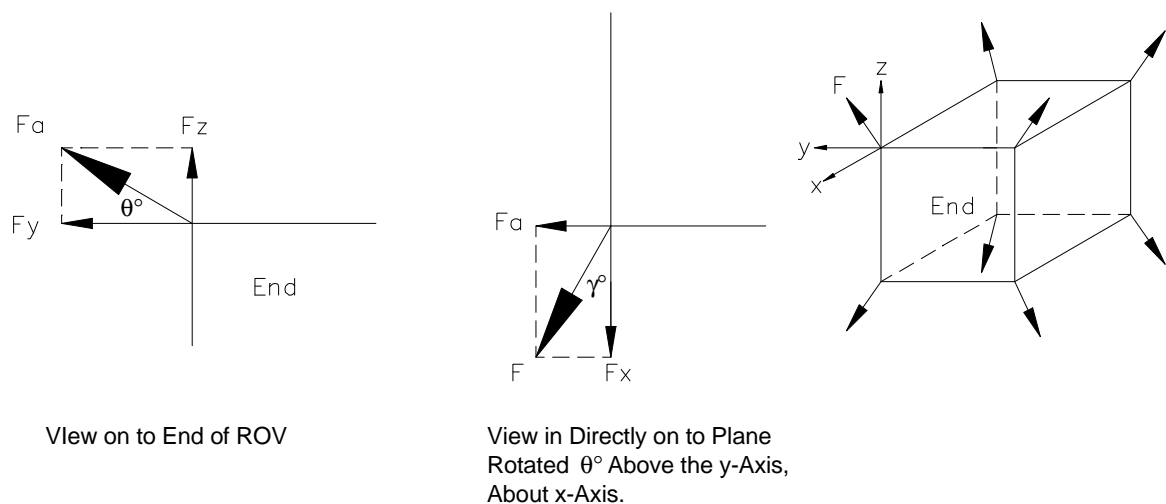


Figure 29 - Pump Force Vectoring

The force, F , generated by one jet is known from the experiments described earlier, this is 4.2N. Due to time constraints, optimisation of the water jet vectoring angles was not conducted. This would require drag testing of the ROV before designing the nozzle mounting system. As a result, θ° and γ° were both chosen to be 30° . This enabled a maximum forward force while still enabling movement in all the other degrees of freedom.

With a single jet force of 4.2N, these angles give the following total forces for water jets working in groups of four in the translational axes:

Axis	Force (N)
X (Fore/Aft)	14.6N
Y (Lateral)	7.2N
Z (Vertical)	4.4N

Table 5 - Total Force in Translational Axis

Internal Structure

16.3 Requirements

The initial concept of the ROV requires a frame that is load-bearing, lightweight, rigid, and that will play a major structural role in the ROV construction. Due to the probable corrosive nature of the operating environment, the internal frame of the ROV should also be corrosion resistant. The frame should be easy to produce and maintain and should provide good support for, and good access to, the ROV internal components. The frame should also provide a platform onto which the exit nozzles of the propulsion system can be securely mounted.

16.3.1 Materials

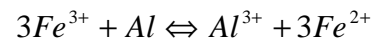
The main constraints for materials used for the design of the internal frame are the need for strength, corrosion resistance, minimal weight and minimal cost. Plastics and aluminium alloys are ideally suited for use in a salt-water environment due to good corrosion resistance. They are also reasonably lightweight.

The properties of polypropylene would be ideal for the corrosive environment encountered in marine applications. It would be sufficiently rigid to use as a frame for the ROV, assuming a suitable thickness and cross section was used. However, polypropylene is too expensive to purchase on the budget. Nylon is also too expensive, but could be used for components, such as the nozzles, due to its excellent corrosion resistance and low friction properties. High-density polythene would also have many of the required properties, but it tends to become embrittled under certain conditions, for example low temperatures or a harsh operating environment. It is unlikely that a plastic frame, made of an affordable polymer, possibly constructed of

tubular sections or similar, would be rigid enough or strong enough for the required application.

Fibre reinforced composites are also ideal in terms of their properties and are commonly used for marine applications. However, it would be costly and complex to produce members for a frame to use in the ROV, due to the necessity of first producing a mould to lay-up on. Also, despite the fact that this type of composite material has a reasonably low density, to achieve the required rigidity, the minimum gauge of a member would have to be rather higher than if aluminium was used. This would mean that overall a composite frame would be heavier than an aluminium frame.

The use of an aluminium alloy for the frame of the ROV presents some easily overcome problems. No metal component can be left exposed in the main structure if made of any other material than aluminium, otherwise an electro-chemical cell reaction will be initiated and the process of corrosion greatly accelerated; for example, in the presence of a ferrous material the anodic aluminium will corrode:



Equation 12

To obtain sufficient rigidity with an aluminium frame, the members could be simple flat strips, but would require a C-section, an L-section, or equivalent. The problem here is that if sheet aluminium is bent sufficiently to form one such section, it can become brittle at the bend. To solve this, an extruded section can be used, although it is slightly more expensive and less widely available than flat sheet.

The other main problem with using aluminium is joining members together. It is well known that many aluminium alloys do not weld well, especially the 2XXX and 7XXX series, so very often rivets, bolts and other such methods are used to join parts of aluminium structures, otherwise a weldable grade of aluminium, such as the 5XXX series, must be used. Rivets would seem the most attractive for application on the ROV because they would be required to take the full load of all the internal components along with the weight of the frame itself and they are strong in shear (although they perform less well in tension). However, in application to the ROV, a small section beam would be used and there would only be sufficient space to position one rivet in the centre of each face of the preferred size of extrusion. This would leave

an unsatisfactory joint since the joined beams would hinge around that one rivet. Only by using at least two rivets at each joint would a rigid enough structure be obtained. However, despite the fact that other methods of joining the structure can be used, welding is still the ideal solution for a totally rigid joint. The 2XXX series and 7XXX series alloys do not weld well, if at all, so the solution lies with the weldable 5XXX series aluminium alloys.

Al 5050: has very good corrosion resistance and workability and can be welded satisfactorily by any commercial method.

Al 5454: is commonly used in marine service and all commercial welding methods work satisfactorily, especially TIG (Tungsten Inert Gas) and MIG (Metal Inert Gas).

Al 5083: has very good corrosion resistance, is easily welded by all conventional means and has good strength and is, therefore used for many marine applications.

Al 5086: is a high strength structural alloy, again used for marine applications and can be welded by conventional methods, especially arc welding.

Al 5456: has similar properties to 5086, but it is not quite as strong and slightly more difficult to weld.

These and other grades of weldable aluminium are available from many suppliers. For the chosen ROV design, 25x25mm L-section extrusions of a weldable grade are obtained from a local company, Metalex.

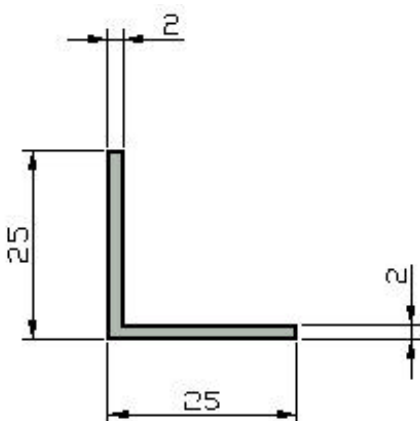


Figure 30 – Theoretical 2mm Gauge

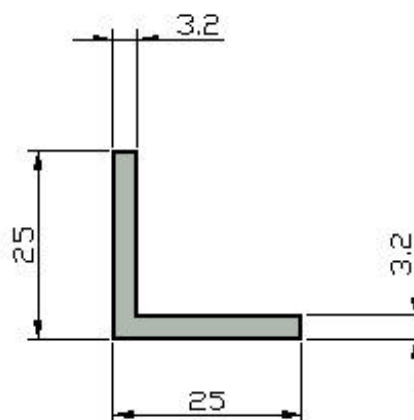


Figure 31 – Readily Available 3.2mm Gauge

From theoretical calculations, shown in Appendix L, it was found that a 2mm gauge (Figure 30) would be perfectly sufficient for the ROV requirements. However, Metalex, in common with many other companies, works mainly in imperial units, so a 2mm gauge was unavailable. The alternatives offered were 1.5mm and 3.2mm gauges. The 1.5mm gauge would be far too thin for use with the final frame design, so it was decided to use the 3.2mm gauge (Figure 31). This means that the internal structure will be slightly heavier than originally foreseen.

16.3.2 Initial Designs

The design of the internal frame was dependent on the size, shape and type of components to be used in the ROV. This meant that the design was liable to change continuously up until the point of manufacture. The main constraints for designing the frame were the need for good accessibility for installation and maintenance, especially due to the prototype nature of the ROV, and the ability to suitably accommodate all the internal components and the required buoyancy.

It was specified to be a free flooding ROV, which made the design of the structure easier due to the fact that it would not need to be watertight or airtight, allowing water to move freely around the internal components. This requirement would have made the ROV integration more difficult and complex due to the necessity for neutral buoyancy and for completely sealed points of attachment for the shell, tether and nozzles.

16.4 Octagonal Frame For Cylindrical Body

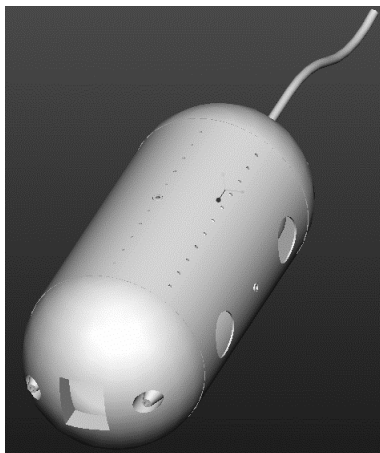


Figure 32 - Cylindrical Body

For use with a cylindrical body, the structure conceived was an octagonal section frame constructed from flat Aluminium strips of about 4mm thickness (see Figure 33). These strips could be welded or riveted together and the end cones of the ROV could be attached to the end faces of the frame. This basic frame would have protrusions attached to longitudinal and bracing beams. These would be specifically shaped to hold the pumps in position once clamped around the protrusions to prevent excess movement of the internal components. This is developed further as shown in Appendix I

To access the components for repairs or modifications, the frame could be lifted out of the ROV through a hinged hatch or by sliding along rails to the opening produced by a removable end cone. The camera box would be secured on the smaller protruding frame. This enables all the internal components to be handled as one unit, again reducing the complexity for access.

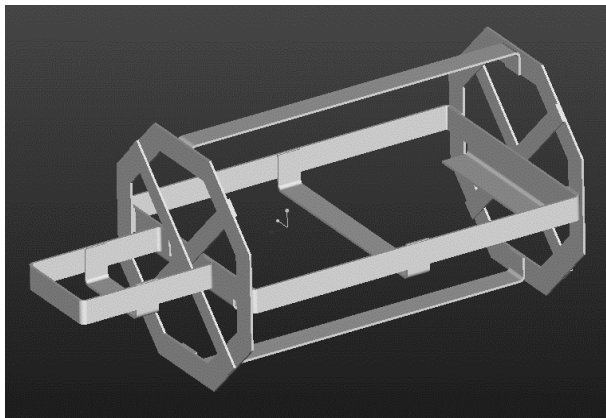


Figure 33 - Octagonal Frame

Whilst this basic frame has the simplicity required for our application, the protrusions (Figure 34) and other parts for attaching the pumps and other internal components would be complex (and, therefore, expensive) to manufacture and these extra parts would also greatly increase the total weight of the vehicle.

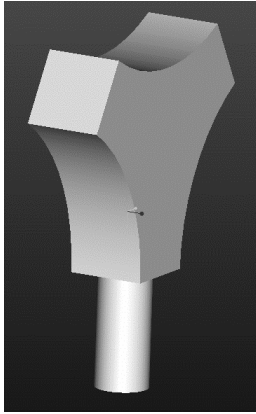


Figure 34 - Example of protrusion to secure components in position

Also, despite the fact that the internal components would be held securely and precisely in a given position, this design does rely on everything being balanced perfectly first time and does not allow any leeway for repositioning.

16.5 Structure For NACA Aerofoil Section

While the possibility of using a NACA (National Advisory Committee for Aeronautics) section body was being explored, it was proposed that the simplest internal frame would be two discs held together by a single tie bar from which all the internal components could be suspended (Figure 35). These discs would be designed to be a tight push fit for the tapering fore and aft sections of the body. If greater accessibility was required, for example to carry out maintenance on the camera, a ring could be used rather than a disc. Using a ring means that it could also be included in the structure of the shell itself, rather than being an entirely separate assembly, if the shell was to be constructed from FRP (Fibre Reinforced Plastic).

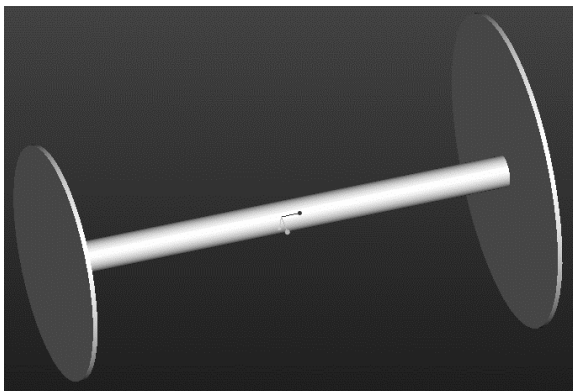


Figure 35 - Internal Frame

However, as it was decided that this body shape would have insufficient volume and that the decrease in C_D did not really justify use of such a complex profile, this

approach was discarded. The proposed internal frame may also have been too simple to adequately prevent the components from moving in a longitudinal direction if the vehicle were to pitch. It may also have proved too difficult to balance properly, due to problems in distributing the components evenly.

16.6 Structure for Wide Bodied ROV

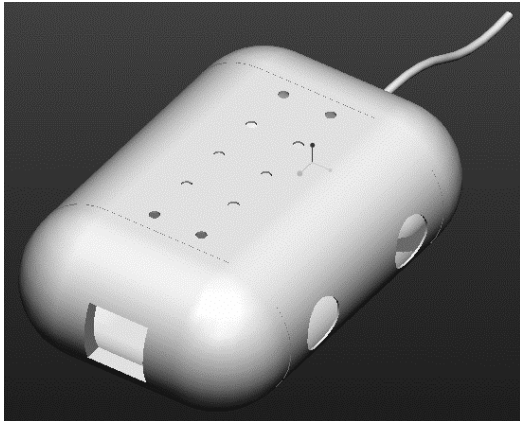


Figure 36 - Initial model of wide-bodied ROV

Once a more flattened shape for the ROV had been decided on (Figure 36), possible ideas were explored to fit a volume of 180 x 180 x 300 mm. This volume was assumed by overestimating the volume of the electronics boxes with the use of the initial eight pump propulsion system.

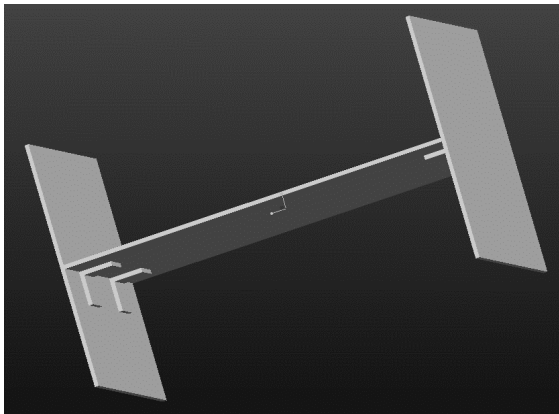


Figure 37 - Flat Plate Structure

With the aim of simplicity in mind, an internal structure was proposed that was formed of 3 metal sheets that could be fastened together by way of brackets to support the central shelf (Figure 37). These sheets could be simply plate aluminium, or perforated sheets. The standard plate could have holes drilled in the positions required to attach the internal components, whereas the perforated plate (Figure 38) allows complete flexibility in positioning the components without the need to drill extra holes.

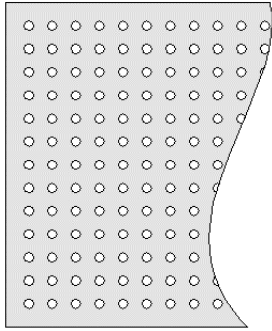


Figure 38 - Example of perforated plate

However, this approach to frame construction would not result in a sufficiently rigid structure. This would be especially true if the plates were only bolted together at the brackets, rather than being welded along the full length of the adjoining sides. As it is an open structure with the main support for the shelf being at either end, the shelf would be likely to sag unless of sufficiently large gauge, and the structure as a whole would not be rigid in torsion. This lack of torsional rigidity could be a problem when it is considered that the ROV could be capable of movement in all 6 degrees of freedom, which may well result in torsional loading of the frame supporting the nozzles.

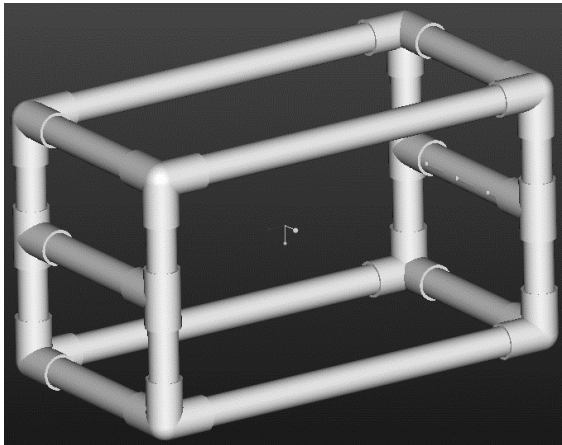


Figure 39 - Plastic Frame

As discussed during the explanations for choice of materials, the possibility of using a plastic frame was explored. In particular, the possibility of obtaining a kit, containing a variety of joints into which the correct length of pipe could be inserted. The plastic frame could be secured using a solvent adhesive to join the parts together (

Figure 39).

By cutting a number of slits in the horizontal pipes halfway down the ends of the frame, a shelf or plate of some description could be inserted, on which the internal components of the ROV could be placed. However, as discussed earlier, it is unlikely that such a frame would be sufficiently rigid for this application without being far too expensive and a plastic shelf, supported only at either end, may well not have proved rigid enough to support the full weight of the internal components without significant deformation.

Using the same basic rectangular section, but this time using a weldable aluminium alloy L-section extrusion, a far more rigid frame can be obtained (Figure 40).

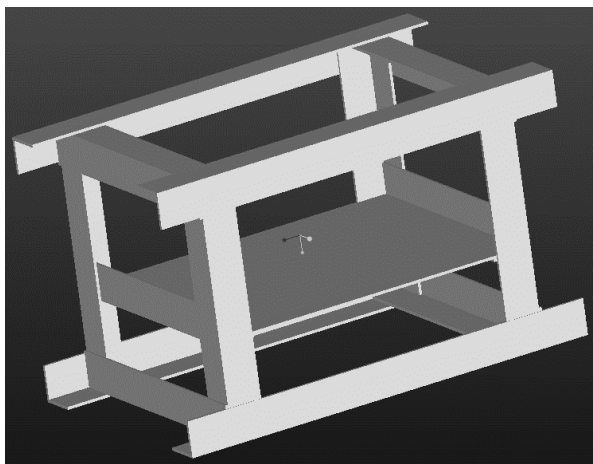


Figure 40 - Aluminium Frame

The Aluminium extrusion can be welded right the way around the corner joints giving an very rigid structure. The lengths of metal protruding from the ends of the framework were proposed as suitable points for nozzle attachment.

It was decided that this type of frame should be used as the internal structure of the ROV and at this stage in development, the volume it occupied was 180 x 180 x 300mm with the sections of extrusion designated for nozzle attachment extruding 30mm from the ends of the main frame. This volume would be sufficient to contain 8 Congo pumps, maximum of 4 abreast, and the required electronics boxes.

The initial design for an aluminium framework, shown above, would require 2.64m of aluminium L-section extrusion. The dimensions initially specified for the extrusion were 25 x 25mm with a 2mm gauge, which would give a total mass of 0.69kg for the ROV frame without the shelf. However, due to the fact that only imperial gauges were available from the supplier, 3.2mm gauge was selected, which would give a mass of 1.08kg for the same length of extrusion used. (Mass calculated using $\rho = 2720 \text{ kg/m}^3$)

value given for aluminium alloys in 'An Engineering Data Book', Munday and Farrar)

To check that the frame would not deform excessively during normal service, a maximum load of 150N was assumed when picking the frame up at the mid point of one of the longitudinal beams, giving a situation like this:

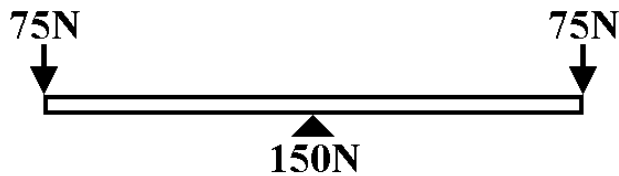


Figure 41 - Weight Balance

This can be seen as a simply supported beam with a point load in the centre:

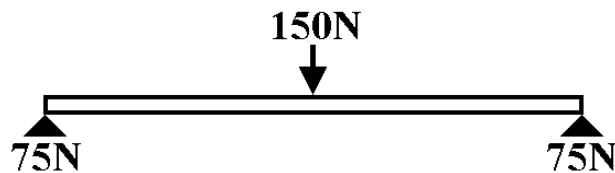


Figure 42 - Simplified Weight Balance

This obeys the equation:

$$d_{MAX} = \frac{PL^3}{48EI}$$

Equation 13

Where:

Maximum deflection = d_{MAX}

Point Load, $P = 150N$

Beam Length, $L = 0.30m$

Young's Modulus of Aluminium, $E = 68.9 \text{ GNm}^{-2}$

2nd Moment of Area is I, from calculations shown in Appendix L.

$$I_{xx} = \int_{dA} y^2 dA$$

Equation 14

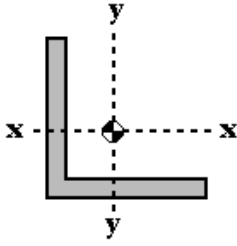


Figure 43 - I_{xx} Diagram

At the load assumed, the 2mm gauge extrusion gives a maximum deflection of 0.21mm, as opposed to a maximum deflection of 0.14mm for the 3.2mm gauge extrusion.

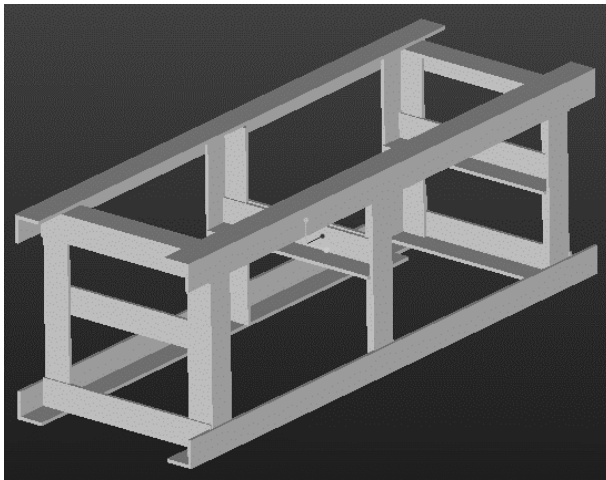


Figure 44 - Longer frame with central support

Various different themes on this basic structure were tried when it became apparent that a longer frame might be required than originally anticipated. To prevent the ‘shelf’ in the frame from sagging, either extra longitudinals would be required, to support it fully along either side, or a central horizontal support to reduce the span of the plate (Figure 44).

16.7 Final Design Of Internal Structure

The final version of the internal frame, shown below in Figure 45, is somewhat longer than the initial version, due to the necessity of incorporating double the number of pumps in the final design of the propulsion system than was originally envisaged. This revised design takes into account the length of a second row of pumps and also the clearance between the rows of pumps to allow sufficient flow into the intakes.

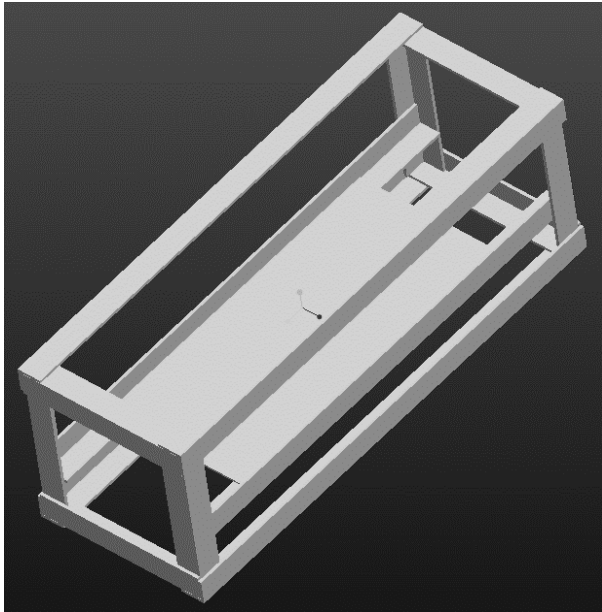


Figure 45 - Final Frame Design

With the length of the longitudinal L-sections at 0.5m, applying the same theory as before, the maximum deflection is given as 0.64mm for 3.2mm gauge extrusion chosen. The originally proposed 2mm gauge extrusion would have given a maximum deflection of 0.96mm. This performance is well within acceptable parameters.

The frame with the longitudinal supports was chosen over the frame with the horizontal central support because, for the designs depicted, the longitudinal support version would require less material. From initial reckoning, it would require about only 4.34m, as opposed to 4.52m for the version with a central support. This has a twofold benefit. Firstly, less material means less mass. Secondly, as the extrusion was to be purchased in a 5m length, the material remaining after cutting the required beams would be sufficient to make another longitudinal beam in the event of a mishap. There would not be sufficient spare material to do this if the other design was used. Another reason for choosing longitudinal supports over the central support is that the presence of the extra length of aluminium between the pump intakes may reduce the amount of flow into the pumps.

The revised frame does not include protrusions onto which the nozzles could be attached, due to the decision to use a different method of attachment.

For the length of aluminium extrusion required to produce a frame with longitudinal shelf supports, the volume of the structure without the shelf is $6.498 \times 10^{-4} \text{ m}^3$ and with the shelf included the volume is $8.065 \times 10^{-4} \text{ m}^3$. Using the value of density of

Aluminium alloy from 'An Engineering Data Book' used in the earlier mass estimations, this revised frame has an estimated mass of 2.19kg.

The extrusion, purchased from Metalex, was well within budget constraints for a 5m length of weldable grade aluminium. Perforated aluminium plate was reasonably difficult to obtain and it was, therefore, decided to use a simple aluminium plate that could be welded, or fixed using epoxy, into place in the structure. This plate was provided by Penske Cars Ltd. Holes could be drilled into this plate where required for positioning components.

The construction of the frame was carried out free of charge by Penske Cars Ltd, although the theoretical cost of their services was £121. The aluminium extrusion purchased from Metalex was cut into more easily transportable lengths by Southampton University EDMC and taken to Penske Cars Ltd for the frame construction.

16.8 Internal Shelf

The final design was to consist of the frame with a shelf to which the internal components could be attached. It was decided that the plate for the shelf should be, initially, left unfixed, to allow easier access to drill holes and position components. The shelf would be fixed into position, using epoxy, after the components were suitably positioned. The plate was to be cut to a length of 13". This length would be sufficient to fix the double row of pumps along, with a gap between the intakes, whilst increasing space available to fit y- connectors between parallel pairs of pumps and to bend the pipes towards the nozzles. The y-connectors, (Figure 7), selected are commercially available from RS.

The use of pairs of pumps per propulsion jet requires Y connectors, significantly reducing available volume for the pipe network. On the underside of the shelf, the pumps were to fit alongside one another, 4 abreast, with alternate pumps constituting a pair. Each pump would be held on at two points along its length, which should prevent movement laterally, and assuming the fastening is sufficiently secure, longitudinally. Holes in the shelf plate form the anchor points for these fastenings.

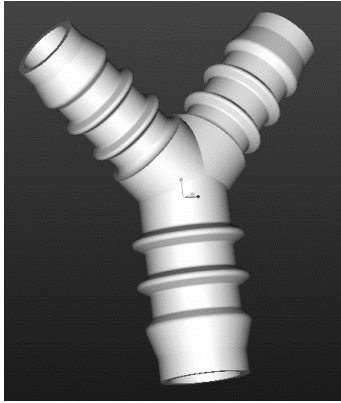


Figure 46 - Y-Connector

The holes, for securing the internal components on the shelf in the frame, were positioned as shown in Figure 47. All dimensions given are in mm. All holes are 5mm diameter.

The pumps above the shelf plate are not required to be held in position flat on the plate and could be suspended from the upper longitudinals of the ROV internal frame and secured by fastening to anchor holes in the vertical face of the shelf support beams.

The main electronics box would be held on separately in the centre of the frame, with its two fastenings passing around it either side of the large connector positioned on its top surface. The holes for anchoring the fastenings would pass through both the shelf plate and the horizontal face of the shelf support beams.

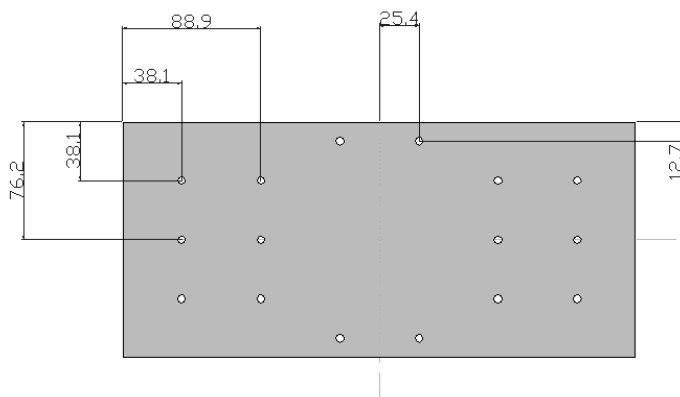


Figure 47 - Supporting Shelf

However, it was eventually decided that, despite the added security provided by attaching components to the plate, the use of a shelf was too constricting when it came to positioning the internal components. Therefore, the use of the shelf was abandoned, and the internal components were left unattached to the frame. Movement of the

pumps and other components was restricted by the addition of buoyancy and, due to its large size, the main electronics box could be adequately secured against the shell.

16.9 Component Attachment

For all the frame options explored, methods of attaching the internal components were examined. It was necessary that, if being securely fixed, the components must be attached to the frame as simply as possible, as firmly as possible and at as low a cost as possible. Ideally, it should be possible to reposition the components very easily, to aid in balancing the vehicle.

The use of epoxy or similar adhesive was explored as a possibility for component attachment. Although a very simple way of attaching components, providing there is sufficient surface area onto which the components can be placed, the permanent nature of the fixing means that it is an unsuitable method for our application.

A framework was considered which would allow the components to be merely slotted into place by means of providing suitable shaped orifices. However, this approach was soon discarded as it became apparent that the resulting structure would be significantly too massive for our purposes. Different methods of component attachment would be required for the more simple designs that were more thoroughly considered for the ROV internal structure.

Jubilee clips would be very rigid and would hold components exactly where required. However, they would significantly add to the mass of the vehicle and would be slightly more expensive than some other options. They would also require solid and well-spaced points of attachment. Jubilee clips were selected to ensure a tight seal between the pipes and the nozzle inlets, but not as a method of attaching components to the frame itself.

Velcro was also considered due to its easy availability, affordability and because it offers a lot of flexibility for repositioning the components. It also retains its grip well in shear. However, because Velcro is mostly available in wide strips, protruding points of attachment would be needed on the frame, which would greatly add to the weight of the vehicle.

Both of these methods of attachment would perform best with a frame with multiple protruding points of attachment. Velcro would be ideal for use with the octagonal

frame described, as it would be the cheapest method of clamping the pumps onto the specifically shaped protrusions. It could also be used for the disc and tie-bar frame. The disc and tie-bar frame would also be suitable for attaching jubilee clips, especially if a square section bar were used, rather than a circular section.

The final design of the ROV internal frame does not lend itself to the use of Velcro as a method of attachment. The use of jubilee clips would be possible to some extent, due to the frame providing some suitable points of attachment. However, this would only be possible at the perimeter of the frame and would not be suitable to secure components to be held in the centre.

The solution to cheap and easy attachment of the internal components of the ROV seems to be the use of cable ties. These can be passed easily through holes drilled in the shelf of the structure and can be tightened sufficiently to give a secure hold on the positioned component. They are cheap to replace if a component needs to be repositioned, they are lightweight and because they are thin and flexible, they can be looped through narrow gaps or holes if a component must be placed in an awkward position and yet will not take up much of the valuable internal volume of the ROV. This particular method of attachment was to be used with the shelf.

Due to the eventual decision to abandon the use of a shelf inside the ROV, it made the necessity of such a method of attachment obsolete. With the pipes, pumps and nozzles all being firmly fixed by the use of jubilee clips, and not to the frame or shelf, and with the electronics box being firmly wedged in place, there was no need for the use of cable ties to secure these components.

16.10 Frame Design Recommendations and Improvements

Due to the decision to use the internal frame without the shelf, it would now be possible to use a significantly smaller and lighter frame. The frame could be reduced to two square frame sections secured separately at either end of the shell, simply to allow the positioning of nozzles. There would be no need to have beams tying these sections together as the sections could be secured directly into the shell structure itself. The reduction in material used would reduce both the mass and volume of the internal structure. The beams used for the square frame sections could also be far smaller in section, as they would not be required to withstand the same loading as if it were supporting the weight of all the internal components. With a maximum thrust of

4.5N or similar from each nozzle, and no added component weight, the forces the structure would be required to stand would be significantly smaller.

The shell of the ROV was also significantly more structural than originally foreseen. Even if the shelf had been used to position the internal components, the frame would not have been required to carry the full load. This means that the frame could have been dramatically reduced in both size and strength, possibly requiring fewer longitudinal members and extrusion of far smaller section because of the load distribution via the shell.

Alternatively, it might be possible to reduce both the size and rigidity of the shell and retain the internal frame as the main load-bearing structure. However, this reduction in rigidity, due to reduction in the shell thickness, would also significantly reduce the strength of the shell and could make it prone to shattering or deformation if dropped. An insufficiently rigid shell might also make the ROV more difficult to store when not in use, possibly requiring it to be dismantled when on shore so as not to damage this non-structural shell.

16.11 Nozzle Design and Attachment

16.11.1 Nozzle Requirements

As with all other aspects of the internal framework, the design and attachment of the nozzles is required to be as simple and efficient as possible. However, the nature of the method of attachment does depend on the precise form of the nozzles.

The nozzles must protrude sufficiently to be just below, or flush with, the outside surface of the ROV shell. They must not protrude too far longitudinally, so as not to interfere with the curvature of the ROV end-cone. There must be sufficient clearance behind the nozzle, once attached, for the tube feeding the nozzle to bend with a suitably gentle radius, so as not to impair flow in the tube.

The nozzles could be manufactured from any suitable corrosion resistant block of material such as nylon or aluminium. It was decided that, as aluminium was cheaper and more easily available, the nozzles should be manufactured from solid aluminium.

16.11.2 Simple Nozzles

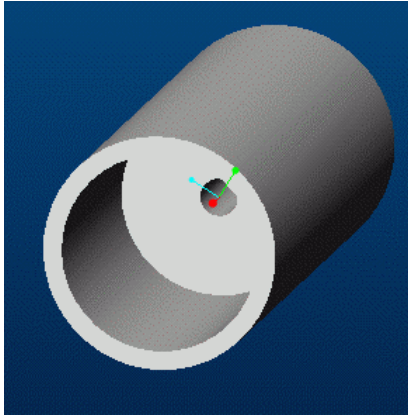


Figure 48 - Simple tube nozzle

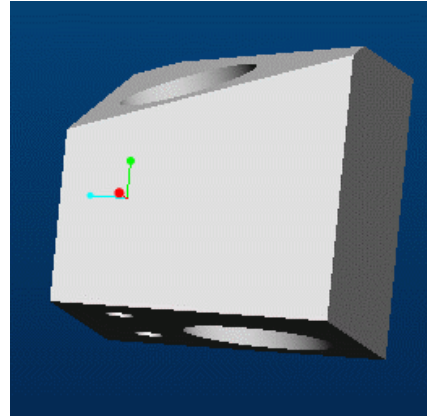


Figure 49 - Nozzle Positioning block

Initially, exit pipes are investigated; an aluminium tube with a sudden contraction, which could be produced by boring out a cylindrical section bar. This very basic nozzle lent itself to being attached using a block with a hole bored at the correct angle to optimise thrust. The cylindrical section nozzle could then be easily inserted into the hole in the block and would be automatically held at the correct angle. This positioning block would then be simple to attach to the end face or onto a flange protruding from the main frame structure.

This simple tube nozzle would significantly reduce production times and costs. If produced from cylindrical bar, no machining, especially CNC machining, would be required; it would simply require the bore to be drilled out. This would be quick and easy to achieve. It is especially advantageous when considering a quoted standard production cost. The rate for both machining and fabrication shop work quoted for external companies at Penske Cars Ltd is fixed at £30 per hour. Whilst a complex machined piece would be a far more precise and efficient product, the use of a CNC machine would significantly slow the process and dramatically increase the resulting cost. Therefore, ideally, the final nozzle design chosen should avoid excessive complexity, which is a criterion that suits the simple, sudden contraction, cylindrical nozzle.

Due to the fact that this simple tube nozzle would give a less than optimum performance, and coupled with the fact that Penske Cars offered to machine nozzles for the ROV free of charge, this approach to nozzle design and manufacture was

discarded. The offer of skilled labour and machine time allowed the proposal of a more complex and efficient design of nozzle to be considered.

16.11.3 More Efficient Nozzles

The nozzle shown in Figure 50 is also reasonably uncomplicated, with a simple external tapering section, comprising a lip part way up the neck of the nozzle, to allow for a more secure positioning of the pipe feeding the nozzle.

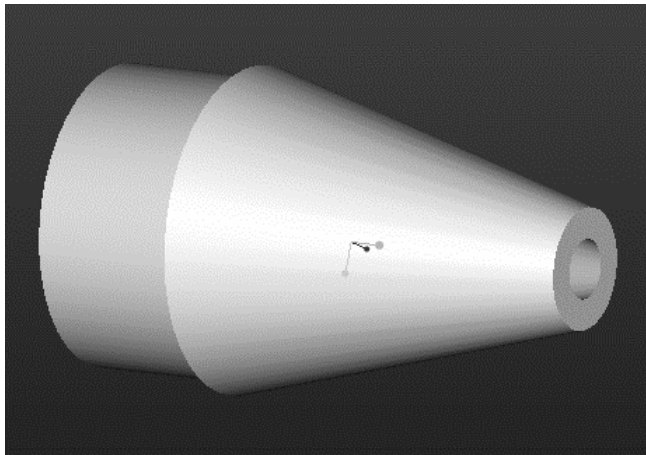


Figure 50 - An example of a more efficient nozzle

This nozzle design is not well suited to fixing using the block shown above, due to its tapering form. There is no flange by which this nozzle could be attached, which would make positioning it on the frame or on the shell rather difficult. However, this nozzle lends itself to being hand machined, for example by turning. This again would be significantly less expensive and easier to produce than a more complex section requiring CNC machining. The possibility of purchasing commercially available nozzles was explored. Most of this research was performed on the Internet. The most promising possibility was found at <http://www.kesmist.com/nozzle.htm>, which would provide a ‘selection pack’ of nozzles, 8 of each type, including suitable filter screens, for \$50. However, these were judged to be unsuitable for our application and were similar in design to the one shown above, so would be difficult to attach or modify. Many other companies offered nozzles of varying shapes, many of which were designed to give a jet that was sprayed as a fine mist, a property that is clearly unsuitable. Some product ranges seemed likely to be suitable, but did not include a nozzle that would be compatible to use with the pipes from the pumps. Other nozzles were manufactured from metals that would be unsuitable for use with the aluminium frame.

16.11.4 Nozzle Attachment

Possible methods were, however, explored to attach nozzles of the type of design shown in Figure 50 and the similar designs available commercially. These included fixing into the corner section of the frame, onto a suitable protrusion, or simply at the correct angle on the end face of the frame by using epoxy to secure the nozzles. A block, such as shown before in Figure 49, could be designed to fit such a nozzle. However, it would be complex to produce and, therefore, expensive. The use of a block machined from solid aluminium would also increase the weight of the ROV.

If a nozzle was to be machined from aluminium, the nozzle could be welded on. However, with such an eventuality, it makes more sense to design a custom nozzle which incorporates a flange, which would allow the nozzle to be more easily bolted or welded or adhered using epoxy onto a suitable surface.

This approach was adopted and more efficient nozzle design was investigated. Shown along with the calculations of nozzle performance, in Nozzles, is a formula for efficient nozzle design, see Figure 4 [Internal Flow *D.S.Miller p.270 Fig.14.16a*]. This formula relies on the designer knowing both the inlet and the exit diameters.

16.11.5 The Final Nozzle

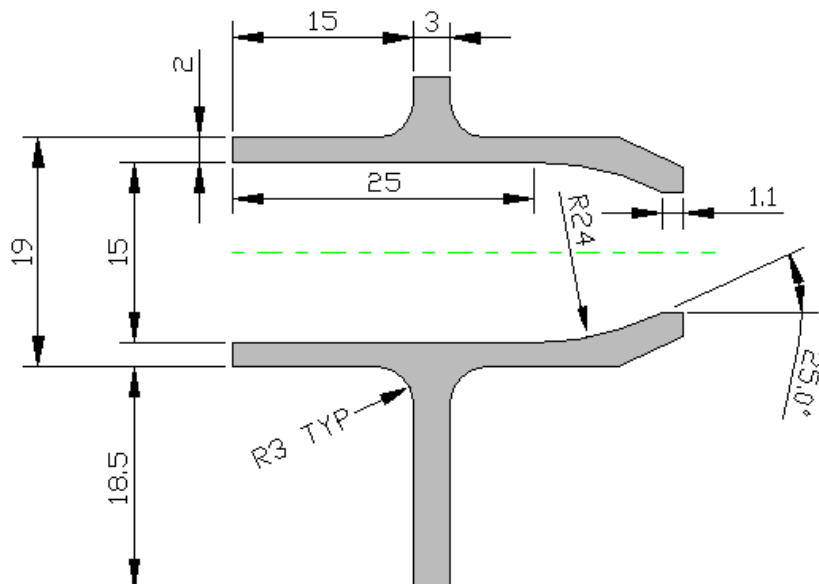


Figure 51 – Final Nozzle Design

The external diameter of the inlet was required to be 19mm to fit the pipe, which would be pushed onto it. It is unreasonable to assume that a machined piece would

have a thickness of less than 2mm, which would leave the internal diameter, D_1 , at 15mm, although even a wall thickness of 2mm could present some problems for machining. Ideally, the exit diameter should be at least 11mm. However, these dimensions are incompatible with the formula shown in Figure 4 [Internal Flow], so the final nozzle design was a compromise based around the formula given by Internal Flow by *D.S.Miller*. The inlet internal and external diameters were considered fixed due to the need for it to be compatible with the pipe leading from the pumps. However, the exit diameter was reduced a little from the optimum to a value of 10mm. It was also required that the radius given for the section be increased a little if the nozzle was to be of the required length. Finally, to obtain a recognisable nozzle shape and to obtain compatible dimensions, the final exit angle was decreased to 25° . However, these modifications were necessary to produce a convergent nozzle of a shape capable of performing the task required.

This “compromise” nozzle incorporates a small flange around the circumference of the nozzle, to prevent the tube from sliding too far up the nozzle once attached. This flange develops into a larger flange on one side, which will allow the nozzle to be attached easily.

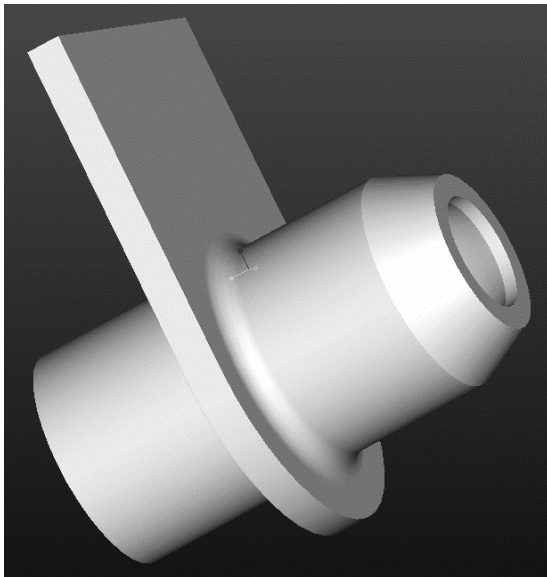


Figure 52 - Final Nozzle

Ideally, this nozzle should be fully machined, which would require the use of CNC machines. However, due to lack of time and severe monetary constraints, the nozzle section itself was hand turned. The flange was added as a separate part by attaching with a $\frac{1}{4}$ ” weld around the top surface of the flange. This position for the weld

prevented any interference when attaching the nozzle to the ROV frame. Assurances were given that the presence of a weld would not deform the nozzle section sufficiently to disrupt flow through it. The method of production used here allowed the piece to be accurately machined in as short a time as possible and at as low a cost as possible.

The theoretical total cost of producing the nozzles was £98. This consisted of material costs and labour costs. With the constraints on the ROV budget, had the offer not come from Penske Cars Ltd to manufacture the nozzles for free, the likely solution would have been to produce the simple nozzles as discussed earlier. As the simple nozzles would require little expertise, members of the group may have been able to produce them. However, using the skills provided by Penske Cars, it was now possible to obtain the more complex and idealised design.

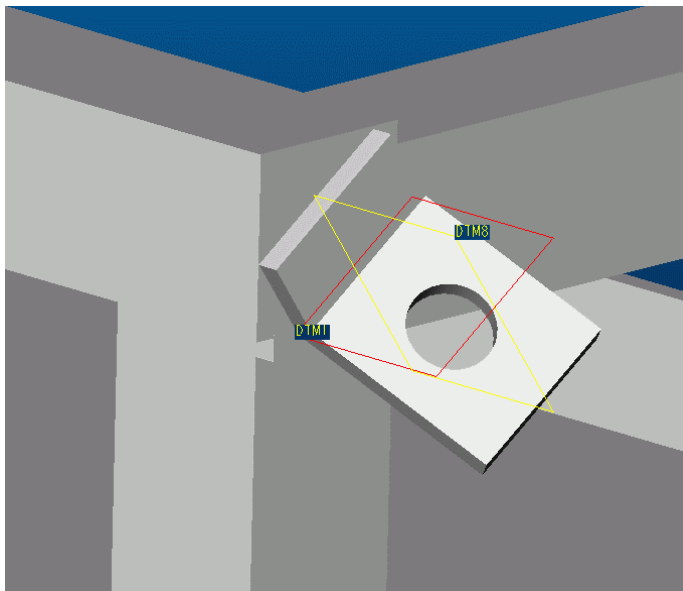


Figure 53 - Initial design of nozzle attachment tab

To attach this nozzle, the initial idea was to have a bent tab of metal, of which one side could be attached to the ROV frame, leaving the other side to project out and form a flange that the nozzle could be attached. Firstly, the plan was to insert the nozzle through a hole in this tab and secure it by its integral flange. Then, due to the need for greater space behind the nozzle, this meant that the nozzle would have to be mounted onto the end of the tab by the nozzle flange. However, eventually, it became apparent that this would leave the exit of the nozzle significantly below the surface of the shell once the frame had been inserted into the proposed NACA section body. The positioning of the nozzles relied on the required angles and on the space available

between the frame and the shell. Therefore, some kind of spacer would be required between the tab and the nozzle flange.

From this, the first type of spacer investigated was a simple block with relevant holes drilled through it, to allow it to be bolted between the two flanges. However, due to the requirement to keep the mass of the ROV to a minimum, a solid spacer fixed on each of the 8 tabs would prove too heavy. Therefore, the spacer concept was developed to be a small length of c-section aluminium extrusion that could be attached between the two flanges. For further clarification of the final design of the nozzle attachment, see Appendix T – 3Dmodelling.

When considering the initial ideas for nozzle attachment, methods of joining the parts were looked at. The tab could be attached to the frame by bolting, welding, or by using epoxy. However, it was decided early on that using bolts would be the best option. By using two bolts as the method of attachment, it would prevent the tab from pivoting as it would if only one bolt was used. This method of attachment could also be used to secure the tab and the nozzle flange either to each other or to the spacer.

The tab could be attached to the frame by bolting, welding, or by using epoxy. However, it was decided that using bolts would be the best option. By using two bolts as the method of attachment, it would prevent the tab from pivoting as it would if only one bolt were used. This method of attachment was also used to secure the spacer to the tab and the nozzle flange to the spacer.

16.12 Recommendations for Nozzle Design

Due to the need to compromise with the dimensions of the nozzle design, the nozzle used on the ROV is not ideal. However, it performs adequately. To improve the performance of the nozzles, a more efficient, ideal design formula would need to be followed precisely, without the use of compromise. Nevertheless, there is still a limit to how much the thrust can be optimised through nozzle design alone.

The main criterion for improving thrust from the nozzles is a need for dramatically improved pumps. There were a very limited number of suppliers producing pumps that could meet any of the desired specifications, even using the pumps in parallel is not ideal. However, on contacting various companies, including Pentair Pumps Ltd, they were unaware of any companies currently producing a pump suitable for our application, or producing a pump that could be easily modified for the purpose.

According to Pentair Pumps Ltd, the development of a small pump capable of producing at least 5N of thrust, in a unit of about 8” maximum length, with a width or diameter of about 2”, would cost between \$10,000 and \$75,000. This is clearly well outside the budget of this project and could, therefore be the subject of future research.

17 Initial Design Performance

The dimensions of the design were initially estimated to be similar to existing ROV's in its class (observation and recreation) and similar in size to previous ROV group design project dimensions. The dimensions being either a box shape: length 60cm, width 30cm, depth 21cm, or a secondary estimate using cylindrical shape with hydrodynamic end cones: length 57cm diameter = 20cm. The actual particulars depend on power and thrust requirements. The initial ROV manoeuvring velocities decided in x, y, and z-planes are $V_x = 0.5\text{m/s}$ and $V_y = V_z = 0.3\text{m/s}$. With the design speed decided upon, the ROV dimensions can be estimated and the drag and thrust requirement of the ROV can be calculated. The performance of the System will also depend on ROV mass. The heavier the tether, ROV and overall system, then due to Newton's 2nd law: $F = \frac{\partial mv}{\partial t}$ or ($F = ma$), the slower the acceleration (or deceleration) will be. The acceleration will be estimated when the overall system mass has been concluded.

18 Initial Drag Estimate

18.1 Thrust requirements.

At the design speed, using Newton's 3rd law, in equilibrium Thrust = Drag. Hence, the thrust requirement for the design speed, given the dimensions of the ROV can be estimated from the equation:

$$D_{ROV} = \frac{1}{2} \rho A V^2 C_{D0}$$

The initial drag coefficient used is 0.31, this is the coefficient calculated from the previous GDP towing tank tests. It should be worth noting that the previous ROV drag coefficient is not as low as it could be if fairing was added around its mid body, and protrusions were kept to a minimum.

If one also takes into account the tether for control and power then, the total drag of the "system" = Drag_{ROV} + Drag_{TETHER}.

18.2 ROV Drag:

Nomenclature

V = Velocity (m/s)

A = Frontal area (m²)

C_D = Drag coefficient of ROV

ρ = Density of standard seawater = 1025 kg/m³

U = Velocity past "pipe" (m/s)

Φ = Tether diameter (m)

A' = Area = Φ*height (m²)

C_{D'} = 0.35 for circular pipe

$$D_{ROV} = \frac{1}{2} \rho A V^2 C_D$$

Equation 15

18.3 Tether Drag

Total Tether drag depends upon the position of the ROV from its origin, and the curvature and path of the tether. An angle of attack of the tether to the free stream flow will change its drag characteristics. In addition, the velocity of the tether may vary with distance from the ROV and the direction with which it is travelling. When on an arc, or circular turn the tether closest to the ROV will be travelling faster than that close to the centre of the turn. The affect of tether weight on total drag is considered negligible, as the tether is assumed to be neutrally buoyant.

As a first approximation for tether drag, not taking into account the angle of incidence, such that the tether is horizontally approximated as a circular cylinder parallel to the flow.

Per unit length horizontally the tether drag is calculated using:

$$D_{T(x)} = \frac{1}{2} \rho \Phi U |U| C_D$$

For the operating speed requirements and using the 3-dimensional drag coefficient C_D from the previous project with a margin of 12% error increase (0.347), calculations are made for variable diameter, drag coefficient and tether length as a circular section ROV to investigate the affect on ROV system drag. Sample calculation of forces required and the initial calculations can be seen in Appendix M.

It is to be noted that ROV drag is small when compared to Tether drag. And for maximum tether the ROV drag should be made as small as possible, and the diameter of the cable reduced to a minimum requirement.

19 Detailed research into components of tether drag

As mentioned previously the estimate of the tether drag is affected by the angle of attack to the free stream. From section 3-11 in Fluid-Dynamic Drag, an empirical fit to experimental data for drag coefficient with varying angles of attack for wires and cylinders is given. By approximating the tether as a cylindrical pipe section, diameter d and length l , inclined at an angle α to the flow at a Reynolds number (Rn) below critical Rn , the following empirical formulae for drag coefficient and lift coefficient can be used.

$$C_D = 1.1 \sin^3 \alpha + 0.02$$

$$C_L = 1.1 \sin^3 \alpha \cos \alpha$$

Although it states for sub critical Reynolds number the experimental data from the reference source: Bursnall and Loftin, - *Pressure Distribution on Yawed circular cylinder in the critical Reynolds number range NACA T. Note 2463 (1951)* indicates that the data can be applied for near critical Rn , hence should be applicable in this case. Figure 54 below shows the geometry for calculation of coefficients.

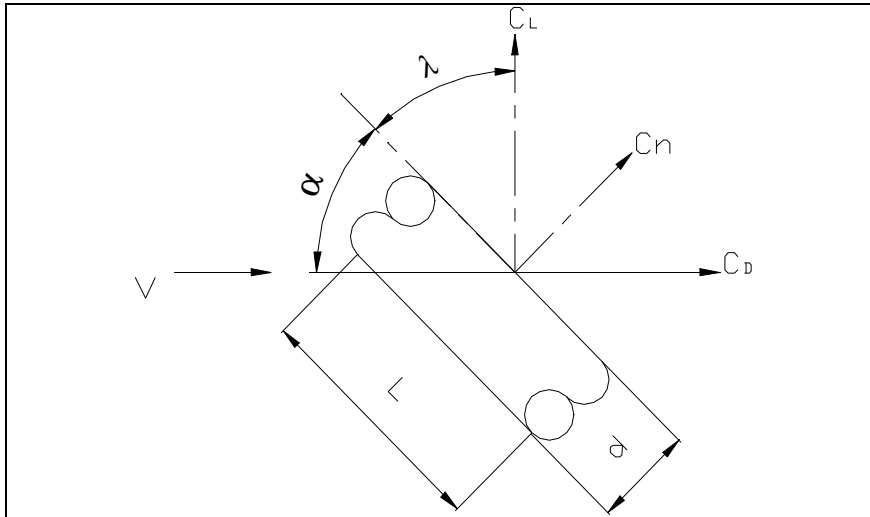
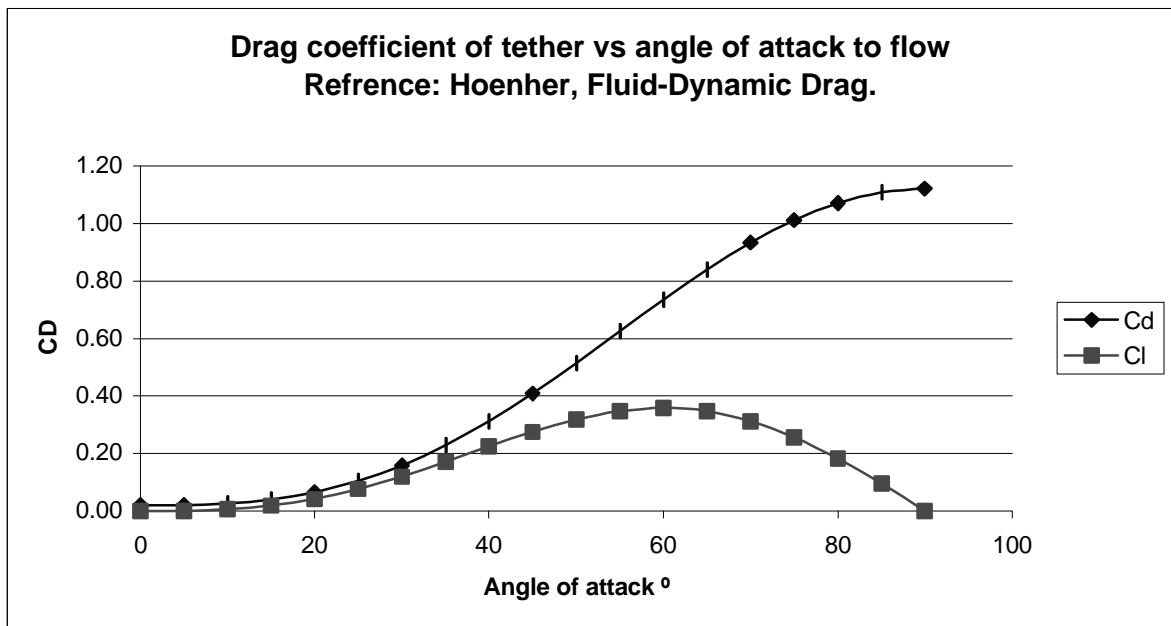


Figure 54 - Tether geometry

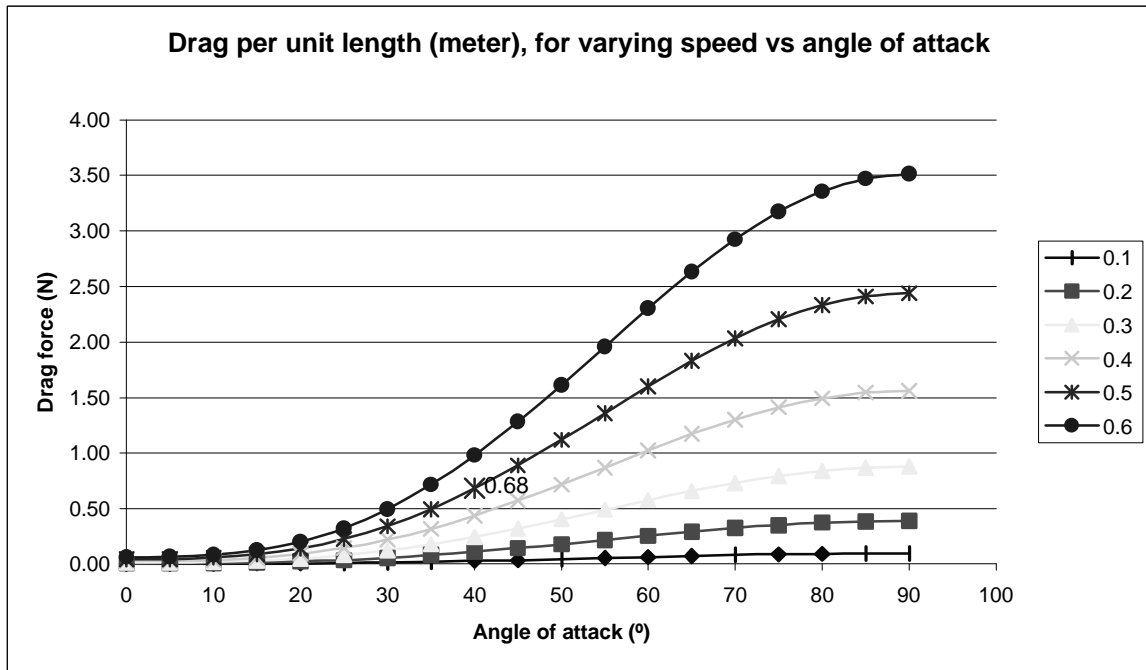
Graph 1 below shows the lines for the two previous expressions for coefficients, and the variation of C_D and C_L with α seen.



Graph 1 ~ Tether Drag coefficient vs. angle of attack

It can be seen that drag coefficient, hence drag increases with angle of attack. From the expression for drag coefficient the drag per unit length of tether can be calculated using the following equation: $D = C_D \times 0.5 \rho A V^2$ Where A is the reference area (lxd)

The sponsor supplies a neutrally buoyant tether. It has a diameter of 17mm (0.017m). The drag per unit length of tether is calculated and this data is represented in Graph 2 below. A full table of data for drag over varying angles of attack and speed can be seen in Appendix N.



Graph 2 - Tether Drag per unit length

For the operating condition of 0.5m/s it is assumed that the tether will not be at an angle of attack greater than 40°, hence the maximum drag per unit length as shown above, is taken as 0.68N 2d.p. This assumption is not unreasonable, as most commercial ROVs make use of a tether management system that consists of a cage of cable lowered to the same working depth as the ROV and then a further coil of tether within the cage that extends with the ROV motion. The use of a tether management system would also give the ROV a much greater operating depth, up to the point at which the control boxes would no longer withstand the pressure. This could be calculated for specifically rated boxes, bearing in mind the modifications for the connectors and camera window.

20 Performance of bare hull form

Due to the low thrust obtained from the water jet propulsion and the increased size of the propulsion system it is required that the ROV be efficient through the water. Due to the low thrust available the hydrodynamics of the ROV are paramount, and it requires a low drag coefficient. Detailed investigation of the affects of fairing on the hydrodynamics of the ROV is required.

21 Effect of fairing on the hydrodynamic performance of a body immersed in a fluid

A more conventional observation class ROV generally has little or no fairing, has a bluff body design for greater positional control. These have little need for fairing since they have much more powerful thrusters than through this design, using water jets.

Due to the lack of very powerful thrusters and the requirement to have a useful amount of tether, then the ROV needs to be optimised for minimal resistance.

In one source of research it was stated that:

"Fairing may reduce the ability to hold position but an elongated after body may reduce C_D due to improved after body flow. C_D can be reduced by a factor of 3 for L/D ratios up to 1/2. Rounding of corners can lead to a reduction of resistance/drag by 5-10% and also reduce the C_D by 20-25%." Source: Research and Development in ROV Hydrodynamics, Sayer P, ISOPE 1993 conference proceedings.

Different shaped bodies have different hydrodynamic characteristics and some have less drag than others for the same projected area. Much research into the different shapes, and the drag of different bodies has been carried out.

21.1 Factors affecting the drag of a body

There drag of a body is dependent upon the cross sectional area of the body moving through a particular fluid, the flow regime that the body is in, the body shape and fairing and the speed at which it is moving. For the flow regime there are four main factors that drag depends upon

- Whether the body is operating in lamina or turbulent flow
- Transition of flow from lamina to turbulent flow
- Whether the flow is attached or separated from the body
- The Reynolds number of operation.

There is a transition region, which is relatively short, when the flow changes from wholly lamina to turbulent. When this occurs there lays a very thin viscous sub layer beneath the turbulent regime where flow is basically lamina. As a result the turbulent

layer has a greater velocity gradient close to the surface and this increases the shear stress and hence the skin friction.

At transition the boundary layer increases in size dramatically. This is shown below in Figure 55.

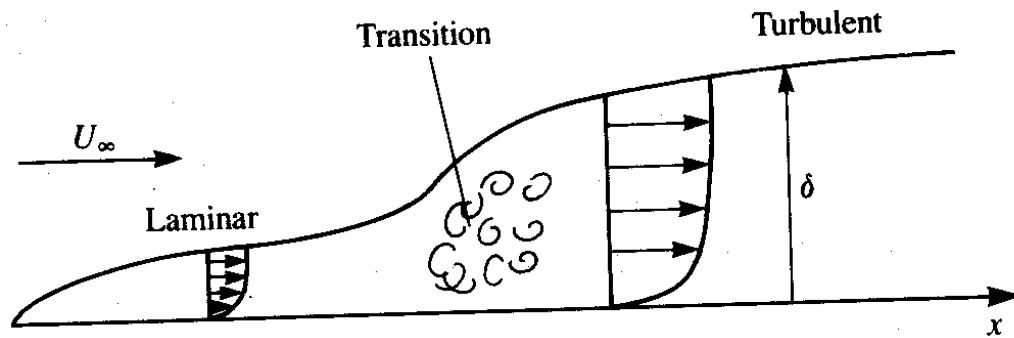


Figure 55 ~ Laminar-turbulent transition

The point at which the lamina flow becomes unstable depends on a number of factors. Roughness of the surface hastens the transition to turbulent flow, as does the intensity of the turbulence of the free stream. The predominant factor however, is the Reynolds number of the flow in the boundary layer. This is usually represented as:

$Re_x = u_\infty x / \nu$ Where u_∞ represents the far field fluid velocity, ν the kinematic viscosity of the fluid, and x , the distance from the leading edge (where the boundary layer starts). When the Rn is in the range of 3×10^5 to 5×10^5 flow normally transitions.

Essentially, separation is when the fluid flow no longer follows the contour of the body. It occurs when there is an adverse positive pressure gradient (opposing flow) and $(\partial u / \partial y)_{y=0}$ becomes zero such that the flow close to the surface of the body tends to zero and is then reversed further along the body, and can no longer follow the contour and separates.

Separation occurs in both laminar and turbulent boundary layers, for the same reason, but laminar flow is much more prone to separate. This is because the in a laminar layer the velocity gradient is much shallower, and the adverse pressure gradient can more readily halt the slow moving fluid close to the surface, a turbulent boundary layer can survive separation for some distance before separating. For any surface, the larger the adverse pressure gradient the sooner separation occurs. Separation radically modifies the flow pattern, causing large scale eddies downstream called wake.

The formation of wake means that the downstream pressure is reduced, and thus the pressure form drag of the body is increase. The magnitude of the pressure drag depends largely upon the size of the wake, which in turn depends on the location of the point of separation. If the separation occurs only to the far rear of the body and the wake is small then the pressure drag is also small, and the drag is made up of mainly skin friction drag. Such a body is a streamlined body, as the flow follows the streamline contours of the body. For a bluff body the flow is usually separated over much of the body, the wake is large and the pressure drag is larger than the skin friction drag.

The total drag is of most interest in this case and is non-dimensionalised with respect to the dynamic pressure of the undisturbed flow, $(1/2\rho u_{\infty}^2 A)$. The non-dimensional coefficient of drag C_D is independent of body size, but not shape.

For low values of free stream velocity the boundary layer is wholly lamina until it separates, but as the free stream velocity increases the transition point becomes closer to the leading edge than the separation point, and the layer becomes turbulent. The separation position then moves further downstream, the wake becomes narrower and the drag coefficient less.

For a body to have a low drag it needs to be in a wholly attached flow, be it laminar or turbulent. For no separation it need be a streamlined body.

21.2 Calculation of ROV Reynolds number

At the forward design operation speed the Re is calculated, with respect to a nominal (or maximum length of the ROV as 1m):

$$Re = \frac{VL}{\nu} \text{ Where } V = \text{Velocity, } L = \text{Reference Length, } \nu = \text{Kinematic Viscosity}$$

$$Re_{x=1m} = 0.5\text{m/s} \times 1\text{m} / 1.19 \times 10^{-6} = 4.2 \times 10^5.$$

Ref Length m	Velocity m/s	Rn calculated
1.00	0.1	8.40E+04
1.00	0.2	1.68E+05
1.00	0.3	2.52E+05

1.00	0.4	3.36E+05
1.00	0.5	4.20E+05
1.00	0.6	5.04E+05
1.00	0.7	5.88E+05
1.00	0.8	6.72E+05
1.00	0.9	7.56E+05
1.00	1	8.40E+05

Table 6 - Calculated Reynolds number of ROV for varying speed

It is clear that the R_n is in the critical R_n range for operating speeds up to 0.6m/s and thus transition could occur, given that the flow may well be disturbed it may be assumed that the flow will be turbulent.

With turbulent flow it is important to keep the flow attached for as long as possible to keep the drag to a minimum. Keeping the flow attached, and finding where it separates can be quite involved.

To work out the most efficient shape of hull for the ROV many hull shapes may be considered.

21.3 Optimisation for least drag

The ROV is to be optimised for bi-directional, forward and backward motion, with lateral motions considered secondarily, whilst still remaining of importance.

Certain parameters of the design are fixed, such as the volume required to fit the internal structure, and supporting buoyancy. Others can be controlled such as surface roughness of the external shell. However, the R_n at the operation speed cannot be altered to a great extent. In the assumed turbulent flow separation may still occur, and almost always does. In order to suppress separation it is necessary to avoid or reduce any adverse pressure gradient, and keep the flow as streamlined as possible. To achieve this a streamlined body is required.

The shape of such a body can be varied quite drastically, from very long thin teardrops with low curvature, to short stubby cylinders with high curvature. From Fluid Dynamic Drag, 1965), the affect of fairing on circular cylinders can be easily

seen. In This reference, Figure 50 shows the influence of various fairings on drag of circular cylinder, at R_n above transition i.e. turbulent. The reference source shows how the drag coefficient of the body is significantly reduced when faired. Figure 51 from the reference source also gives details of sleeved fairings. As a rough estimate of drag coefficient one would expect that for a sleeve like fairing, similar to a NACA section (see next section) the drag coefficient would be from 8-20%. Experimental and computational tests will be used to assess this.

To fit the required volume, a very low curvature streamlined body will be longer than that of a higher curvature body, hence the skin friction drag will be increased, whilst the pressure/form drag is reduced.

In this optimisation a family of streamlined curves will be investigated and the results commented upon.

NACA Four-digit section designs

From the Theory of wing sections, the thickness distribution along the chord can be calculated using the following equation:

$$\pm y_t = \frac{t}{0.2} \left(0.29690\sqrt{x} - 0.12600x - 0.35160x^2 + 0.28430x^3 - 0.10150x^4 \right)$$

Equation 16

The leading edge radius is expressed as:

$$r_l = 1.1019t^2$$

Equation 17

The digits represent the camber and the thickness chord ration, for symmetric sections about the chord, there is no camber and the first two digits are represent the location of maximum thickness, 00 represents mid chord. The second two digits represent the thickness chord ratio, for a chord of 160 and thickness 32 then the $t/c = 0.20$, that is 20%

Using Equation 16, a series of sections could be drawn up. These sections are aerofoil shaped. An example of such a foil is a Figure 56 below:

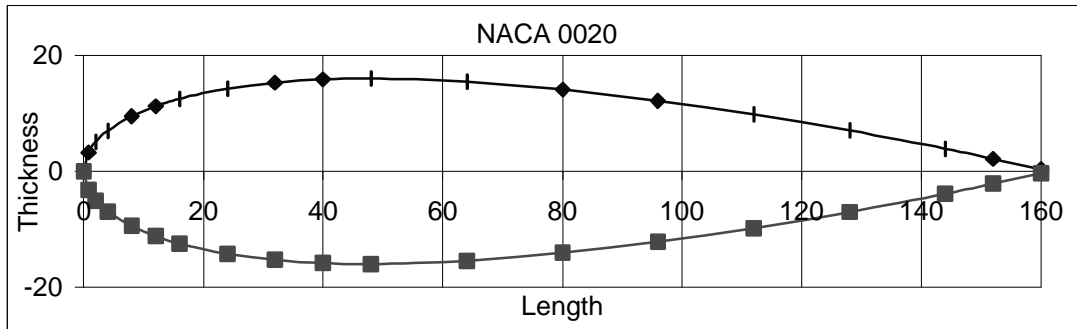


Figure 56 - NACA0020 section

Initially the geometry of the ROV was to be that of a revolved NACA section, resembling a teardrop, for minimal drag. This was not pursued, as the size of the ROV would be far greater in length than required due to the tail. This shape would also lead to some interesting force balancing and movement control systems, as the shape is not symmetric fore and aft. Also as the ROV is designed to be bi-directional it is required to have equal performance characteristics in both directions.

To generate accurate, fair sections, which are symmetric fore and aft, the NACA thickness distribution was used. Offsets are calculated up to the point of maximum thickness, and then it was reflected about this point to give a symmetric shape for and aft. **Error! Reference source not found.** below shows the mirrored section with some parallel mid body added.

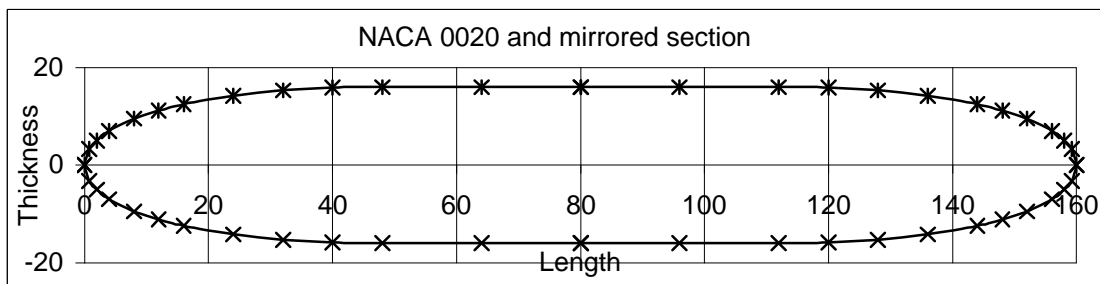


Figure 57 - Mirrored NACA0020 section with some parallel mid body

22 Estimation Of Drag Coefficient Of Modified NACA Sections

22.1 Computational methods available

There are a few different computational methods for assessing fluid-body interactions such as drag and lift. These vary in complexity and accuracy, generally the more complex the more accurate, but the more user-intensive and complicated to use.

One such programme is CFX, a computational fluid dynamics package. Although more accurate solving for full Navier-Stokes viscous flows, this program however is quite complicated to set up and get reliable results without spending a long period of time on a problem. To generate a collection of data for multiple problems would take a very large amount of time indeed, especially with limited knowledge of the program.

A more user-friendly solution is sought in the way of a linear 3D surface panel method to solve for invicid potential fluid flow over a body relatively quickly with useful results.

The key to any computational method is to know the limitations of the package being used.

22.2 Use Of Panel Methods

An estimate of the drag, and the coefficient of drag for the body of revolution can be made using a panel code, namely PALISUPAN, which is a PARallel LIFTing SURface PANel code.

The use of a panel code allows the drag of different bodies of revolution can be calculated, and their respective drag coefficient, with respect to frontal area, calculated also. This therefore means that the body of revolution with the lowest C_D will represent the most efficient shape for a speed tested.

The panel code uses potential flow to solve for lifting surfaces at an angle of attack to a fluid flow, however, the pressure form drag and required (C_D) is zero at zero angle of incidence (due to potential flow). In reality this is not the case, and the panel code makes an estimate of the pressure form drag, which for a lifting body is a good approximation. However in this case where the body is at zero angle of attack, and a more accurate estimate of the drag is required then a coupled method for solving the pressure drag at zero angle of incidence is required.

22.3 Coupled Boundary Layer And Potential Flow Panel Codes

The coupled codes are the panel code PALISUPAN and a boundary layer program SUBBL. The program SUBGEN is used to combine the two codes in an iterative loop.

SUBBL was developed in a PhD thesis by written by Thibaut Jacquet-Lagrece, and has been modified to suit a single body of revolution, as in the case of a revolved section. This program solves the boundary layer of submarines, it reads the streamline data from a file .bli (boundary layer information produced by Palisupan) and outputs a source file (.00) that can be used by Palisupan. This program also outputs files with the skin friction coefficient and evaluates the total drag due to the skin friction.

Palisupan takes the .bli file and solves the flow, along each streamline of the boundary layer (the boundary layer being calculated from subbl), to solve the pressure form drag.

The two programs then iterate until the forces calculated are within a tolerance level which can be specified (1%).

22.4 Geometry Definition

The geometry needs to be defined and set up in a specific manner so that the panel code will understand and function. SUBGEO is the program that generates a geometry file for Palisupan (.pan file) by reading the description of the transverse of a submarine from a file with the section data, and outputting the geometry file. Christos Pashias, from Part III Ship Science wrote the program as part of a 3rd year dissertation.

By using the geometry definition programme it is possible to generate a large number of geometry files from section offsets derived from the NACA equation given previously.

22.5 Previous work

Researchers at Massachusetts Institute of Technology (MIT), USA have successfully attempted the interactive use of panel codes and boundary layer solvers, but this code was not accessible. The boundary layer programme in the ship science department is still in the beta testing stages of design, but the turbulent section of the boundary layer interaction has been used and seems to give encouraging and good results.

22.6 Wind Tunnel Validation Of Computational Panel Technique

To check to see if the results yielded from the interactive codes are worth using, it is necessary to validate them with experimental data. This is done using data from a PhD thesis.

The PhD thesis is that of K. Putama. In the PhD wind tunnel tests on a 3D ellipsoid of revolution are made and the drag recorded. The drag coefficient of the ellipsoid is calculated at 40m/s, as is the Reynolds number (Rn).

The drag at 40.3m/s is 2.367N, the frontal area being 0.3m²

The Drag coefficient calculated:

$$C_D = 2.367 / (0.5 \times 1.2 \times 0.3 \times 40.3^2) = 0.0809$$

A geometrically similar body of revolution's geometry is created and set up to be run in the panel interaction programme; subgen. A Naca0020 mirrored and revolved as detailed previously is used.

The Reynolds number of the wind tunnel tests at 40m/s in air, for a 1.2m length body is calculated as:

$$Re = \frac{\rho V L}{\mu} \text{ Where } \rho = \text{density of fluid, } \mu \text{ Dynamic viscosity; noting that } \frac{\rho}{\mu} = \mathbf{u}$$

$$Rn = 1.2 \times 40 \times 1.2 / 1.825 \times 10^{-5} = 3.156 \times 10^6$$

From this the test velocity for equivalent Rn in salt water, $\rho=1025\text{kg/m}^3$ is calculated.

$$V = \frac{1578 \times 10^6 \times \mathbf{u}}{l} = \frac{1578 \times 10^6 \times 1.19 \times 10^{-6}}{0.66} = 4.96 \text{m/s}$$

Fortunately this test speed is large enough for turbulent flow transition to have occurred, and the use of the panel code interaction.

The panel code drag is found to be 8.79N for the 1/4 body, at a panel ratio of Nt=120, Ns=13, with a cross sectional area of 0.031. The total drag coefficient is calculated from the panel code as:

$$C_D = (4 \times 8.79) / 0.5 \times 1025 \times 0.031 \times 4.96^2 = 0.08995 \sim 0.09$$

From inspection it can be seen that the values are very close indeed. The actual difference is 10% and thus the panel code does yield a close approximation to experimental data.

22.7 Choice Of Shape Due To Time Restrictions

Due to timescale limitations, it is necessary to make a decision unto the shape of the hull of the ROV, before optimisation-testing process could be completed.

Of the possible geometries the shape chosen was a streamlined NACA0023 section, mirrored about the Y-axis at 450mm from the leading edge with a maximum diameter of 310mm and a portion of parallel mid-body, which would then be revolved about its longitudinal X-axis.

The section is moderately slender with relatively low curvature compared to shorter alternatives. Due to the internal structure dimensions, and the required minimum diameter of the ROV, a more slender shape than the NACA0023 would mean a much greater length (greater than 1m), which is not desirable.

It is expected that the flow will separate at or just after the start of the rear shoulder of fairing where the hull tapers inwards. The amount of separation will depend upon the curvature. The more blunt the shape the earlier separation is expected, and the greater the pressure form drag. It is assumed that the pressure drag will have a large contribution to the drag and possibly dominate over the skin friction drag. Hence a slender shape is desired.

This section is chosen as a compromise between that of a longer more slender shape which may have less total pressure form drag, with greater lateral resistance, and lower all round manoeuvrability, and one that would be shorter, with higher curvature streamlines (hence greater adverse pressure gradient affect), with higher pressure form, and total drag, whilst having more uniform manoeuvrability in all degrees of freedom.

The profile area of each NACA section is found and the NACA 0023 has one of the lower profile areas, this means that the penalty of loss of some lateral manoeuvrability is reduced.

22.8 Variables defined for the programs

The programs used require the nose-tip radius, which is calculated from the expression given from the NACA series data. For all sections tested the nose-tip radius is 0.10m.

The program will also allow the separation point to be defined, but it is not specified and as such the program calculated it. The transition Reynolds number is also specified in the program and is set in the order of 5.0×10^4

Note that this is the local Reynolds number based on the velocity of flow at that point, a distance s from the leading edge.

The transition Reynolds number is less than the maximum local Reynolds number. This means that the sections are being tested a theoretically almost fully transitioned turbulent flow, regardless of real life fluid flow.

The program will calculate the transition node and a text file will allow one to check its value.

22.9 Limitations of the programme

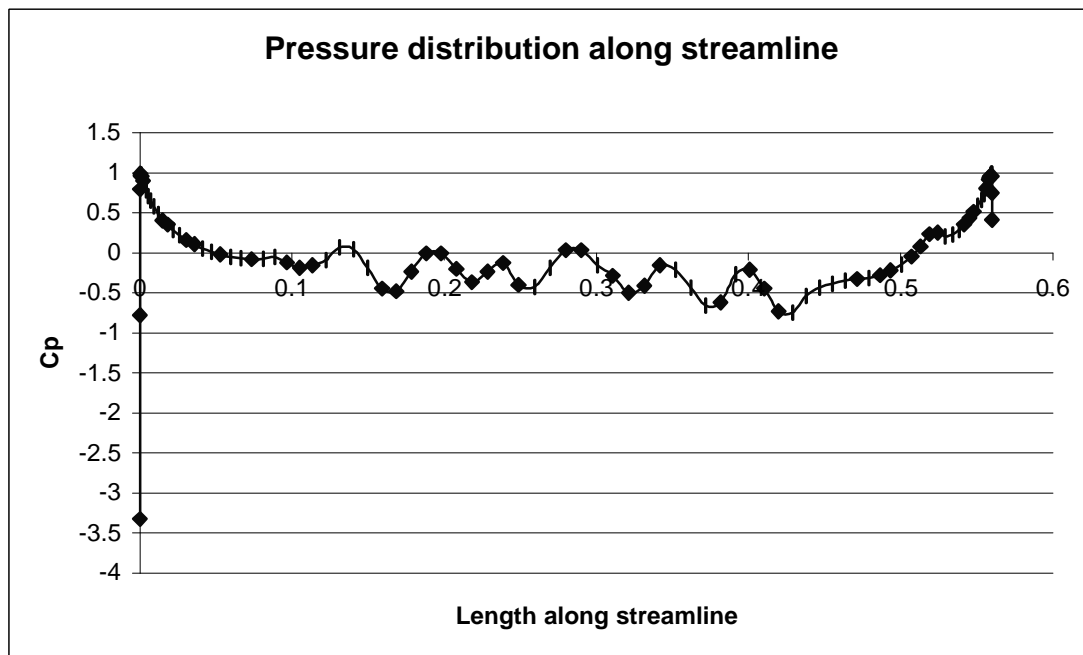
The program subbl considers that the flow can separate. After the separation, only an approximation can be obtained for the boundary layer and the skin friction coefficients. An approximation that the source strength correction is only set to the value before the separation is used in the programme.

The affect of this assumption will vary depending upon the position of the separation, as described earlier, and if the flow is laminar or turbulent and when the flow separates. If for example the flow was to separate at the first shoulder of the body then using the assumption would over estimate the skin friction due to shear, and the result may well be invalid. However, as it is expected that the flow will separate after the second shoulder (at the rear of the body) then the assumption will not greatly affect the overall result and as such will yield a good approximation.

The program also allows for separation at the tip of the body and for almost immediate reattachment, which is as good as that is what happens to the flow.

At the present time of testing the laminar section of the code is not working correctly The models can not be run at low speeds, equivalent to the operating speeds, if the

model is in a range of R_n where there is a transitioning boundary layer. This is because the code uses two different methods for solving laminar and turbulent flow, namely Thwaites and Head. When the flow starts to transition the code switches equations. Because the boundary layer changes in size and properties, the force values start to oscillate and the solution when iterated would not converge. A good example of this can be seen in Graph 3 below. In this test the body was running at 2m/s with a sinusoidal clustering at the ends of panels, distributed as of $100(N_t) \times 6(N_s)$.



Graph 3 - Pressure distribution at low speed / transition

As such at low speed (in the ROV operating range) where the body is in the transition of laminar-turbulent flow, the code did not function as desired.

It is also seen that using the sinusoidal distribution means that the C_p is not 1 or close to 1 at the extremes of the body, in the free stream, which is obviously not correct. As such an even distribution of panels, rather than clustering was used in test cases, which yields the correct result for C_p close to 1 at the free stream.

Due to the sensitivity to flow speed the body was run at a higher speed than actual operation, in a fully turbulent regime, which may or may not be the actual case. Verification is made by tank testing the final ROV shape. This issue renders any optimisation as dubious as the body is operating in transitional flow, which is difficult to model computationally without a more involved 3D viscous flow solver.

A more complex computational solution using CFX was not attempted, as there was insufficient time to carry out single, or multiple body optimisation problems

22.10 Families of geometries tested

After the internal structure had been designed it was possible to generate geometries based upon the maximum diagonal distance of the end of the structure, which was a square face 180mm x 180mm. By simple trigonometry this gives a minimum diameter of the ROV shell of 255mm. If one then includes a shell thickness of 6mm (12mm total) then the minimum shell diameter is 267mm. However, due to the size of the watertight electrical connector being used and the amount of usable space available, and an allowance for syntactic buoyancy foam the actual minimum diameter is close to 300mm. The final diameter with a margin of 10mm for a variable/different shell thickness is 310mm.

With the diameter of the ROV set a group of NACA sections is created to fit around the internal structure with as small amount of clearance of the vertices of the structure from the internal diameter of the shell.

The sections designed are as follows: NACA 0016, NACA 0020, NACA 0023, NACA 0025, NACA 0031, and NACA 0041. These can be seen in Appendix O.

The geometries of the revolved section were created using subgeo and the .pan files modified so that the distribution is set to 0, no clustering, and the flow speed is set to 4.96. The panel aspect ratio is also set in the geometry file. The aspect ratio used for all shapes is 120x15; this was determined from a sensitivity study of aspect ratio and panel distribution. The corresponding number of blocks, being $Ns-1 = 14$, which is divisible by 2, making the matrix quicker to solve than if it were an odd number of blocks.

The proportion of shape tested is a quarter section along the longitudinal (X) of the revolved body. This makes the solution in a 3D panel code possible, and quicker than for a half body, and more accurate as the panel aspect ratio is kept more constant.

A more accurate method would be to do smaller angles, but the quarter body is satisfactory. The resulting forces outputted thus need to be multiplied by four.

22.11 Sensitivity study for panel aspect ratio and minimum cp

The convergence test for C_p was not carried out for the minimum number of iterations for an insignificant change in force due to C_p . The minimum C_p was set at 0.001, which takes a moderate time to compute.

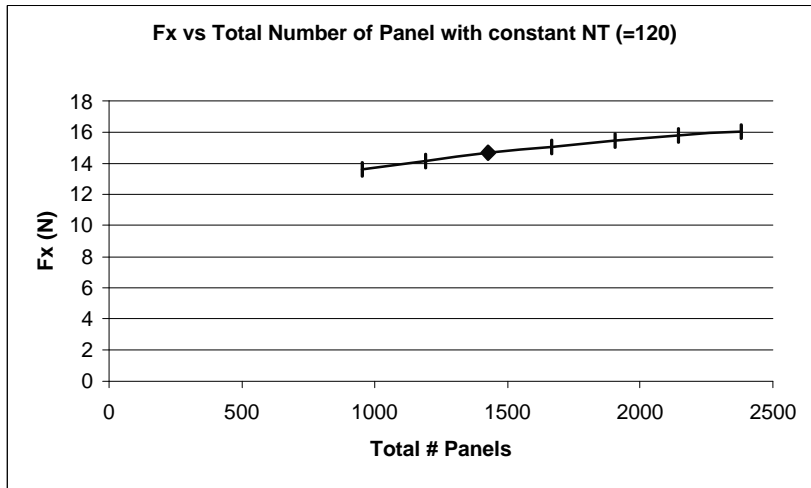
The number of panels, along the length (N_t) and around the radius (N_s) is changed such that panel aspect ratio gives even quadrilateral panels with a moderately constant aspect at the ends of the body. The increase in the number of panels increases the force computed, there would be a convergence if one were to carry on increasing the number of panels, giving rise to a more accurate result, although increasing the computational time.

When calculating, the maximum N_t for an N_s of 21 was 120, else the program did not have enough room for the matrix, hence could not continue, hence a maximum N_t was taken as 120. The Value of N_t was set to 120 and N_s varied and the results outputted for F_x for the NACA 0023 section shape.

NT	NS	(NT-1)(NS-1)	FX
120	9	952	13.61
120	11	1190	14.17
120	13	1428	14.66
120	15	1666	15.05
120	17	1904	15.46
120	19	2142	15.82
120	21	2380	16.05

Table 7 - Variation of N_s with constant N_t

Graph 4 below shows the total force on a quarter body slowly converging.



Graph 4 - Convergence of force for increased number of panels

The final choice of panel distribution, is 120x15, which when observed from the data exchange file in AutoCAD gives satisfactory quadrilateral panels at the ends, where the pressure change is more variable. If clustering had not given Cp errors then it would have been used and the number of panels could have been reduced.

Figure 58 below displays the panel distribution for the NACA 0023 section at 120x15 panels along one quarter (revolved four times).

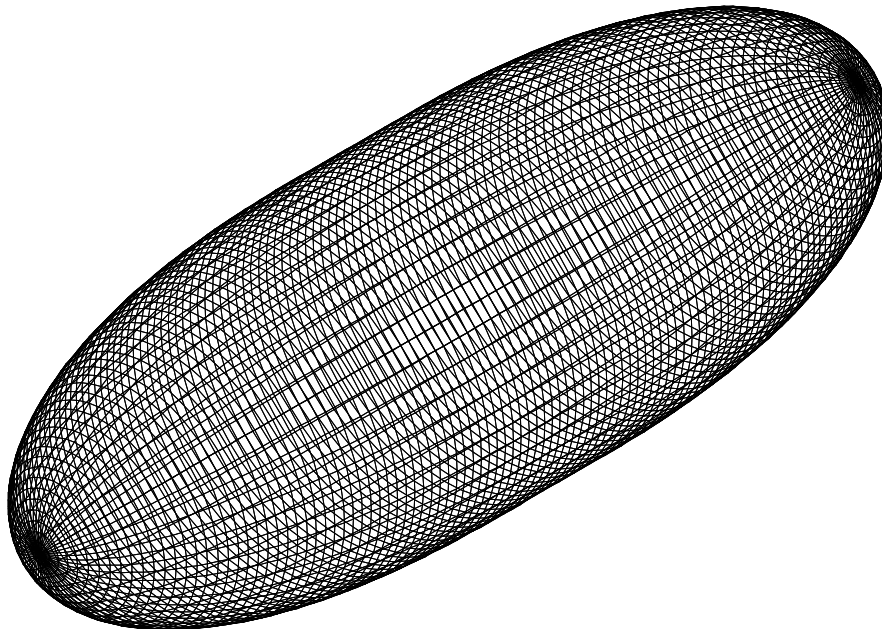


Figure 58 - Panel distribution 120x15

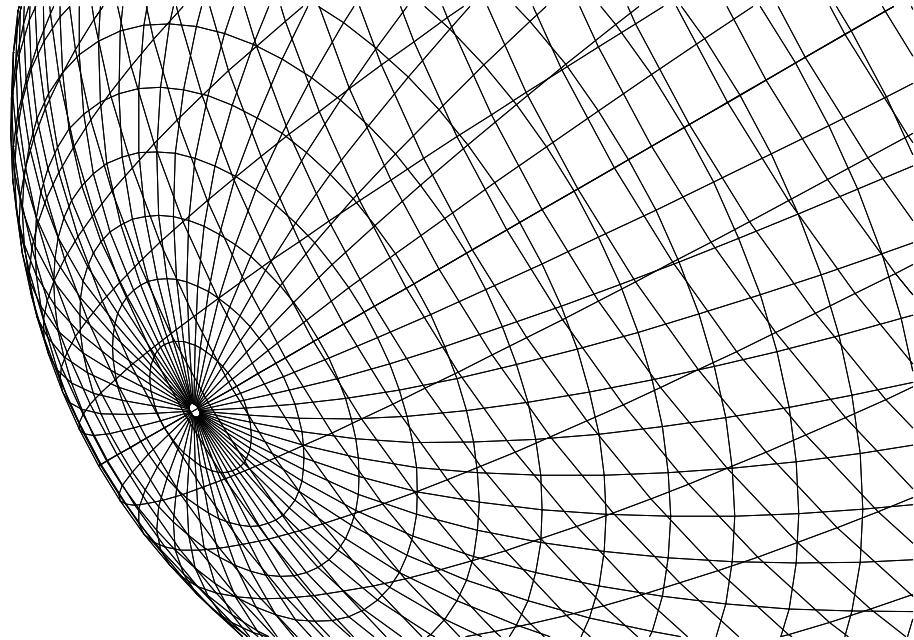


Figure 59 - Close up of Panel distribution at ends

The panels are well proportioned, except right up close to the end, unfortunately the limit on N_t meant that this is the best distribution possible without decreasing the number of radial panels, a computer with more memory might solve this problem. The panel distribution of all other sections tested is shown in Appendix P. The geometry files are included on the accompanying CDROM.

22.12 Outputs from the programme

A log file of the forces is outputted which also contains the pressure distribution along the hull form. An AVS compatible .inp file which gives the panel and pressure distributions along the quarter body of revolution. However, these cannot be shown in the report, as the file allocation could not be converted from the AVS to a postscript file for plotting or otherwise. The .inp files and the AVS network are included on the CDROM if one wishes to read these and view the 3D pressure distribution. The 2D representation taken from the C_p values in the log file show the pressure distribution and the graphs can be plotted with ease. As the body is axis-symmetric the pressure distribution along all streamlines is identical

The NACA 0023 log file, for one streamline up to the 118th panel can be seen in Appendix Q. All log files for tested sections are included on the CDROM.

22.13 Results

The results from the panel code are quite interesting. The first comment is that the revolved body is very efficient, with a low estimated drag coefficient in the range of 4% to 9%.

The body with the most streamlined shape (NACA 0016) has the greatest drag, hence greatest drag coefficient. This is because skin friction dominates drag, (this is found in the log file) and the reduction in length of the ROV for a given diameter and shape gives rise to a much greater reduction in drag than the shape does to pressure from drag.

By calculating the drag coefficient with respect to the length squared it can be seen in Graph 6 that the drag coefficient of a NACA 0016 over its length is less than that of the NACA 0020, 23, 25 and 31 but still greater than that of the NACA 0041.

As one might expect from fluid flow theory the results show that the more streamlined the body, then the longer the flow stays attached to the body.

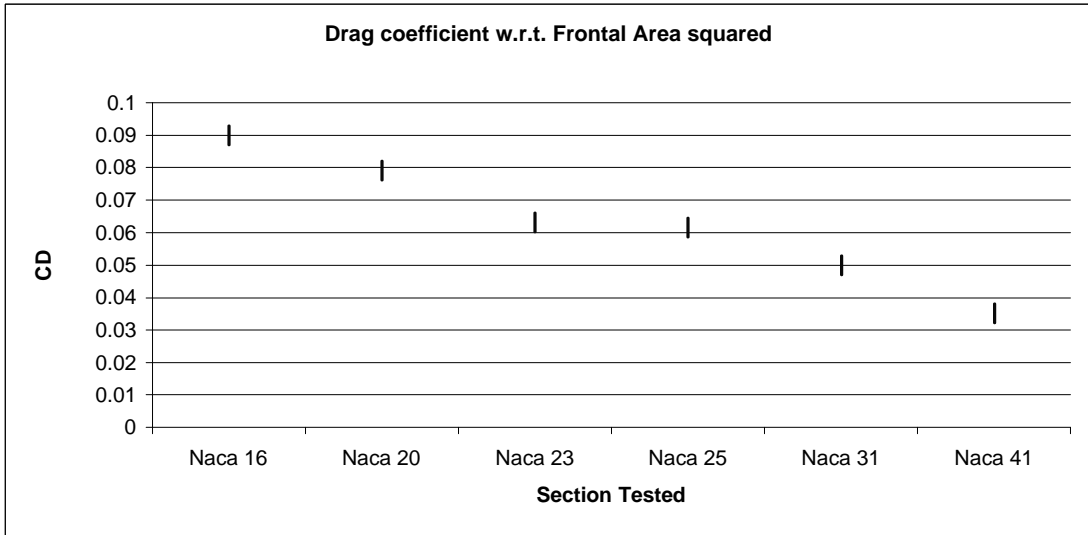
Graph 7 shows the percentage of length of attached flow along a streamline. This is also related to the pressure distribution along the streamline.

Section shape	Quarter body force		Length m	Length squared m ²	Velocity m/s
	Fx	Frontal area m ²			
NACA 0016	21.39	0.075476764	1.15	1.3225	4.96
NACA 0020	18.83	0.075476764	1.05	1.1025	4.96
NACA 0023	15.05	0.075476764	0.91	0.8281	4.96
NACA 0025	14.64	0.075476764	0.9	0.81	4.96
NACA 0031	11.87	0.075476764	0.82	0.6724	4.96
NACA 0041	8.35	0.075476764	0.75	0.5625	4.96

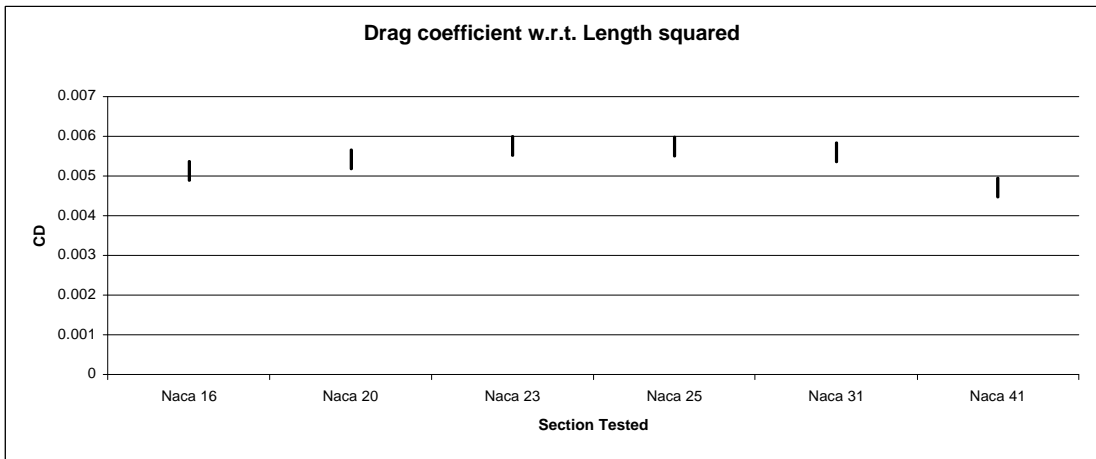
Section shape	Density of Fresh water kg/m ³	Total force (4 x Fx)	Drag coefficient (Frontal area m ²)	Drag coefficient (l ²)	
NACA 0020	1000	75.3307	0.0811	0.0056	
NACA 0023	1000	60.2038	0.0648	0.0059	
NACA 0025	1000	58.5597	0.0631	0.0059	
NACA 0031	1000	47.4849	0.0511	0.0057	
NACA 0041	1000	33.4034	0.0360	0.0048	

Section shape	Transition node	Transition point (laminar flow length) m	Length of Streamline m	Separation Point m	Attached flow length %
NACA 0020	3	0.026928	1.139891	1.121938	0.98
NACA 0023	3	0.024121	1.013069	0.972866	0.96
NACA 0025	-	-	-	-	-
NACA 0031	4	0.029875	0.941047	0.888765	0.94
NACA 0041	4	0.028274	0.890627	0.827010	0.93

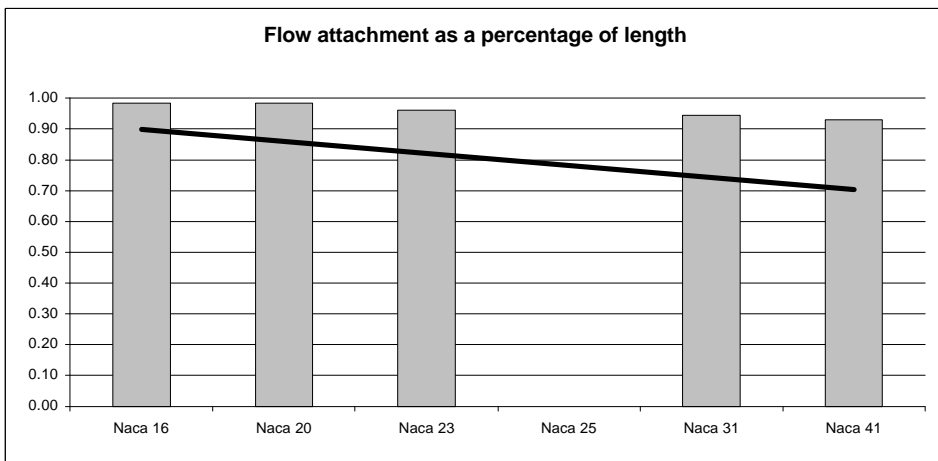
Table 8 - Panel Code Results



Graph 5 - Change in Total drag coefficient (C_{D0}) with section shape



Graph 6 - Drag coefficient by length squared



Graph 7 - Streamline flow before separation as a % of streamline length

A better, more comparative study would be if all the sections were the same length, encasing the same volume, rather than encasing the structure alone. However, with the structure previously designed the method is quite useful for optimisation.

22.14 Transition and Separation

From the output files the transition and separation of flow is obtained. The results show that there is a very short laminar section before the flow becomes turbulent and then stays turbulent and separates far down the body as expected.

22.15 Pressure and Velocity distribution

From the log files it is possible to graph the pressure distributions along the streamline. It is seen in Graphs 1a-6a in Appendix R that the peak suction pressure is higher for the NACA 0041 than for subsequent lower t/c ratios, and the NACA 0016 has less of a suction along the parallel mid body.

It is also seen that the peak pressures are at the shoulders as expected and that they coincide with maximum high velocity, close to the free stream.

The pressure distribution also gives a representation of the adverse pressure gradient affect upon flow velocity. If one looks at Graphs 1b-6b in Appendix R the change in pressure gradient matches the change in velocity.

The NACA 0016 streamline velocity is not accelerated to as great a degree as any other section. This also means that the section design will have less wave making in shallow water. The flow over the NACA 0041 is being accelerated much more than that over the NACA 0016 and it is also clear that the NACA 0041 is approaching the point at which the adverse pressure gradient will start to make a marked affect. It is also worth noting however that the NACA 0041 is a lot shorter, and if a similar section, with more parallel mid body were to be tested then the pressure and velocity gradients would most likely be less.

The peaks at the shoulders affect the separation of flow from the body, and this greater pressure exhibited on the fuller form of the NACA 0041 is one reason why the flow separates further forwards than for other sections.

22.16 Drag penalties not accounted for

The program calculates the drag assuming that the body is an uninterrupted smooth shape. However, this will not be the case. The drag due to the lip and the intakes is not modelled and these could mean an underestimation of actual drag. Data for the Drag due to circular cavity are investigated in Engineering Sciences Data Unit, item number 74036. But the corrections cannot be readily applied to this problem, as the cavities are all the way through the body not blanked off. This data is also designed for very high speed, and is probably outside the range of the subsonic tests.

The alternative is to seal the cavities when drag testing the towing tank.

22.17 Alternative choice of section, if any

At first glance it would seem that the best choice at such low speed would be the NACA 0041 body, with its short length and lower skin friction drag. However, from 3D modelling in AutoCAD, and from the construction of the actual ROV it is found that the NACA 0041 would have been too short to enclose the camera box in its forward location, or encase the pipes and fittings. The NACA 0041 would have had to be lengthened, increasing its skin friction drag.

Compared to the NACA 0041 a more streamlined body such as the NACA 0023 will have less shallow water wave making.

The choice of the NACA 0023 gives a good compromise of slenderness and space, it will be seen that the design is also very compact with virtually no wasted volume. Over all it is a good choice of section. Again, a more comparative study of similar length would be beneficial.

22.18 Unidirectional Optimisation

If the ROV were to be unidirectional, similar to an autonomous underwater vehicle (AUV) then it could be made more efficient if the shape was more elongated, or teardrop shaped. This was the finding of a PhD on the optimisation of an AUV where the optimised shape of a unidirectional AUV is shown in the Figure 60 below.

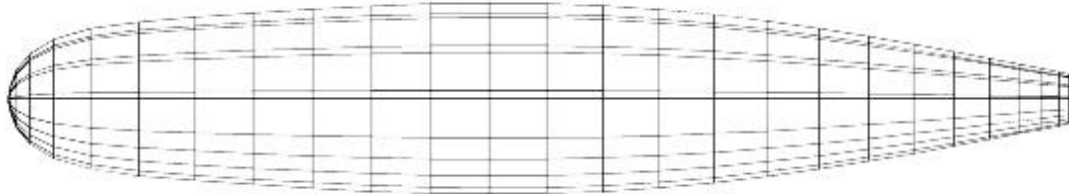


Figure 60 - Optimised Unidirectional AUV design Source: Thibaut Jacquet-Lagrece, MSC Thesis University of Southampton

23 General Arrangement and 3D Modelling of ROV components

To ensure that all components would fit into the NACA0023 body volume and for visualisation purposes it is necessary to do extensive 3D modelling. AutoCAD 14 is used for this. The general arrangement is also drawn in AutoCAD 14. The design drawings can be seen in Appendix S.

All of the main components of the ROV except for pipes were drawn in 3D and rendered to ascertain if the components would fit. This process enabled the detailed design and the general arrangement to be finalised.

The most complex geometries of the pipe networks were not modelled in 3D due to time constraints and complexity, although samples of pipe section and orientation is made in real life 'spatial availability' tests, showing that there is room for a very compact pipe network with minimal pipe distortion.

Detailed rendered images showing various stages of the 3D modelling process can be seen in Appendix T.

There were several co-ordination problems which needed to be solved due sizing of certain components such as the Buccaneer water tight connectors, Electronics box

sizes, internal structural design, and location and orientation of the nozzles and interference with the shell. This made the 3D modelling quite challenging. These items are modelled and located such that they do not interfere with the shell or the connectors and cables do not intersect the frame.

For construction and shell design purposes the location and orientation of the holes in the shell for the nozzles is critical, so that the water jet is not obstructed or misaligned with the holes and channel through the shell.

The main electronics box and its five connectors is quite high up in the structure, high is not ideal for stability, but it was later found that the box when sealed is positively buoyant, which improves the stability in water.

There were also potential problems with the tether entry into the ROV, due to its bending radius. It is decided that the tether would be fed through a hole at the stern, in the top shell, close to the centreline such that there is minimal bending of the tether - this also improves drag characteristics, as the tether is horizontal with the flow and does not contribute to frontal area.

Using AutoCAD it is also possible to draw in the buoyancy in its desired location, and by using the programs mass properties dialog accurately ascertain the location of the centres of mass of complex shapes such as the buoyancy nose and stern cones, top, and side curved buoyancy panels. This information is then used in the weights and centres, to ensure that there is enough buoyancy and in the correct location such that the ROV is at level trim in pitch and roll.

24 Shell Design Manufacture and Construction

With the shell section shape determined it is necessary decide upon the materials to use. These should be low-density materials to keep the weight of the ROV to a minimum.

The shells are designed and made in two halves cut along the horizontal transverse centreline, to give a top and bottom shell. They are to be joined by means of a joggle or internal lip, which protrudes up from the horizontal centreline.

Internal framework support rails at 90mm depth are to be fitted level and at 180mm apart from their centrelines. The rails are the same thickness as the framework

The shells will have 11mm profile holes for cut through them for the water jets to discharge through. Which will require a chamfer so not to disturb the jet.

A profile cut will be required for the drag support strut in the top shell, along with a 18mm hole at the centreline at the stern, and a 35mm hole cut through the centreline at the bow for the camera lens.

Intakes for the water jets will be required in the shell such that there is sufficient mass flow rate through, with a zero net force.

24.1 Possible materials and methods of manufacture

24.1.1 *Wood construction*

This includes making the shells from a lightweight material in panels or strips similar to a rugby ball. Side by side panels in a carvel design would produce a seamless outer hull rather than overlapping panels in a clinker design. Another alternative is strip planking comprising of narrow, almost square planking, secured with edge-nailed fastenings. They are glued together not caulked, which produces a smooth seamless hull. The shape could also be carved from a laminated or single wooden block of the correct dimensions, although this would take much time.

Wood construction is highly labour intensive requiring a skilled pattern maker, this process is a similar cost to composite construction for a one off, but the process would take a very long time to complete. One merit of wooden construction is that the shell is buoyant, which has its merits, reducing buoyancy required and disadvantages, with all round buoyancy and thus a loss in stability. Counter weights could be used to solve this, but requiring more volume of buoyancy, which is not desirable.

24.1.2 *Metal construction*

A welded multi chine construction with round bar or tube welded into the soft chine can produce a quite shapely hull form, however, to make a highly curved body of revolution the panels would need to be very small and the process would take much time and the finish would not compare to the alternatives. This type of manufacture does not lend itself to small size construction. Other factors such as corrosion and magnetic interference with compasses and electronics can also add complexities.

24.1.3 Glass Fibre Composite Design

A polymer composite or glass fibre/epoxy composite could be used to make the shells. This requires a mould and a pattern or plug to make the mould. This route is costly for one off, but the benefit is that once the mould is made it can be used many times for construction, also complex geometries can be made with relative ease and in a relatively short time. GFRP design is also lightweight and low density thus the required volume of buoyancy material is reduced. The relative densities of the top and bottom of the shells can also be controlled ensuring static stability.

For a complex shape, which is relatively small, the lay-up would be by hand and can be quite labour intensive, and this dominates the cost more so than the materials. Once an accurate mould has been made the manufacture of the shells is quick and efficient and the shells can be made exactly the same every time.

The fact is that there is no cheap and easy solution once the fairing and the hydrodynamics become unusual in design compared to say, a cylinder with two hemispheres at either end.

The factors that dominate the manufacture are accuracy, time and cost. The shell is a one off and is required very quickly, for slightly less cost the GFRP will yield the shells and a mould in a preferred material to wood, with lower maintenance. One can also customise the GFRP to suit a customer's preference in say colour.

Due to the complex geometry time available and the size of the shell, it is decided to make it out of a composite glass fibre.

25 Buoyancy

There is a wide choice of buoyancy material including, syntactic foam, closed cell PVC foam, cork, polystyrofoam, and gas. The least deformable, water absorbent and most easily available is syntactic foam (provided by a previous sponsor). The next most malleable, although a little difficult to contain while setting is expanding closed cell PVC (similar to cavity wall insulation), which could be used in a production model to fill the top half of the shell and incorporate fixings such as nozzles and connectors on the top of the internal structure for perfectly uniform buoyancy with limited waste.

The material used is syntactic foam, which is can be easily cut shaped with time. It is specially shaped by hand into buoyancy blocks, at the bow over the camera box, at the stern, in the upper half of the shell, along the top and either side of the internal frame. All buoyancy is in the upper part of the shell. The exact amount and location of the buoyancy is determined from the weights and centres data and 3D visualisation before being made. It cannot be made and place accurately until all other components are ready to be constructed so that the buoyancy can be designed to fit.

The volume of the buoyancy that is shaped and which can be installed is shown in Table 9 below.

Location	Volume m ³
Bow	0.0011429
Aft	0.0020714
Port	0.0017857
Starboard	0.0017857
Forward wedges port	0.0002143
Forward wedges starboard	0.0002143
Top	0.0033571
Forward top	0.0003571
Side panel stbd	0.0007143
Side panel port	0.0006429
Aft internal	0.0006429
Forward 1	0.0004000
Forward 2	0.0002571
Forward 3	0.0000714
Aft wedge port	0.0002000
Aft wedge stbd	0.0002000

Aft 2	0.0002429
Aft 1	0.0001571

Table 9 - Buoyancy available

The Hand carved buoyancy took two solid 12-hour days to complete, with one main shaper and one cutter to model, cut and start symmetrical shapes once a parent had been shaped to fit. The main tools used are a hand rasp file and saw. The completed buoyancy can be seen in Figure 61 and Figure 62 below.



Figure 61

Figure 61 Left: Crafted Buoyancy laid out including one shaper: Karl Randle

Figure 62 Below: Buoyancy when inserted into ROV



Figure 62

26 Weights and centres

All the ROV components were weighed and their positions in relative to amidships recorded. The longitudinal datum is amidships, the vertical datum is from mid plane of the profile, and the transverse datum is from the centreline, along the longitudinal axis, as shown in Figure 63 below, positive sign convention is shown.

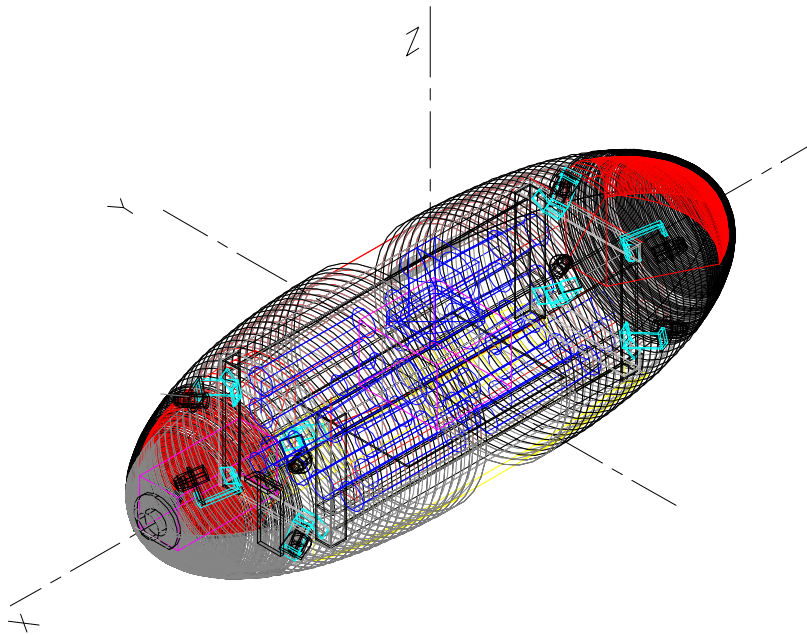


Figure 63 ~ Centrelines and Sign convention

The centres of mass are estimated as the centre of volume for some of the components such as the control and camera boxes, which are evaluated as such with some offset towards the heaviest components. 3D modelling is used for complex geometries.

Each component that displaces water contributes to the vessel buoyancy (volume displaced x density of fluid displaced). The sum of the masses and buoyancy divided by the sum of the moments in X, Y, and Z gives the location of the vessel centres of mass and buoyancy.

$$LCG = \frac{\sum Moments_x}{\sum weights} \quad TCG = \frac{\sum Moments_y}{\sum weights} \quad VCG = \frac{\sum Moments_z}{\sum weights}$$

$$LCB = \frac{\sum Moments_x}{\sum Buoyancy} \quad TCB = \frac{\sum Moments_y}{\sum Buoyancy} \quad VCB = \frac{\sum Moments_z}{\sum Buoyancy}$$

With the 3D modelled Buoyancy and locations of components, the weights and centres are as follows:

LCG mm	-0.58	LCB mm	50.82
TCG mm	0.00	TCB mm	0
VCG mm	-0.01	VCB mm	9.25
Mass	24.86	Buoyancy kg in SW	25.93
BG mm	9.26	Buoyancy in kg FW	25.30

Table 10 - Modelled weights and centres

With the actual buoyancy and location of components the weights and centres are as follows:

LCG mm	-0.55	LCB mm	-18.50
TCG mm	0.00	TCB mm	1.08
VCG mm	-0.01	VCB mm	29.41
Mass	24.75	Buoyancy kg in SW	27.41
BG mm	29.13	Buoyancy kg in FW	26.74

Table 11 - Actual weights and centres

The two weights and centres tables for 3D modelled design and actual build ROV can be seen in Appendix U, Tables 1 and 2 respectively. The bow down trim indicated from the 3D modelled location of buoyancy can easily be rectified, with adequate reserve of buoyancy if the aft cone is removed completely or sliced in half with removal of some the buoyancy.

The main change from design to build is the location of the pumps, which are not situated as per the General arrangement, but instead are placed under the frame, and either side as can be seen in the Figure 64 below, which also increases BG and hence improves static stability.



Figure 64 - Actual location of Pumps

There is quite clearly enough room for buoyancy and extra payload, such as tether (small but cumulative) or extra cameras and equipment e.g. oil in the electronics box, should it be required.

27 Stability

27.1 Static Stability

It is necessary to have the buoyancy and mass centres in X and Y coincident for level trim, in pitch and roll. It is necessary to have the centre of buoyancy in X-axis (LCB) vertically inline and above the centre of mass in the X-axis (LCG), this ensures static stability of the vessel. Having the main buoyancy in the top half of the shell helps to ensure static stability with the LCB above the LCG. This is achieved with the general arrangement as shown in Appendix S.

It is also desirable to have the mass distributed evenly such that the centre of mass lies between the water jets, providing equal moment arms for control.

The metacentric distance between the centre of buoyancy and the centre of gravity (BG) is 29.13mm and G lies below B and the ROV is in stable equilibrium. Both the

transverse and longitudinal stability of a submerged body are the same and GZ curves and righting moment curves become single sine curves.

Depth maintenance stability of the ROV is required such that when given a disturbance such that the ROV is sent deeper, and the hydrostatic pressure increases, that the buoyancy does not shrink and take up less volume, hence having the buoyancy for a constant mass. If this occurs then a resultant downward force is created and the body is said to be unstable in depth maintenance. Also when in descent, the down force is effectively added weight and thus the effective BG will be reduced. Given a vertical force of 4.4N the added mass is calculated as 0.4485Kg, which is not significant enough to affect stability.

Depth maintenance stability is tested in full-scale tests and when a downward force is applied the ROV sinks slightly before returning to its original position. The ROV is depth stable.

The ROV total mass is 24.75kg

The righting moment is calculated using $RM = \Delta BG \sin \alpha$ where α is the pitch or roll angle of the craft and Δ is the mass displacement of the ROV.

The righting moment curve and GZ curve is given in Appendix V.

27.2 Directional Stability

Further stability analysis and estimation of oscillatory coefficients and slow motion derivatives, for vessel equations of motion could be found using a Vertical and Horizontal Planar Motion Mechanism (VPMM and HPMM). However, there is not sufficient time to do so. Also, only the HPMM is available at the University of Southampton, which would require major modification of components to fit the ROV (the base plate is larger than the ROV and not designed for submersibles), also it is the only one available at a university in the country, there is not a VPMM in the country, but there is one being built by the ship science department at the University of Southampton. The closest is possibly in Denmark.

If one were to gain such information then a full rigid-body directional stability analysis could be fulfilled. In any case the test equipment would have to be custom made.

28 Full-scale Tests

28.1 Immersion and Floatation

With the designed amount of buoyancy installed the ROV was immersed in the Tank. It did not sink, and was quite positively buoyant with some bow down trim. This is adjusted as mentioned previously. Figure 65 below shows the first time flotation and the ROV lie in the water.



Figure 65 - Floatation Test

In operation this will not be as great an issue as the increase in buoyancy aft will be counteracted by the weight of the tether, bringing the nose back level for the design 10-20m of tether.

The first time error in trim and buoyancy was not unexpected due to the complexity of accurately shaping and forming the buoyancy blocks and also due to some air entrapped in the pumps and pipe work. The excess buoyancy is removed such that the ROV is neutrally buoyant and at level trim.

28.2 ROV and Strut Drag Tests

The ROV is drag tested attached to the low drag strut in the Ship Science towing tank. The strut is slightly modified from the previous ROV project and bolted to the internal frame such that only the vertical strut protrudes from the ROV shell. The 3D layout can be seen in Appendix W. A photo of a test run is shown below in Figure 66 below.

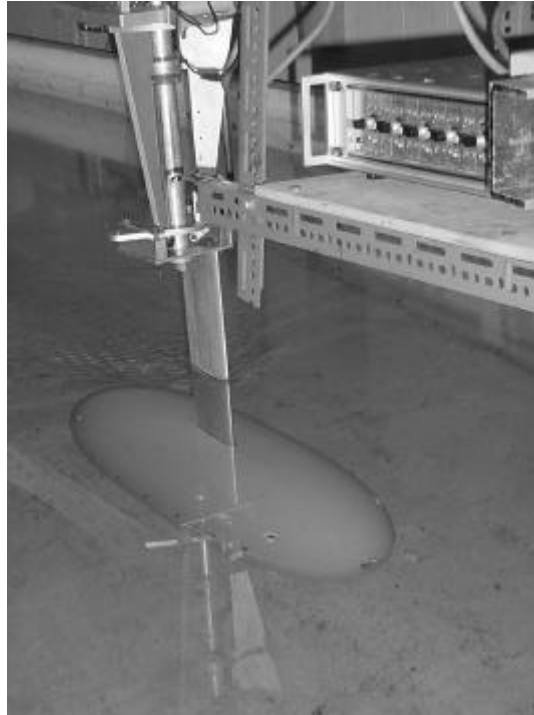


Figure 66 - Drag testing ROV

Firstly the Dynamometer is calibrated with the strut only attached. The strut is then drag tested at a range of speeds to find its drag and average drag coefficient. The ROV is then attached and the dynamometer re-calibrated with a mass offset of 2.5 N. The calibration data and graphs are in Appendix W. There is little no change in the multiplier value for the force between the two calibrations because the ROV is neutrally buoyant. A linear fit was made to the calibration data and the equation of the line used to convert the reading into an actual force value.

The strut extends 0.35m below the surface in a 1.2m tank. From the photo above (a larger image is included on the CDROM) a Kelvin wave from the strut can be seen. There is also a wave hump generated in front of the strut, this is a free surface effect due to the low immersion of the ROV and flow acceleration over the fore shoulder of the ROV. The free surface effect will increase the drag read by the dynamometer. There will also be a drag increase due to blockage affects. A blockage affect has not been applied to the results, although this will not be too significant.

The deeply submerged drag of the ROV in open water will be less than calculated in the test tank.

The linearity of the calibration is excellent, and deemed accurate over the range tested. It was not possible to test the dynamometer at a low enough range for the strut.

The drag of the strut is very small and the dynamometer is not designed for such a small force, as such the results from the strut drag test are not a smooth curve with increasing velocity. This can be seen in Graph 2 of Appendix W.

The calibration range is satisfactory for the ROV expected drag characteristics.

Actual speed is calculated for the timed 10m run and used in calculations.

28.3 Tether Drag Tests

The tether is attached to the strut in the manner shown in Figure 67 below. The drag tests on the tether are done in two sections, firstly the vertical component of tether including 0.2m of tether horizontally is calibrated and drag tested over a range of speeds as before. Next, 5m extra tether is added and drag tested. In the shorter tether test the 0.2m length of tether is observed to oscillate at higher speeds.

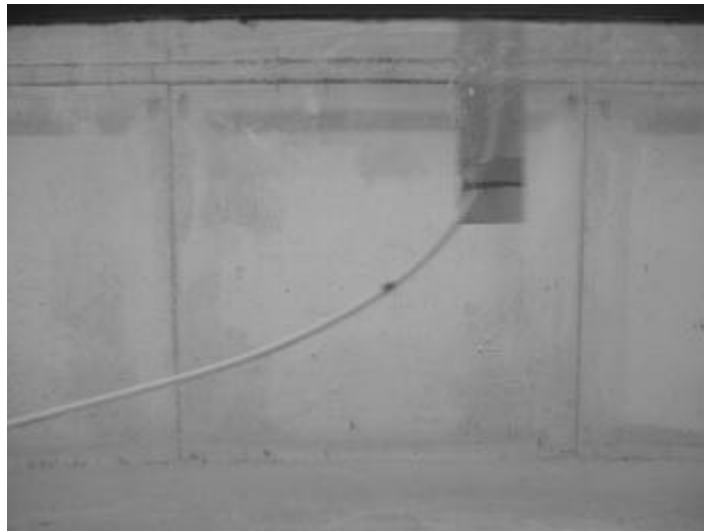


Figure 67 -Tether and strut drag arrangement

From observations it is noticed that the tether is not horizontal and the last 1m of tether touches the tank bottom and curls up. This is due to some residual curvature of the tether after being uncoiled.

This leads to some large inaccuracy and it is seen from data Tables and Graphs 5-7 in Appendix W that the drag readings of the horizontal component of tether decrease with speed. This is due to two reasons. Firstly at higher speed the tether becomes more horizontal, secondly when more horizontal, less of the tether touching the tank bottom, reducing drag.

Unfortunately the validity of the tether drag tests is vague. A larger, deeper towing tank would be required to more accurately test the drag. It is also recommended that a more streamlined approach to attaching the tether to the dynamometer be sought to eliminate any wave making and disturbance at the free surface.

29 Comparison of Drag Test and Panel Code Results

The estimated drag coefficient was 0.0648 and the average tank test drag coefficient is 0.0850. The actual test result is higher than the panel code as expected due to the way the program calculates. The free surface and blockage effects will also contribute as stated. A difference in result of 0.02 that is 2% is very small indeed and this validates the computational technique used.

This also means that the flow is most probably turbulent at low speed, or has been tripped due to the camera lens and the join of the lip around the bow, and possibly the bolts attached to the sides. Some flow may also be entering through the nozzle holes.

Overall there is excellent comparison between the computational and experimental results. This implies that further work with the panel code could make even further refinements to the hydrodynamic performance of the ROV shell.

Due to the time scale the ROV hull was not tested with the intakes and nozzles blanked off.

30 ROV Operational capacity

Using full-scale test results for Drag coefficient and the Hoenher prediction for drag coefficient of the tether, at an angle of attack of 20°, compared to the observed angle in the tether drag tests which is calculated as:

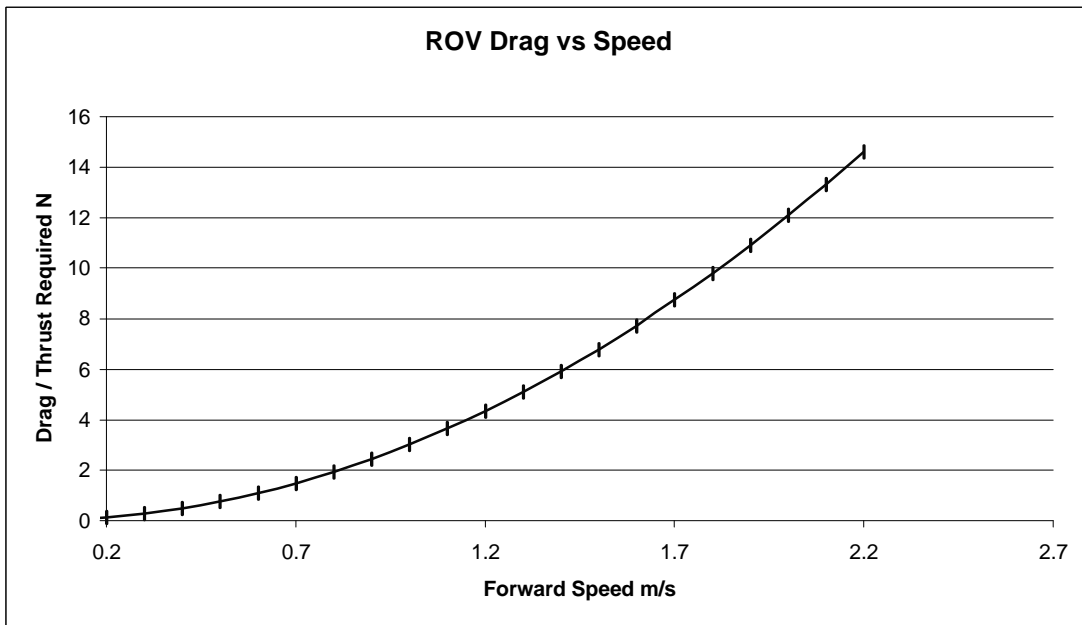
$q = \sin^{-1} \frac{0.9}{5.2} = 9.97^\circ$ where depth of tether is $1.2 - 0.3 = 0.9$. It is possible to calculate

the length of tether sustained for a given speed.

Given the maximum thrust force calculated for the four vectored water jets, 14.6N, 7.2N and 4.4N in forward, lateral and vertical planes of motion are respectively then this information can be used to estimate the forward, lateral and vertical operating conditions.

30.1 ROV thrust and drag

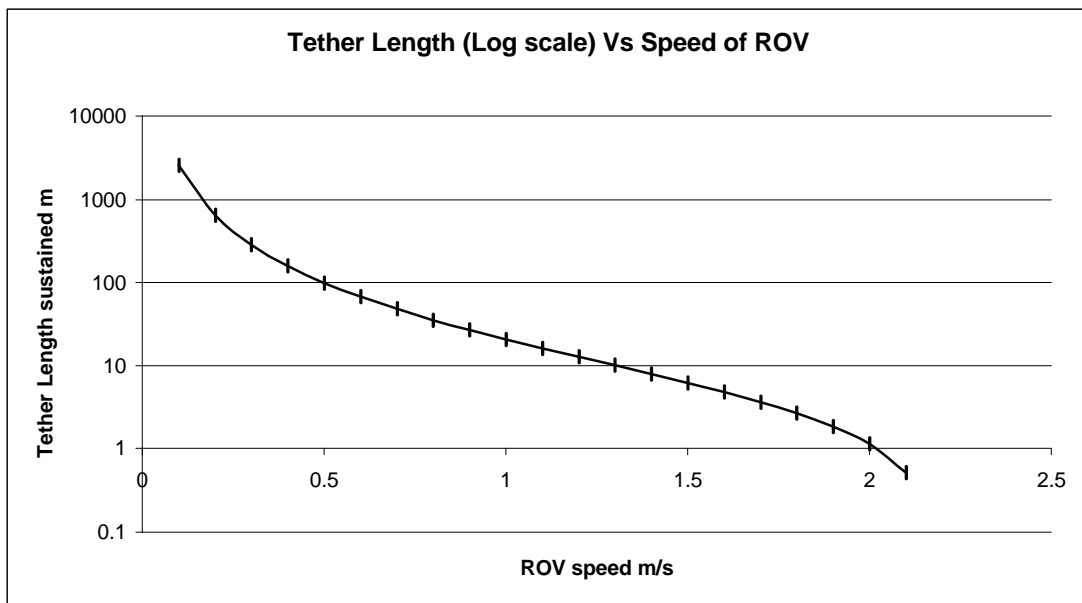
Graph 8 shows the thrust and drag requirements over a range of forward speeds.



Graph 8 - ROV Thrust and Drag for a given speed

30.2 Tether length sustained

Graph 9 below shows a graphical representation of amount of tether for a given ROV speed. Due to a more hydrodynamic hull form and an increased thrust available quite a substantial length of tether may be towed at a low angle of attack.



Graph 9 ~ Tether length for given ROV speed

30.3 Performance and manoeuvrability

With a maximum forward thrust the ROV alone should move forwards at over 2.0m/s this is four times the design requirement.

The maximum lateral translation speeds are calculated using a drag coefficient of 1.2 side ways and vertical (approximated as a circular cylinder in axial flow). The velocities are 0.23m/s sideward and 0.18m/s vertically. Pitching it down with the front jets and diving forwards can improve the ascent and descent of the ROV, although this will slow the ROV transit.

It is expected that the lateral and vertical motions are less responsive as it has been designed and optimised for forward motion. To improve the vertical rate of motion it might also be advantageous to add small hydroplanes, to make the ROV more like a submarine although not part of the objectives.

The forward acceleration of the ROV alone, at maximum thrust is calculated $14.6/24.75 = 0.56\text{m/s}^2$. The lateral acceleration (excluding intake affects) $=7.2/24.75 = 0.29\text{m/s}^2$. The vertical acceleration (excluding intake affects) $= 4.4/24.75 = 0.17\text{m/s}^2$.

It is considered that this loss in lateral and vertical speed is acceptable given the increased range of the ROV.

Further self propelled tests are required to give the ROV yaw rate, its turning circle radius would be zero if there were no tether, but it is limited to the tether minimum bending radius.

30.4 Intake slots and their implication on the ROV operational performance

Intake slots dimensions and their implications on the ROV performance can be assessed using the expressions based on momentum transfer. For a given volumetric flow rate, at maximum thrust = 4.6litres/s.

If only the bottom slots contribute and the profile hole is considered negligible then: With a combined slot area of 0.009m^2 the flow velocity is 0.51m/s. This equates to a suction force in fresh water of $1000 \times 0.009 \times 0.51^2 = 2.3409\text{N}$ and in standard saltwater 2.3994N.

In such a case, at maximum thrust the theoretical rate of descent when operating forwards propulsion is calculated using thrust equations from those used at initial design. With an ROV profile area of 0.2345 in standard saltwater the rate is 0.129m/s. At maximum forward velocity of 2.17m/s (no tether, from maximum thrust available at vectored pumps at estimated C_D of 0.08) this works out at a dive plane angle θ , of $\sin^{-1}(0.235/2.17) = 6.2^\circ$. This is quite small. However if 10m of tether is taken into account then the forward velocity is decreased to roughly 1.0m/s the dive angle of descent is thus 13.56° , which is undesirable.

If the strut profile hole is included as an intake, then the intake area (0.0018m^2) the total area is 0.01008m^2 the average velocity is 0.45m/s this is a total force of 2.15N, which is a small net force. This is assuming that the inflow does occur from the profile strut and is not constricted.

The only solution is to remove the net force is to have unconstrained equal opposite intakes to the pumps. This is not as simple as it sounds due to the main electronics box and connectors in the path of the top profile hole. Re-engineering the design such that the intakes are on a horizontal plane is not possible with the joggle in the way unless a there were four slots at equal opposite locations about the centreline, although the stress in the shell might cause warping. Having four intakes means smaller areas per intake, which is better for reducing warp than one large hole. In addition, cutting lots of slots all around the streamlined body will have an adverse affect on the flow, having the slots inline reduce any adverse affect.

The net force is dynamic with speed and pump flow rate, as such the problem cannot be solved as an added mass problem and the ROV should not be designed positively buoyant by the same amount as the net maximum downwards-suction force, because when the ROV stops or is not at full speed or a speed such that the suction force is equal to the added buoyancy, it will surface. It is an interesting problem if the intakes are not equal in area and opposite each other.

Another consideration due to the intakes is the change in the pressure around the ROV, which will alter the drag characteristics of the ROV. The suction pressure over the intakes, if equal and oppoite would be 107N/m^2 . This could stop the boundary layer from separating, or slow the flow and increase the pressure form drag if the

suction draws water from the opposite direction do motion, hence instigating separation. It is quite a difficult problem to model and solve.

When the ROV is self-propulsion tested with all four jets and eight pumps running the ROV did not have any noticeable uncontrolled downward movement. This therefore means that there is inflow from the top intake and that the force is over estimated in the calculations.

31 Electronics Section

31.1 Requirements

Through analysis of the general ROV requirements it became known that the electronics must be able to:

- Switch pumps on and off.
- Sense the ROV's surrounding environment by use of a camera and positional sensors (e.g. orientation and depth sensors).
- Read commands from a PC in a serial data format to keep connections to the ROV minimal.
- Act on sensor information and user requests to switch on the correct water jets and move the ROV as desired.

The design of the electronics in this project concentrated on minimising the size of the control system.

31.2 Microprocessor selection

To allow the electronics to interpret sensor data and user input into the required ROV movements, it was decided that a microprocessor should be used as the core of the ROV control system. The microprocessor would communicate with a shore based PC, receive and interpret data from any sensors, implement feedback and then control the pumps based on all the information it has received. Two main methods were considered as detailed in the following two sections.

31.2.1 CANbus

31.2.1.1 Reason for Investigation

At the start of the project, a few control systems were investigated for the purpose of communicating between the shore side computer and the ROV. One of these systems was CANbus (Controller Area Network bus), since it appeared to be very compact and easy to set up.

31.2.1.2 What is CANbus?

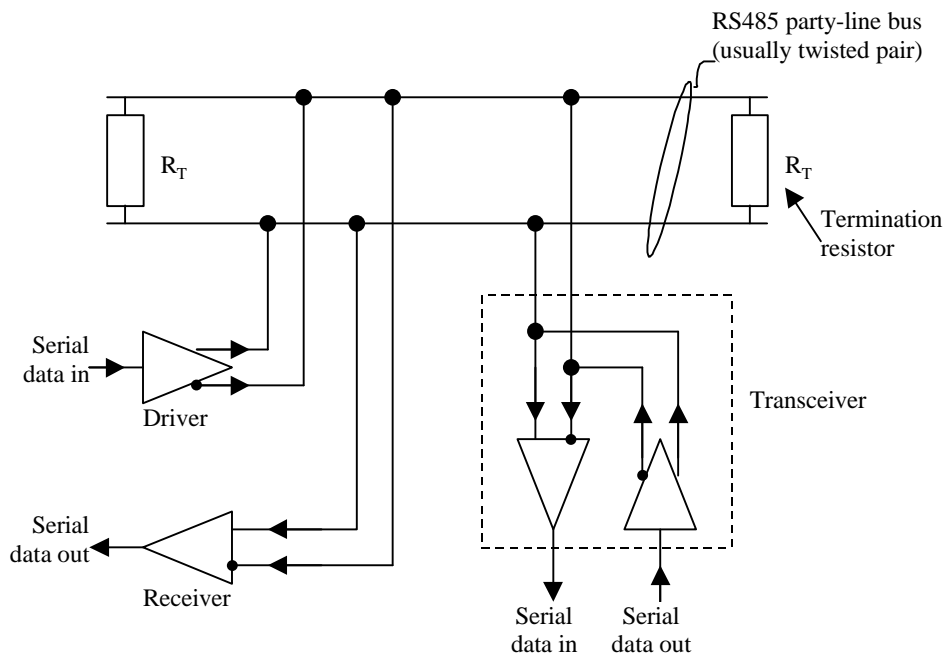


Figure 68 - RS485 standard using half-duplex transmission, as found in CANbus.

Robert Bosch developed CANbus in the 1980s for the purpose of creating better wiring looms for cars that contained an increasing number of electronic devices. The basic principle is that signals are sent between nodes (electronic send/receive devices) via a single twisted pair using the RS-485 standard, Figure 68, thereby reducing the number of wires in a complex system quite considerably. The signals are controlled by a master node (usually a computer) to determine which node can send a message, depending on the priority setting designated to that device. One great advantage is that all the protocol is contained in the CANbus microprocessor itself, almost totally eliminating the need for complex software and control programs. Another advantage is that each node verifies whether it is working or not, and so errors can be detected very quickly.

31.2.1.3 Results of Investigation

After researching the equipment available, it was found that a number of CANbus microchips could handle multiple Pulse Width Modulation outputs, which would be very beneficial in terms of controlling the pumps. In this way, only one or two CANbus controllers would be needed in total to handle all of the output requirements of our system, see Figure 69, while also being able to verify whether the pumps were functioning or not, thanks to some of the basic CANbus features.

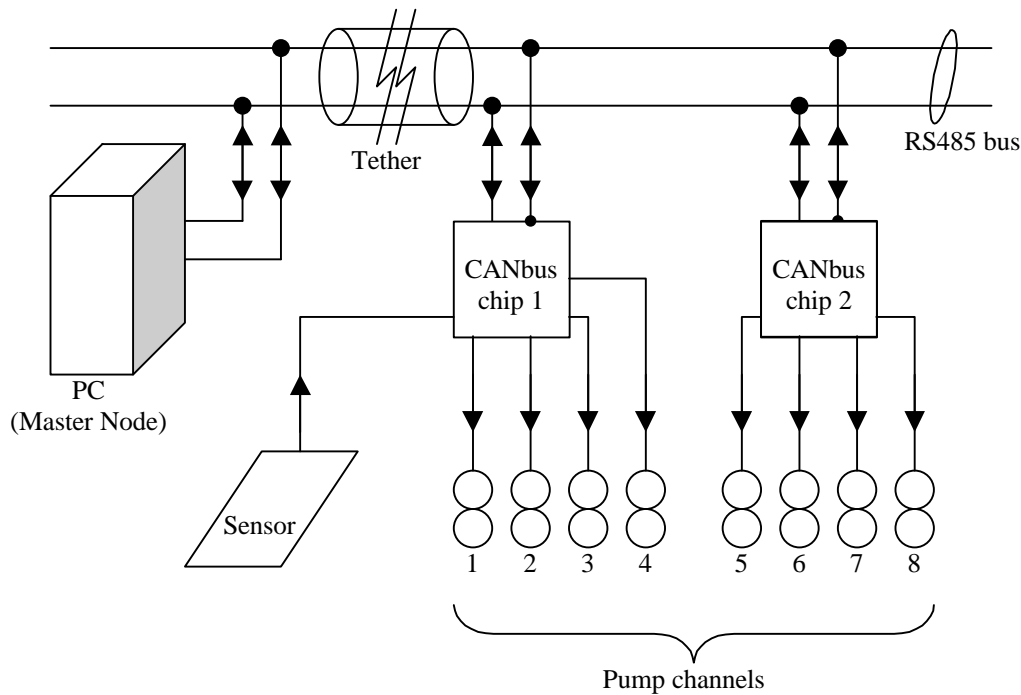


Figure 69- A Potential CANbus Setup For The ROV

This option appeared very favourable since it would reduce the circuit complexity greatly, thereby reducing the size and mass of the circuit itself, and only require two wires in the tether.

Unfortunately, due to certain information regarding the availability of CANbus microcontrollers and general technical information not being very forthcoming from technical offices by email, it was not possible to proceed further in developing a CANbus solution for the ROV. However, given sufficient time and information, a CANbus system could be incorporated into a future ROV with relative ease.

31.2.2 PIC micro-controller

The PIC (Peripheral Interface Controller) micro-controller incorporates a number of functions on a single chip and as such can help reduce the number of additional

components required in a control circuit. This makes it a very attractive solution for devices such as a small ROV, where space and weight are paramount. The PIC can be chosen to have serial communication ports, analogue to digital converters and pulse width modulation (PWM) outputs amongst others. Pulse width modulation can be used to control the speed of motors or pumps. The PWM signal has a fixed period, but the ratio of the on time to off time is controllable. The shorter this on time is, the slower the pump speed, as on average it sees a lower voltage level. The period of the signal is usually short and so the repeated switching of the pump or motor is not noticeable.

Programming of the PIC can allow interpretation of the different inputs for calculation of feedback and setting outputs.

31.2.3 Chosen control device – the PIC microcontroller

Due to its versatility and the ease of programming, the PIC was chosen to be the core of the ROV system. In particular the PIC16C7X range was considered as they had all the required features – PWM outputs, analogue to digital converters, a universal synchronous asynchronous receiver transmitter (USART – for communicating with the PC) and digital inputs and outputs (I/O). From this range the PIC16C73A was chosen as, despite its small package size, it had more digital I/O pins than needed and enough analogue to digital converter channels (5 channels) for the circuit requirements.

31.3 Sensor Selection

In order to control an ROV, it needs to have sensors that will interface with the world around it. It was felt that of most use to an ROV operator would be a camera and depth sensor. In terms of control feedback, an orientation sensor was felt to be of most importance.

In the previous ROV project the sensors were looked at separately, but for this project the search for suitable devices concentrated on finding an integrated device to save on space in the ROV. It was decided that the sensor would need to sense the roll, pitch and yaw of the ROV and that a depth sensor would also be useful to an operator, but not required for control.

An initial Internet search came up with a seemingly perfect solution - a combined roll, pitch, yaw and depth sensor. This was the OceanTec Electronics model 428 sensor. However the large size (5.08cm diameter and 20.96cm length) and high cost overwhelmed the advantage of having all four sensors in one.

From then on it proved impossible to find any other sensors combining all four variables, and orientation sensors proved far more common (combining roll, pitch and yaw). The model 543/4 micro orientation sensors by Crossbow Technology have a very small package size (2.03cm x 2.03cm x 11.68cm), but proved very expensive at US\$4400 for model 544 and US\$2,100 for model 543. This would take a large proportion of our budget and so was discarded. A number of other sensors were considered including the EZ-Compass-Dive/Magnetometer from AOSI (Advanced Orientation Systems Inc.), which comes in a submersible package, and the 3DM solid-state orientation sensor from MicroStrain.

The TCM2 sensor, from Precision Navigation, was chosen over these as the specification claimed that it could output data in an analogue format that could then be very easily read directly by the A/D converters of a PIC microprocessor. The range of the sensor was chosen to be +/- 50 degrees tilt, as it was felt the ROV would never need to pitch or roll beyond 45 degrees. Since the sensor contains a compass and as such is sensitive to changes in magnetic field, it was decided to mount the sensor alongside the camera in a separate box to the main electronics.

A suitable depth sensor for the project was not found and is not required at this stage. If the ROV were to be produced commercially, then a depth sensor would need to be included. Paroscientific Inc. produce a number of suitable submersible depth sensors that could be looked at for this application.

31.4 Camera selection

31.4.1 Requirements

One of the key requirements of the ROV is that it can see underwater, both to enable the operator to navigate, and also to allow the operator to inspect the underwater environment. To facilitate this task, it was believed that the employment of an infrared light source would be advisable to illuminate the area to be observed. The

final section of the requirement was to present the image on the shore in some viewable form.

31.4.2 Previous ROV camera

It was decided early in the project to test the camera used by the previous GDP group to see whether it still worked before considering the purchase of a new camera. Therefore, the old camera was tested, and after wiring it to a suitable power supply and connecting the signal to a SCART plug, it was found that the old camera did work. The camera was of the infrared type, and so presented a greyscale image on the television screen to which it was connected. However, since it had no form of IR illumination associated with it, the camera did not pick up any image when all the lights in the test room were turned off.

Following these results, it was concluded that, although the old camera did work, a new camera would need to be purchased that incorporated an IR light source.

31.4.3 Choice and specification of new camera

The search for a suitable new camera was very quick due to the range of small, circuit-mounted, security and CCTV camera modules available through the major component catalogues (Maplin, RS, etc.). The most suitable camera was found on the Maplin catalogue website, see Figure 70, and consequently ordered. After arrival and testing, it was found to be very effective at its task, even when viewing objects through water. By using its six IR LEDs to illuminate its surroundings, the camera supplies a very good scanning resolution on the screen of 500 by 582 pixels, despite the compact size of the module. Measuring 57mm wide by 38mm high, protruding only 27mm and having a mass of only 33 grams, it was ideal for fitting into a small enclosure and thereby reducing the space taken up inside the ROV.

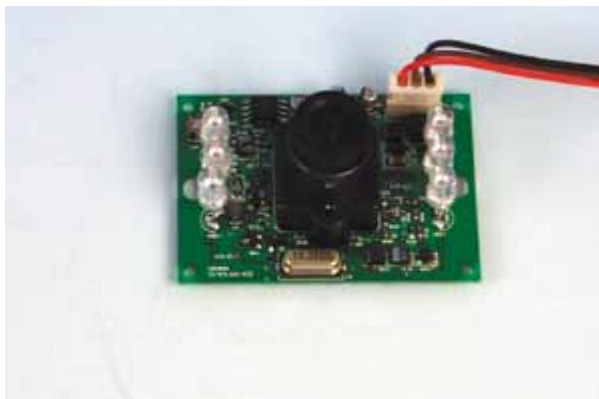


Figure 70 - The chosen Black and White Board Camera with Infra Red LEDs.

The wiring is very simple, consisting of only three lines – a 12V power line, ground line, and one-volt peak-to-peak signal line.

31.5 Initial Circuit Design

Circuit design was based on the choice of microprocessor and the chosen ROV configuration of eight pumps. From this it could be seen that a number of factors needed considering:

- Communicating with the sensor.
- Communicating with the PC.
- Power supply.
- Switching the pumps.

31.5.1 Pump Interface

It was initially considered that the circuit should allow speed control of the pumps. To get to a location a top speed of 0.5m/s would be used, but this could be reduced once the ROV was in its desired location to allow more precise manoeuvres. Complicated manoeuvres could be achieved by varying each pump's speed individually.

To control the pump's speed, a pulse width modulation (PWM) signal would need to be sent to each pump. However, since a suitable PIC with eight PWM outputs could not be found, other solutions were looked for:

- The use of external PWM producing chips that would act on the level of an analogue input to determine duty cycle. The analogue input could not be directly produced by the PIC. Separate digital to analogue converters could be used, but would require a large number of digital outputs from the PIC to get a reasonable resolution and would increase the physical size of the PIC (see Figure 71). The component count and overall circuit size would therefore increase, but the fine control desired could be achieved.

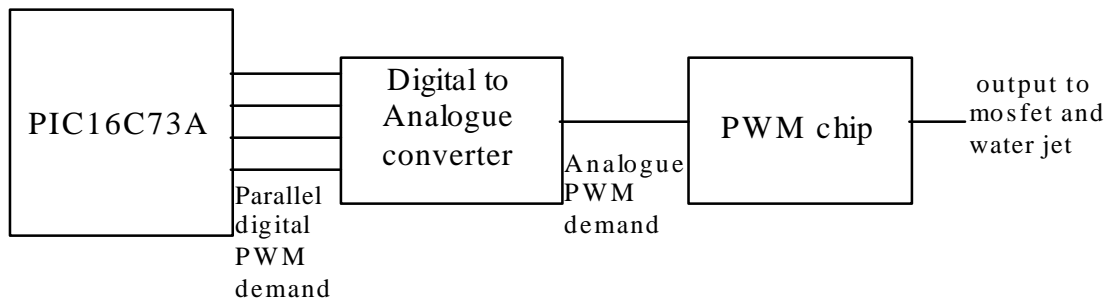


Figure 71 - Block diagram of the PWM chip control scheme

- Implementation of PWM in software onboard the PIC. This would require no extra components, but the software would be complicated to implement.
- Using one PWM output from the PIC to control the speed of all the pumps. This would not allow the complicated manoeuvres, but simply overall speed control. Again the external component count would increase as an AND gate chip would be required to combine the PWM demand with the on/off signal from the PIC's digital I/O.
- Using two PWM outputs on the PIC permanently set to 1/3 on and 2/3 on respectively. These two speeds would then be combined with a two-bit output from the PIC that would select either full on, full off or one of the two PWM outputs (see Figure 72). This would allow a limited range of speeds and combined manoeuvres, but would increase the component count and double the number of PIC outputs required.

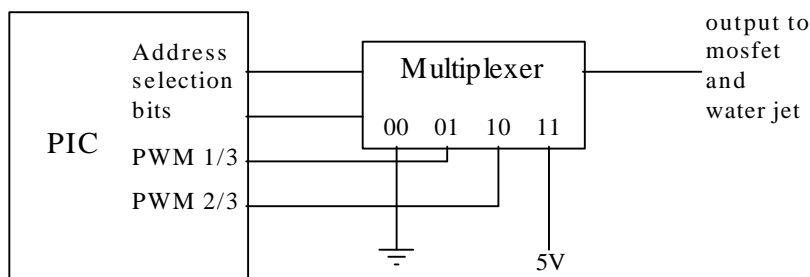


Figure 72 - Block diagram of limit speed selection

It was decided that, to simplify circuitry, the need for speed control would be left to the software. This would give a more compact circuit design and the possibility of

future implementation of more complicated manoeuvres (such as combining moves forward and left).

In terms of hardware, the pumps that were chosen required 24V and 3A each. In order to switch these on and off intelligent MOSFETs were chosen that could handle these requirements and could be switched directly from the outputs of the PIC. However, the design later changed so that two pumps would power each water jet and so a MOSFET with double the current rating was found. This MOSFET is the IRSF3010 from International Rectifier. The specification of this MOSFET allows it to be connected directly to the digital outputs from the PIC with no need for an additional driver chip. It is extremely rugged and has onboard over-current, over-voltage, over-temperature and ESD (Electrostatic Discharge) protection.

It was decided to place diodes across each pump so that when the MOSFETs are switched off there will not be a large voltage spike destroying the MOSFETs. These diodes also help improve the pulse width modulation control, as the fast switching of PWM will cause continuous cycling of charging and discharging of the inductive load of the pump.

31.5.2 Sensor Interface

The TCM2-50 sensor was initially chosen over other small orientation sensors because the specification detailed that it had analogue outputs that could be routed directly into the PICs analogue to digital converters. When the sensor was received it was discovered that in fact it could only output yaw in analogue format and the rest could only be transmitted via RS232 serial communications. Unfortunately, the chosen PIC only had one suitable serial communications port (the USART), and the PC communications lines would take this up. It would therefore be necessary to implement an additional USART in software. To keep the software as simple as possible, the yaw would be received in the analogue format and the sensor would be set up to continuously transmit only the roll and pitch. This would mean there would be no requirement for the PIC to send commands to the sensor; it would only need to receive data.

The analogue output range is from zero to five volts. As this is exactly the same as the range of the analogue to digital converter on the PIC, no changes are needed and the analogue output can be wired straight to the PIC.

The RS232 communications lines need to be converted to TTL logic levels before entering the PIC. Since this also needs to be done for the PC communications, a two-channel transceiver chip was chosen. The MAX233CPP chip was chosen for this purpose. This component requires no external capacitors, reducing the component count further.

31.5.3 PC Interface

As mentioned above, this uses the USART hardware port on the PIC. The receive- and transmit- lines on the PIC are put through the MAX233 chip to convert from TTL to RS232 levels. The outputs from the MAX233 chip are then connected to separate twisted pairs of the tether, with the other wire in both pairs connected to ground. Other pins on the MAX233 are connected together to produce the correct levels. The hardware USART is simple to operate in software, as described in more detail in PIC Software.

31.5.4 Power Supply

The pumps chosen either operate on 12V and 6A or 24V and 3A. In order to reduce losses in the tether and reduce the required current rating of cables and connectors, it was decided that the supply to the tether should be 24V. The initial design was based on the use of eight pumps resulting in a maximum current of 21A (assuming a maximum of seven jets on at any time). However this was increased to 16 pumps to provide a greater thrust resulting in a huge required current rating of 42A. To bring this back to the original rating, it was decided to have a maximum of four jets operating at any time. Combined moves would have to be done by switching certain pumps on and off for a short period like a crude form of PWM.

The electronics would draw very little current, but the PIC and the MAX233 chip require a 5V supply, the camera needs 12V and the sensor can operate on either 5V or 12V. Two voltage regulators were needed to provide these levels. Since both the camera and sensor would be in the same box (see Loom Configuration), they would both be fed by 12V from the main electronics enclosure.

Voltage regulators are known to overheat easily and it is necessary to limit the power dissipated in them. To do this the, voltage is dropped first from 24V to 12V and then

the 12V output of the regulator is used as the input of the 5V regulator. Each voltage regulator came in a TO-220 package that has a tab on the back for easy attachment of a heatsink. To improve heat dissipation heat sinks were attached to these tabs. The heatsinks will quickly conduct heat away from the components into the air that fills the electronics box, which in turn will conduct the heat to the cold surrounding water.

31.5.5 Tether

From the design of the circuit, the requirements for the tether became apparent. The tether is the only cable that attaches the ROV to the surface and so must carry all power and signals. The ROV design requires two wires for power, a twisted pair for the camera signal, and two twisted pairs for PC to PIC communications. It is also useful for the tether to be neutrally buoyant so that when attached to the ROV it does not pull the aft down or up too much. For this reason a small neutrally buoyant ROV tether was sought. One of the project's sponsors, Halliburton Subsea, was able to provide a tether free of charge. The smallest tether they could provide contained four twisted pairs, a coaxial cable and ten individual cable cores. The ten cores were split between ground and power, and one twisted pair and the coaxial were left spare.

31.6 Final Circuit Design and PCB Fabrication

The final circuit design incorporates all of the above factors into a single circuit. The entire schematic was drawn using OrCAD software and then converted into a double-sided PCB layout (see Appendix Z). The only additional components that are not mentioned above are the crystal oscillator and two capacitors used to provide the 20MHz clock of the PIC16C73A (see C1, C2 and OSC in Figure 73).

In designing the PCB, the components were laid out within a constraining area that related to the internal measurements of the enclosure and the size of connectors protruding into the box. The wires were then routed until none overlapped and extra copper was attached to paths where possible to provide better conduction. In particular the power and ground lines were increased in size where possible.

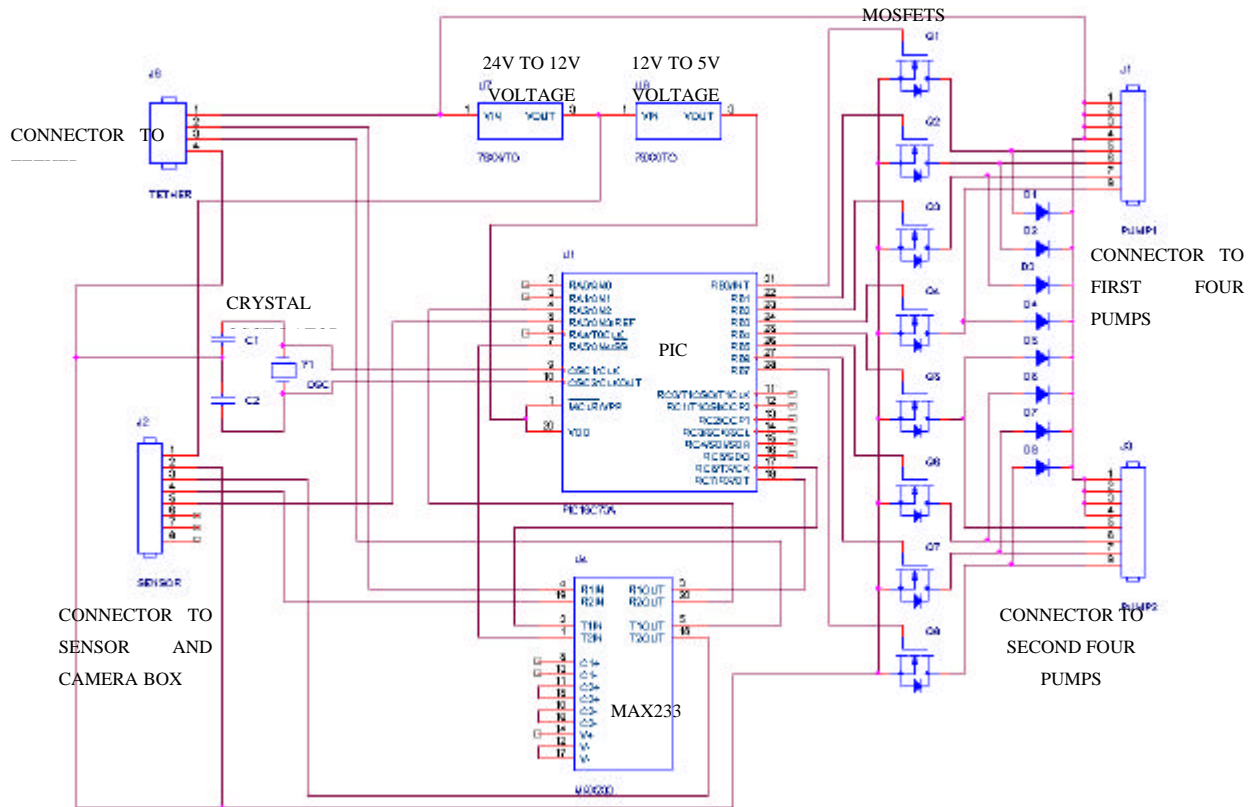


Figure 73 - Complete circuit schematic

Mr D. Russell of the Electronics and Computer Science Department fabricated the PCB for the group. The first version was produced from printed acetates of the layers. However, the grainy finish of the acetate combined with the small width of some copper paths resulted in many copper tracks being formed with breaks in. For this reason the tracks on the circuit were increased in thickness and then the design was printed using a laser printer, giving a much improved board.

Once the PCB was produced and all components purchased, assembly could begin. The PIC was mounted in a ZIF (zero insertion force) socket, for ease of removal for reprogramming if required during testing. The short pins on the ZIF meant that it needed to be mounted flush to the board, making soldering to paths on the top side very difficult. It was therefore necessary to add a number of wires to the underside to reconnect points where soldering on the top had failed.

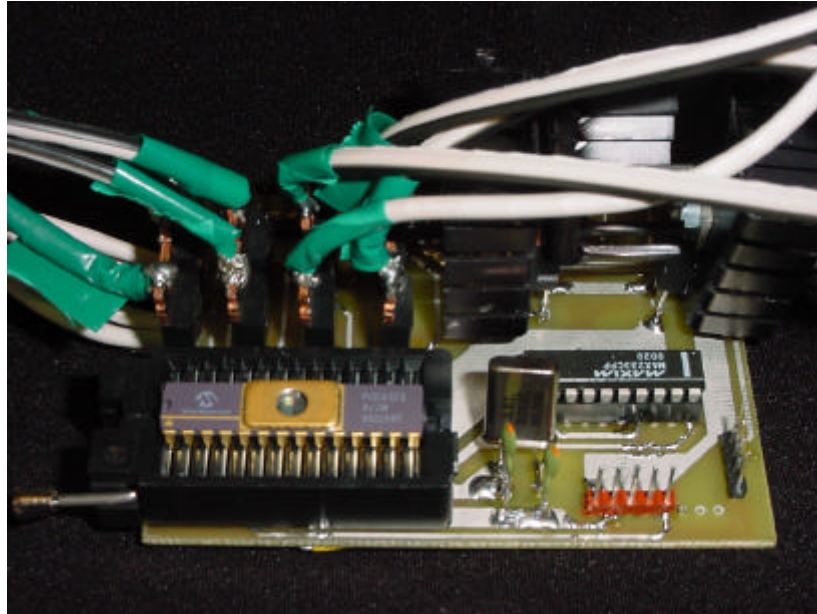


Figure 74 - Completed Circuit

It was realised after construction that the current flowing through the MOSFETs would be very high – 6A each – much more than the PCB paths were designed to handle. It was therefore decided to add connections directly to the drain and source for better conduction. The tab on the MOSFET TO-220 package is connected to the drain and so these were used to attach wires. In this case, this was done with solder (see Figure 74) but a better way would be to screw on connectors utilising the hole in the tab. Connection of the source pins to ground was more difficult as there were no easy attachment points. Wires were stripped and soldered between the pins along the copper ground strip on the bottom layer of the board.

31.7 Enclosures

31.7.1 Requirements

An important need for the electronics in the ROV was to ensure that everything is protected from the outside environment – i.e. waterproof. After researching the standards used in this form of protection, it was found that the enclosures to be used would have to be protected to a specific IP rating. IP (Ingress Protection) ratings determine the limits for both liquid and solid ingress that an enclosure can maintain. The first number relates to the mechanical ingress limit (from no protection, up to dust proof), while the second number determines the limit of liquid ingress (varying ranges of waterproof / splash proof protection). Therefore, for this project, which involves nearly continuous immersion at depths of a few metres, IP68 enclosures would be needed.

Further requirements for the enclosures were that it should be large enough to contain all the necessary electronics, while at the same time being small enough to fit in the assigned space inside the ROV itself. They should also be of a suitable material to prevent dissimilar metal corrosion with the internal frame of the ROV – namely to be either plastic or the same metal as the frame.

An extra requirement was imposed by the electronic orientation sensor, in that it would operate better when there were minimal sources of electromagnetic interference. Therefore, since the main circuit could cause problems in terms of electromagnetic compatibility (EMC), it was decided to place the sensor in the same enclosure as the camera, leaving the main circuit to be contained in a separate enclosure, which could hopefully be EMC shielded. This would prevent undesirable noise emanating from the main circuit to affect the sensor.

Protection against solid objects		Projection against liquids	
<i>First Number</i>	<i>Definition</i>	<i>Second Number</i>	<i>Definition</i>
0	NO PROTECTION	0	NO PROJECTION
1	Protected against solids over 50mm (e.g. accidental touch by hands)	1	Protected against vertically falling drops of water
2	Protected against solids over 12mm (e.g. fingers)	2	Protected against vertically falling drops of water
3	Protected against solids over 2.5mm (e.g. tools and wires)	3	Protected against direct sprays up to 60° from the vertical
4	Protected against solids over 1mm (e.g. tools, wires and small wires)	4	Protected against sprays from all directions - limited ingress permitted
5	Protected against dust - limited ingress (no harmful deposit)	5	Protected against low pressure jets if water from all directions - limited ingress permitted
6	Totally protected against dust	6	Protected against strong jets of water e.g. for use on ship decks - limited ingress permitted
		7	Protected against the effects of temporary immersion between 15cm and 1m. Duration of test 30 minutes
		8	Protected against long periods of immersion under pressure

Table 12 - IP (Ingress Protection) Ratings Table

31.7.2 Enclosures considered and chosen

The Internet was thoroughly searched to locate companies that produced or distributed IP68 rated enclosures, and quite a few matches were found. After examining all the options available, it was decided that the most promising company was Weidmüller, with their “Kestrel” range of IP68 enclosures. These came in a wide range of sizes and also had the option of EMC protection. After consulting their technical assistants, it was found that the IP68 rating had a limit inside it, determining the length of time and depth of immersion allowable. These limits did not match our requirements, and so the enclosures did not appear as suitable as previously thought.

However, after consulting an engineering lecturer, it was discovered that enclosures could be modified to either increase or decrease the rating specification by, for example, adding sealant or waterproof tape to the sealing glands on the outside of the enclosure. Therefore, after returning to Weidmüller, they suggested contacting the actual manufacturers of the enclosures, Crouse Hinds. After further communication, it was found that the “Kestrel” enclosures could be modified to satisfy our requirements.

The next task regarding the enclosures was to select the correct size to ensure that the circuit and sensors would fit in them. As the dimensions of the camera and sensor were already known, the enclosure containing them was easy to size. The enclosure that was to contain the main circuit was harder to size, since the dimensions of the circuit were unknown at that time. Therefore, a size was decided upon that seemed to fit well inside the ROV. From this, a limit was set on the size of the circuit board. The sizes of both enclosures also took into consideration the space needed inside for the parts of the connectors that would protrude into the enclosures.

The final step in the selection process was to order the enclosures. This proved harder than imagined since most of the enclosures are made to order, resulting in lead times of around seven weeks. However, a local distributor, R&M Electrical, was found who could obtain the correct enclosures in approximately two to three weeks. Therefore, the enclosures were purchased through this distributor.

With regard to the camera enclosure, a window would have to be attached to the front to allow the camera to see out of the box. Therefore, a hole was cut to accommodate

this, and a piece of clear plastic was sealed over this hole by superglue. This ensured that the IP68 rating was maintained.

31.7.3 Special notes

It was planned to fill the main circuit enclosure with a special oil used for exactly the same purpose in commercial ROVs. This oil reduces the pressure difference between the inside and outside of the enclosure, which could lead to both ingress of water and damage to the circuit. However, since the camera / sensor enclosure includes the camera, which must see out of the window, this was not oil-filled since the oil would obscure the camera's view.

Unfortunately, due to the oil not being supplied in time, the main electronics box was not filled with this oil.

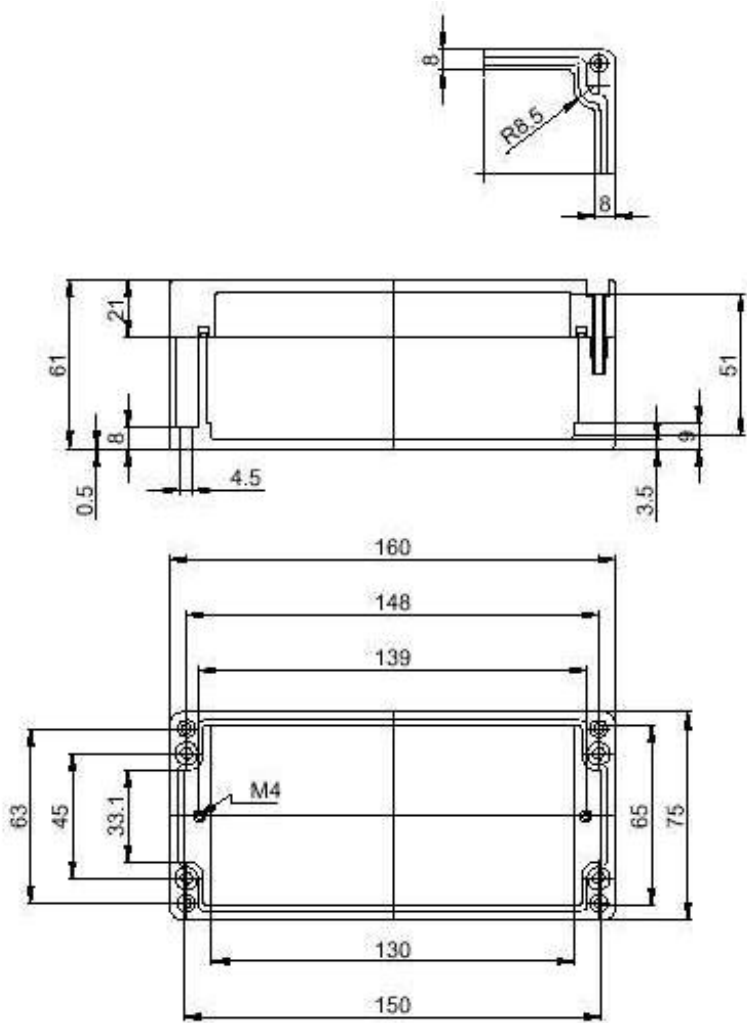


Figure 75 - The Kestrel IP68 rated enclosure used for the camera and sensor.

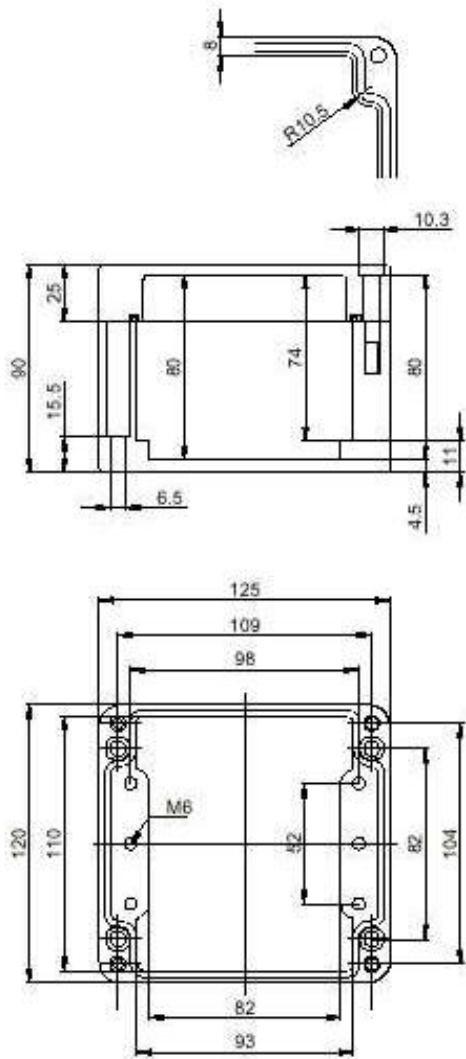


Figure 76 - The Kestrel IP68 rated enclosure used for the main circuit.

31.8 Connectors

31.8.1 Requirements

As with the enclosures, an IP68 rating was required for the connectors. The other key consideration for the selection of the connectors was to match the current ratings required in the ROV systems. This was particularly important since some quite large currents would be drawn from the pumps with respect to normal circuit currents. As a final restriction on selection, they would have to be of a suitable size to fit on to the enclosures and to mate with the cables at their other end.

31.8.2 Specifications for circuit

Another important factor in selecting the connectors was the number of pins required for each connector. Fortunately, most connectors are available in a variety of pin numbers.

Since there would be two enclosures, these would need to be linked so that the camera and sensor can receive power and transmit their respective signals. The sensor has two power lines and three signal lines, while the camera has two power lines and one signal line. Therefore, it was easy to determine that the connectors between the two enclosures would need to have eight pins (as would the link cable itself). The current limit for these would not be of concern since the smallest rated connector was easily above the very small currents used by the camera and sensor.

With the configuration of pumps used in the ROV, a maximum of four out of the eight channels would be used at one time, and since two pumps were connected to make one channel, a maximum of eight pumps would be active at any one time. Therefore, since each pump drew three amps, a total of 24 amps would be required when the maximum of eight pumps were operating. This set the current rating for both the pump connectors into the main circuit enclosure and also the rating for the tether connector. The number of pins required for the pumps would be two per channel (24 volts and ground), giving a total of $8 \times 2 = 16$ pins. However, since the 24 volt line is common to all the pumps, this could be shared among them, and so the pin requirement can be reduced to one per each of the eight channels, plus one other for the 24 volt line, giving a total of nine pins.

The tether connector requirements are quite complex, due to the varied signals and voltages travelling along its length. The tether included two power lines (24 volts and ground). The signals involve three twisted pairs consisting of a camera signal twisted pair, shore-to-ROV signal twisted pair, and an ROV-to-shore signal twisted pair. This gives a total of 8 pins for the connector between the tether and main circuit enclosure. The current rating would be 24 amps from the pump requirements, plus less than one amp for the normal circuit requirements, giving a total of 25 amps minimum.

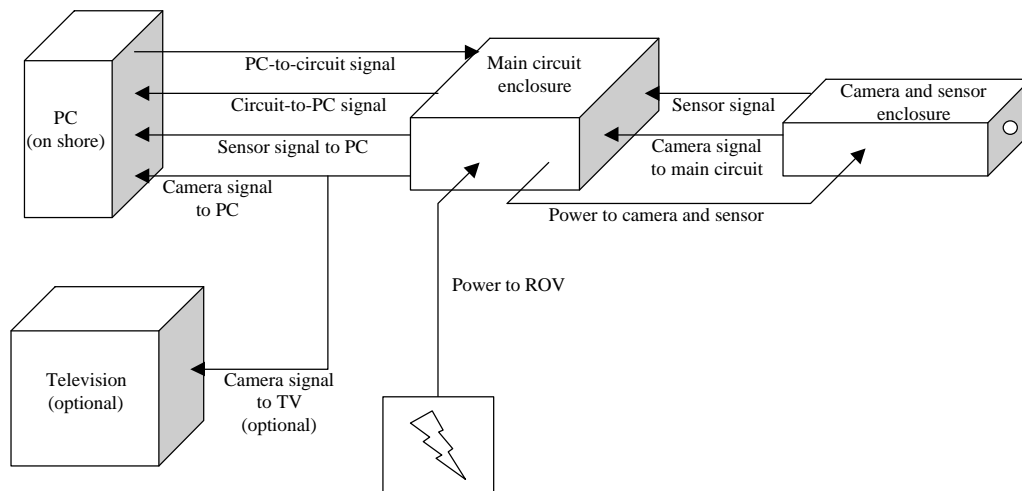


Figure 77 - Diagram of all of the signal and power lines in the ROV system.

31.8.3 Options available and chosen solution

A number of companies were found on the Internet that could supply IP68 connectors, but the best range and availability were found in Bulgin. The connectors came in three series – Buccaneer, Mini Buccaneer and the 900 Series Buccaneer. The differences between these ranges came in their physical size, number of pins and current ratings.

For the small current connectors, the Mini Buccaneer series was found to be the most suitable, with ratings of between three and ten amps, and pin options of 2, 3, 4, 6, and 8 poles. The eight pins required for the link between the two enclosures was perfectly satisfied by the eight-pole Mini Buccaneer connector with a rating of 5 amps.



Figure 78 - Examples of the Mini Buccaneer connectors by Bulgin

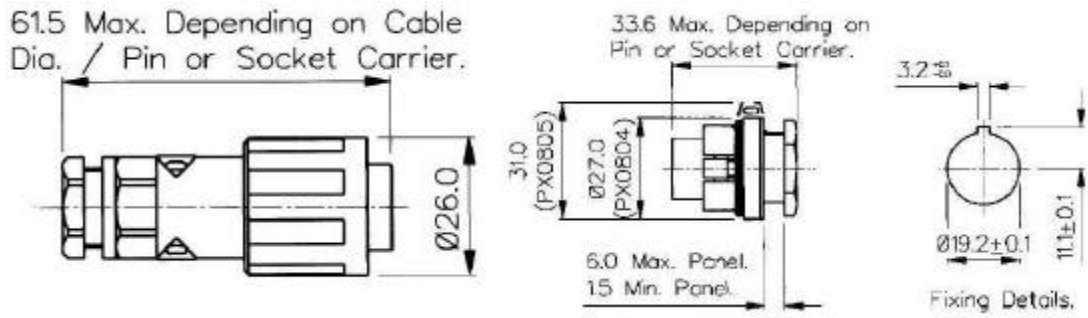


Figure 79 - Technical dimensions of the Mini Buccaneer connectors

For the current intensive connectors, the 900 Series Buccaneer range was chosen since it was the only range that would satisfy the 24 amp current requirement, presenting a number of connectors with a current rating of 32 amps. The pin options consisted of 2, 3, 4, 5, and 7 poles.



Figure 80 - Examples of the 900 Series Buccaneer connector range by Bulgin

The angled chassis mounted connector (top right with respect to Figure 80) combines with the bulkhead adaptor moulding (bottom right) to form a 90° connector.

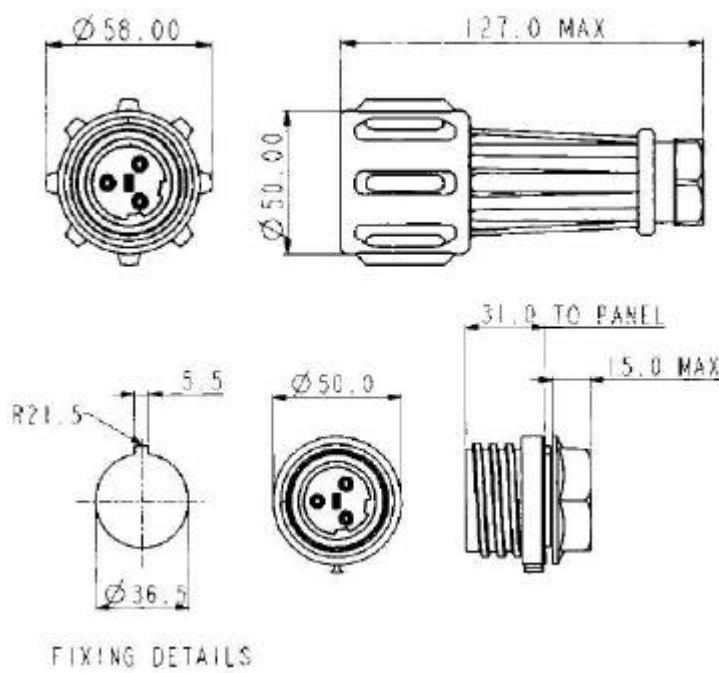


Figure 81 - Technical dimensions of the 900 Series connectors

The only task remaining in the selection of the connectors was to choose the right configuration. However, this proved to be a balancing act, due to the limited number of pins available in the 900 Series range. Firstly, it was decided to join the ground lines of the twisted pairs together for the shore-to-ROV and ROV-to-shore signals, so the number of lines was reduced to seven pins. Now a 7-pole 900 Series connector could be used. However, when companies were contacted with respect to ordering parts, it was discovered that the 7-pole 900 Series connectors were not available, the highest number of pins available being only 5-pole. This was an unfortunate setback for the connector configuration, but another solution was found by rearranging the connector layout for the tether. It was decided that instead of using only one connector for the tether, two connectors could be used – one for the power lines, and one for the signal lines. Therefore, it was resolved that a two-pole 900 Series Buccaneer connector would be used for the two power lines (24V and ground), while a 6-pole Mini Buccaneer connector could handle all three twisted pairs used in the tether. This would require the tether to be split into two parts, but this would not be too hard, as can be seen in the next section (Loom configuration).

The pump connectors were quite simple to select, since the total number of pumps could be split into two groups, each comprising eight pumps equalling four channels. If all the 24V lines for each group were combined onto one pin, then each connector would only need four channel control lines and the 24V line (five lines in total),

resulting in two 5-pole 900 Series connectors being used for the whole task. The 900 Series were chosen due to their current handling capabilities, since the pumps are the main current draw in the system. Just as the tether had to be split into two parts, so the pump cables would have to be joined together, changing four two-core cables into one five-core line. This is further detailed in the next section.

In summary, the connectors chosen for the main circuit enclosure are as follows:

- Sensor enclosure link – 1 x 8-pole Mini Buccaneer connector
(plus one at other end of cable to connect onto sensor enclosure)
- Tether – 1 x 2-pole 900 Series Buccaneer connector
1 x 6-pole Mini Buccaneer connector
- Pumps – 2 x 5-pole 900 Series Buccaneer connector

Now that all the connectors had been chosen, the next step was to position them on the main circuit enclosure. The main difficulty in placing the connectors lay in the fact that the 900 Series connectors are approximately 50mm in diameter and extend about 130mm from the enclosure wall. The Mini Buccaneer connectors were less of a problem with a diameter of 26mm and length of around 60mm.

Another catch in the positioning of the connectors on the enclosure walls was due to the fact that, although the external dimensions of the enclosures seemed favourable, the internal dimensions were smaller because of wall thicknesses, corner shoulders for the lid connecting screws, and the height of the enclosure without the lid attached. This was overcome by careful consideration of how to mount the connectors, and also the ability to attach connectors with a special 90° mounting fixture.



Figure 82 - The location of the connectors on the main circuit enclosure

Since it was not possible to attach connectors to the left and right sides of the box, due to the location of the pumps in the internal structure, the final layout consisted of the tether signal and one of the pump connectors side by side on the rear face, and the sensor signal and the other pump connector on the front face, see Figure 82. Meanwhile, the tether power connector was attached to the top of the lid by a 90° mounting fixture. It was not possible to attach the connector straight onto the lid since it would protrude too far upwards, interfering with the external shell location. This layout can be seen in Figure 82.

31.9 Loom Configuration

31.9.1 Tether

An important consideration in the loom configuration was to calculate the voltage drop across the tether, so that the supply voltage on the shore was set correctly to provide 24V at the ROV itself. Therefore, the first task was to establish the resistance of the tether power lines. Five wires in the tether are used for each power line, since ten non-signal wires are provided in the tether. The cores of these lines are believed to be copper, and the expected peak current is approximately 24A (the current drawn by the circuit is almost negligible).

Therefore, using the below equation, the resistance per metre of tether was calculated, where \tilde{n} is the resistivity, l the length and A the area of the material.

$$R = \frac{\tilde{n}l}{A}$$

Equation 18

The resistivity of copper is $1.72 \times 10^{-8} \text{ } \Omega\text{m}$, while the radius of the core is 0.41mm, giving an area of about 0.53mm^2 per core. Therefore, for five cores, the total area cross-sectional area is $2.64 \times 10^{-6}\text{m}^2$. When these values are entered into the equation along with a length, l , of 1m, the resulting resistance is $0.652 \times 10^{-2}\text{ } \Omega$ per metre. This value can then be fed into the Ohm's Law equation, below, with a current value, I , of 24A.

$$V = IR$$

Equation 19

The resulting voltage drop per metre is, therefore, 0.156 volts. When this is applied to a tether length of 20 metres, the total voltage drop is 3.12V. Therefore, the supply voltage on the shore should, in fact, be $24 + 3.12 = 27.12\text{V}$.

31.9.2 Cable combination and splitting

As mentioned in the previous section, some of the cables connecting devices together have to be split or combined to suit the connectors on the main circuit enclosure. This can be achieved by joining the relevant lines together with an appropriately rated junction block (readily available from most DIY stores) and then sealing the section of cable with self-amalgamating tape to ensure that it is waterproof. A diagram of this is shown below.

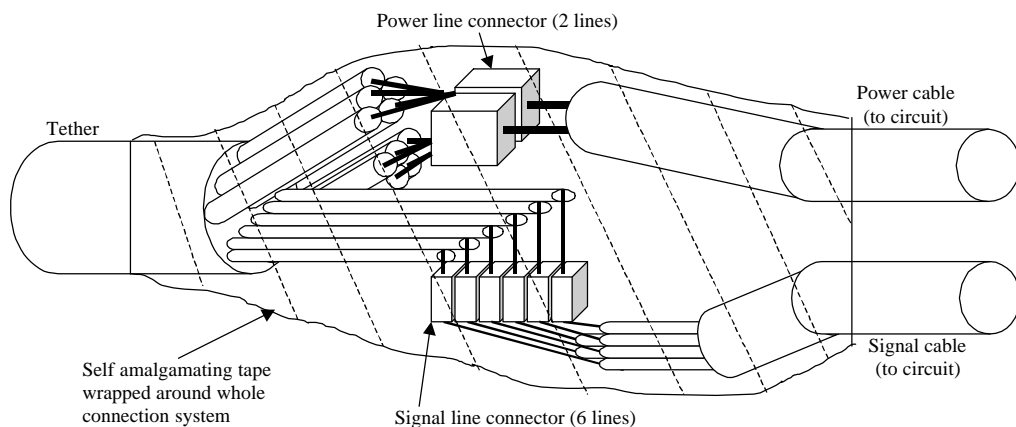


Figure 83 - Diagram of the split of cables on the tether

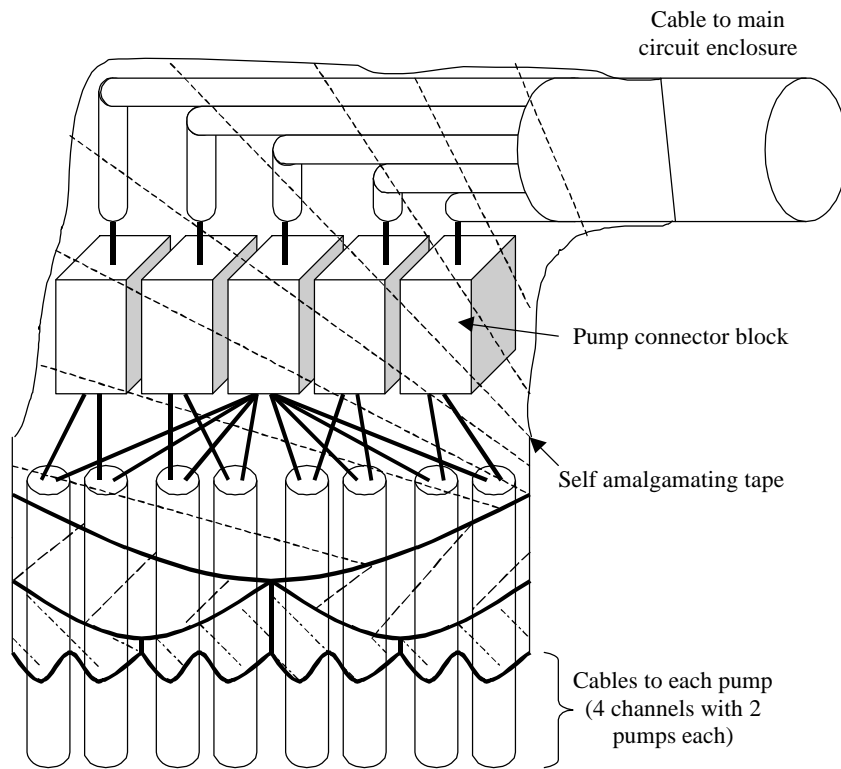


Figure 84 - Diagram of the combination of the pump cables into one single cable

31.9.3 Loom layout in ROV

As the final part of the total solution involving the enclosures and connectors, the wiring loom can now be laid out to show the final set up of the electronics systems in relation to each other inside the ROV.

The cables connecting the various devices are all to a suitable current rating, large core cable handling the high currents in the tether power lines and the pumps, while smaller core cable was used for the signal lines in the tether and the sensor / camera link cable. All cables incorporate a certain amount of slack to allow enclosures and systems to be moved around inside the ROV, if adjustment of position is required, without stressing the connections and connectors.

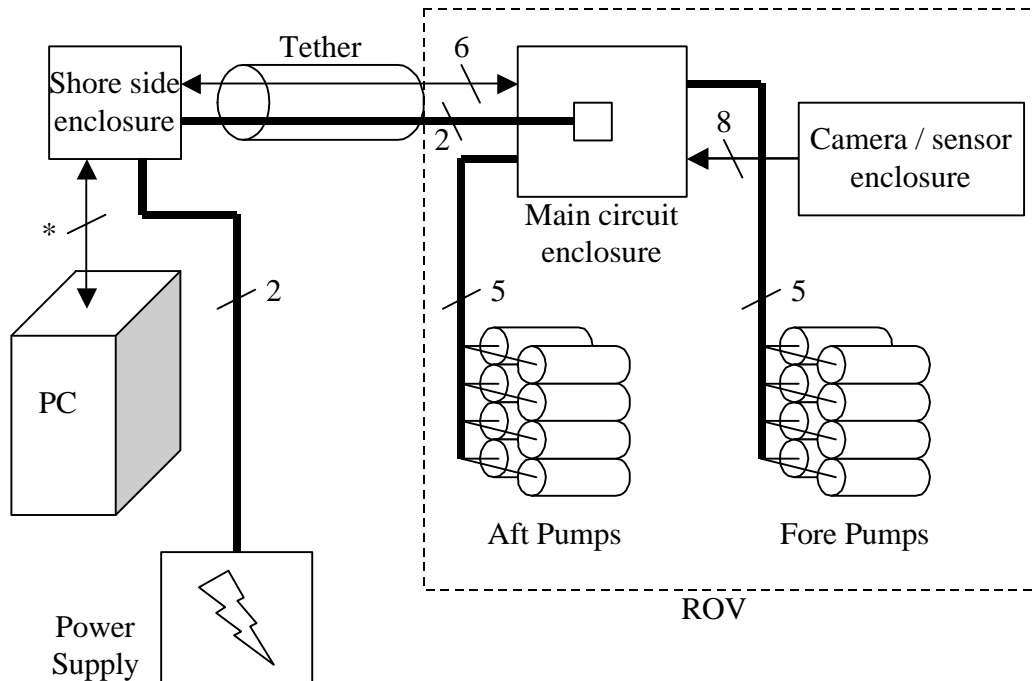


Figure 85 - Diagram of loom layout

Referring to Figure 85 the '*' means that the link between the shore side enclosure and the PC consists of three lines for communication with the ROV, and can also include SCART and S-Video signals (2 lines each) that can either be connected to the external TV card of the PC, a television, or both devices, depending on the user's preference.

Referring to the above diagram, the lines in each cable are as follows:

- PC to shore side enclosure: PIC to PC signal, PC to PIC signal, ground, SCART pair, S-Video pair.
- Power supply to shore side enclosure: 24V, 0V.
- Tether: Three twisted pairs, consisting of PIC to PC signal, PC to PIC signal, and camera signal. Also, two power lines (24V, 0V), each of which takes up five physical lines in the tether to accommodate current requirements.
- Camera / sensor enclosure to main circuit enclosure: Power (12V), signal, and 0V for camera; power (12V), receive, transmit, analogue signal, and 0V for sensor.
- Main circuit enclosure to pumps (x2): 24V supply, and four channel lines (controlled by MOSFETs).

(All thick lines in diagram denote higher current carrying capabilities to deal with requirements of pumps.)

31.10 The Future

The circuit design was moving on the right lines to produce a very compact design. However, there are a number of improvements that could be made:

- The use of surface mount technology – this could dramatically reduce the board size
- The use of CANbus technology – this would simplify the whole communication system and also provide feedback confirming whether the pumps were working properly.
- A change of microcontroller – If a microcontroller featuring two USART ports can be found this would simplify the software. If the same chip had eight PWM outputs this would allow far greater control and more complex manoeuvres.
- A change of sensor – the sensor chosen works very well. With a larger budget, a smaller sensor package could be purchased or one that incorporates a depth sensor.
- Improved design for the connection of pumps to the MOSFETs
- Gimballed camera this would enhance the observation ability of the ROV by being able to look around whilst keeping the ROV stationary.
- 7 pin 900 Series connector for the tether – this would simplify the wiring of the ROV system, and also reduce the volume taken up by the main circuit enclosure.

32 PC Control Software

The requirements were determined so that the scope of the software could be determined and hence the program could be designed and written in a logical manner.

32.1 Functional Requirements of the Software

32.1.1 Initial Main Problems

A new system is required to control the ROV because the old system was based on opening and shutting 12 valves and running the pump at variable speed, whereas the proposed ROV will have multiple pumps that are switched on and off and can run at independent speeds. This should increase performance by minimising the losses due to the valves in the old system but it requires a more complicated approach to control since the system is switching between manoeuvres to perform the desired motion.

Speed, in this case, is determined by running the pump at full power for varying amounts of time to lower the average current. For example:

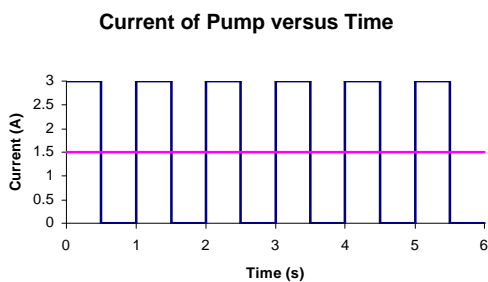


Figure 86- Average Current 50%

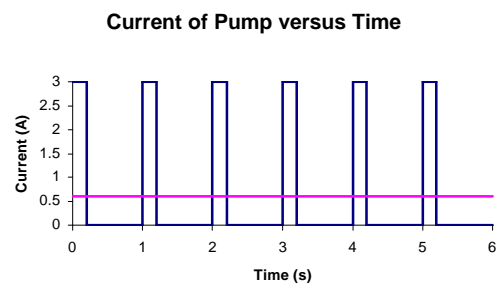


Figure 87 - Average Current at 20%

This average current is then proportional to average mass flow rate of the jet, which is a measure of the velocity of the jet:

$$\frac{dm}{dt} = rAv$$

Equation 20

The nomenclature for this equation is:

- $\frac{dm}{dt}$ = mass flow rate
- r = density
- A = cross sectional area
- v = flow velocity

However it is likely that there is a constant period that the pump is on in all cases so that the ROV actually moves in the desired direction.

32.1.2 Main Requirements Of The Application

The primary functional requirements of the software interface with the ROV were determined by the group to be:

1. Communication with the ROV is required for the control software to be successful.
2. To allow the user to control the pumps of the ROV for the desired motion.
3. To give feedback on the ROV's attitude and other information in a user-friendly manner.
4. To allow control of the ROV by the use of a joystick.
5. To keep the ROV's roll at zero. It was also proposed that a secondary functional requirement would be:

1. To display the output of the camera on the computer screen.

32.1.3 Internal Processing of the System

Figure 88 shows the system overview of the software code. When the application is first run the setup window is opened, which provides the user with a set of options:

1. Select Primary Control
2. Keyboard Configuration
3. Detect Joystick
4. Calibrate Joystick
5. Configure Joystick
6. Simulate ROV
7. ROV

When the program is first run, most of these options will be greyed out since the control interface has to be set up before the user can control or simulate the control of the ROV. Once everything is configured to the program's satisfaction, then the "Simulate ROV" and "ROV" buttons become enabled to allow the user to access the control of the ROV.

The simulation mode of the application allows the user to test how the control set-up works and how the ROV responds to the user's input. It also allows the user to become familiarised with the displays.

The control mode of the program allows the user to communicate with the ROV and send the desired signals to the PIC, where they can be processed and used to control the switches to the pumps.

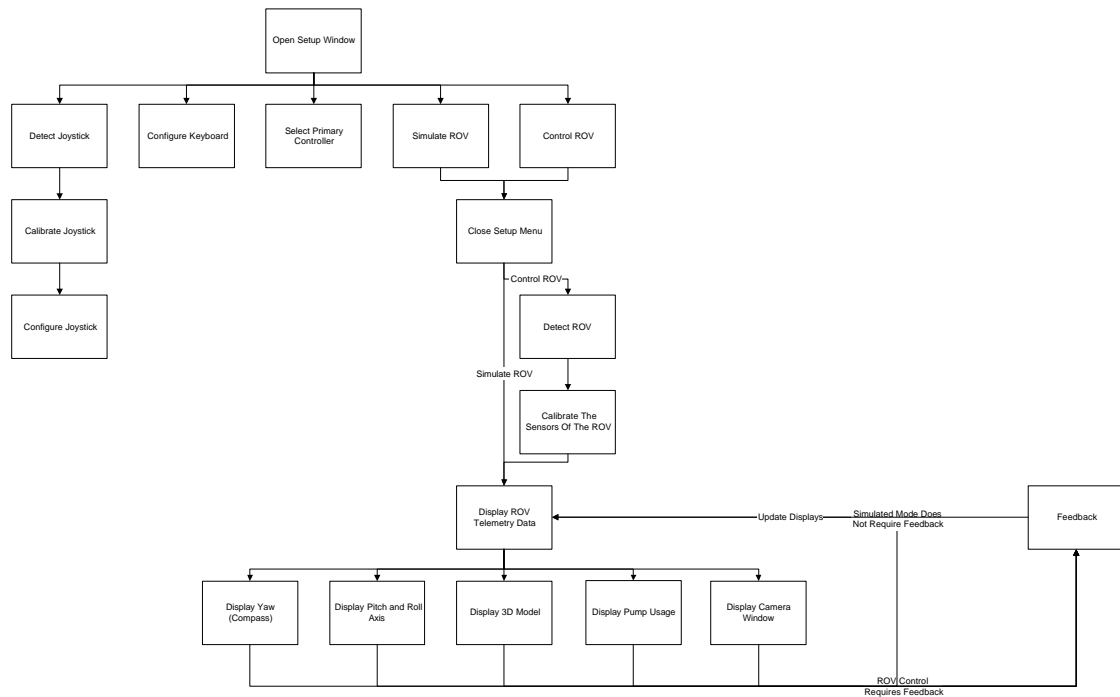


Figure 88 - Software Overview

The feedback will be provided by the PIC since this speeds up the overall time of the ROV's response to changes in its environment (for example currents and eddies) and changes in the user input that lead to changes in its attitude.

32.1.4 Logical Design of Windows Within The System

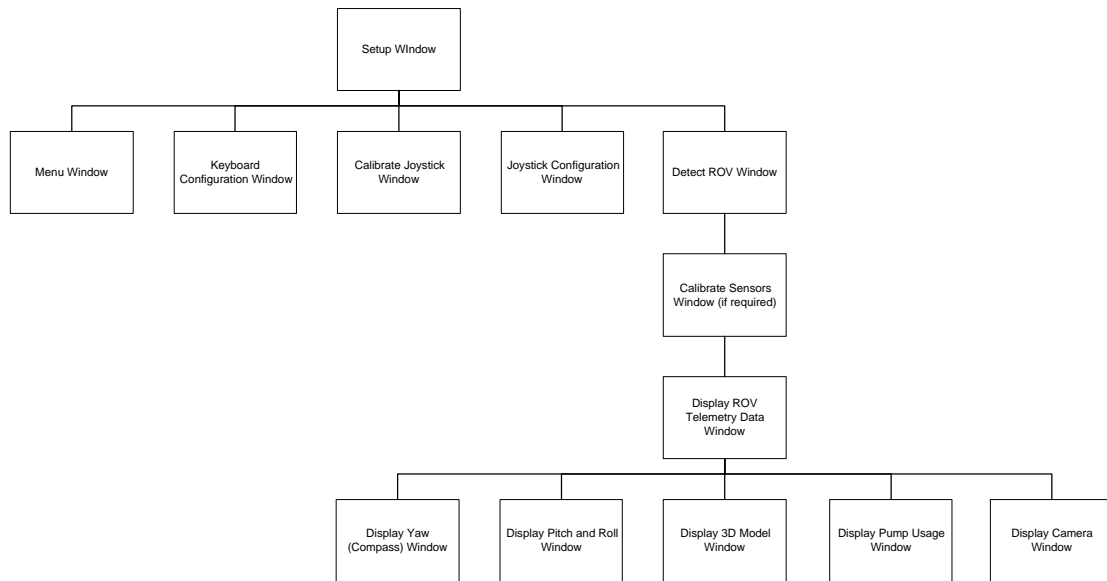


Figure 89 - Logical Design of Windows

32.1.5 Integration / Communication with Other Systems

There are only two external software programs that the current control software communicates with in any way. These are the camera software and the PIC software. The potential exists to split the camera signal to multiple televisions, via SCART cables and / or computers, currently via the S-Video input in Hauppauge's WinTV cards.

The camera is currently proposed as a separate software program so that the control program does not have to be installed on multiple computers. Each extra computer only requires the camera program.

32.1.6 Users Of The System

The intended users of the system are dependent on the market for the submersible ROV. The market is currently seen to be:

- Observational roles (searching for faults in pipes, cables etc.)
- Recreational roles (the latest must-have gadget)

Hence the intended users are seen to be companies working in maintenance of underground pipes, cables etc. and relatively wealthy people who would use it as an executive toy.

The ROV only requires one user to control it. There is no requirement for co-operative control or multiple-access to the same data on various computers.

32.2 Non-Functional Requirements of the Software

32.2.1 Hardware Configuration

The hardware configuration of the control system is as follows:

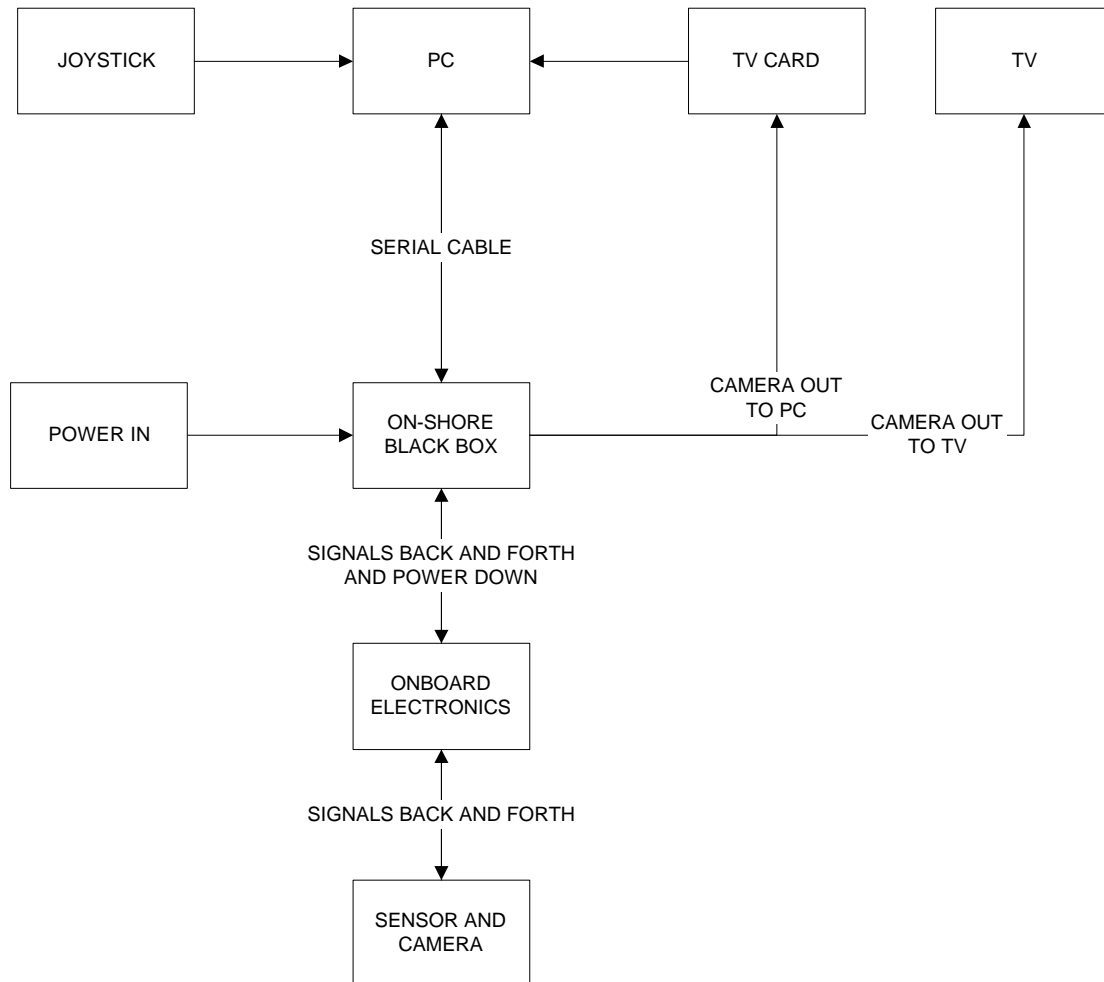


Figure 90 - Hardware Configuration

32.2.2 Hardware And Environmental Constraints On The System

A laptop PC is ideally suited for the task of controlling a small, low cost ROV because it is as portable as the ROV. The laptop does not degrade the transportation performance of the entire system nor does it affect the performance of the control system as a whole.

The only disadvantage with the use of a laptop is that currently it requires an external TV Card to display the camera output on the screen. It would be more convenient if the TV Card was internal. However with the limited space in a laptop this is not practical.

The laptop, if the system was to remain portable, could potentially get wet in the use of the ROV, hence an alternative or some form of waterproof protection needs to be studied.

32.2.3 *Alternative Technical Environments For The System*

It is possible and perhaps beneficial to have a dedicated on-shore control system. However this then poses a problem with upgrade-ability and growth of the system. It could also have cost implications.

32.2.4 *Other Considerations of the System*

The system is stand-alone.

For the growth of the system it will be required that additional easily installed configuration models are available if and when the consumer purchases a new ROV. This would then require the control software to understand a simple configuration file, containing amongst others, number and layout of the jets, mass and buoyancy of the ROV, the force an individual jet produces and characteristic lengths (e.g. moment arm(s) and buoyancy to centre of mass distance).

Also our particular ROV has a cylindrical cross section and so implementing roll is unnecessary, hence the requirement to maintain the roll angle at zero. However other configurations of ROV may not be cylindrical so it may be beneficial to implement roll as a controllable manoeuvre. The 'test' mode shows that roll is feasible with our configuration and water jet propulsion.

The control software can be maintained by re-installing any damaged files that occur, simply by re-running the installation program again.

32.3 Development

32.3.1 *Gantt Chart of Progress of Software Development*

The Gantt Chart, see Appendix AA, shows the proposed software development plan and the actual progress made. The actual development differed from the proposed development in two major areas. Two tasks had to be split – for external reasons (revision and exams). For other tasks the duration was either longer or shorter than predicted due to unexpected difficulties or ease of the actual task.

32.3.2 *Constraints*

The constraints were time and the fact that many of the software techniques were unfamiliar at the beginning of the project. For example:

- Camera Interface
- Serial Communication
- OpenGL
- Independent Threads

32.4 DirectX – An Overview

32.4.1 Goals

Microsoft's DirectX® Standard Developer's Toolkit (SDK) provides resources to develop high performance, real-time applications on current and future systems.

The DirectX SDK provides a robust and standardised operating environment for the development of DirectX applications. Most importantly it was well documented within Microsoft's Developers Network Library with plenty of samples and other information required to use it.

DirectX gives the benefits of device independence without losing the benefits of direct access to the hardware.

DirectX provides a consistent interface between hardware and applications, reducing the complexity of installation and configuration. It uses the hardware to its best advantage. By using the interfaces provided by DirectX it is possible to take advantage of hardware features without being concerned about the implementation details of that hardware.

This then allows the software to be portable to other systems with different hardware.

32.4.2 DirectInput

DirectInput is a facet of DirectX and is the only aspect of DirectX used in this control software. It is used to provide support for the input devices used in this application, namely the joystick and the keyboard.

It can also provide support for force-feedback (input/output) devices. Therefore it would be possible to add extra code to generate the feedback response of the actual ROV, therefore giving the user a more accurate and intuitive feel as to how the ROV

is responding to his commands. However this requires a joystick that supports force feedback. This then generates an additional requirement on the joystick.

32.4.3 Architectural Overview of DirectInput

The basic architecture of DirectInput is the DirectInput object, which provides the interface between the software and the device, and the object for each input device that provides data, for example the joystick or the keyboard. In addition each device has objects that represent the functionality of said device, for example keys, axes or buttons.

In the interests of speed and responsiveness, DirectInput works directly with device drivers, bypassing the Windows message system.

DirectInput enables an application to gain access to input devices even when the application is in the background. This is useful if you are manipulating data in more than one window via the use of DirectInput data when any or none of the windows may be selected. This is the case in the current PC control software where there are multiple windows (telemetry data, graphical displays, camera display) any one of which can be the active window. In the interests of ease of use it was decided that the use of the joystick and keyboard would be non-exclusive to the “*host*” window, so that it would not matter which window was selected. In addition this meant that as the camera window was the last to be created it was the default active window and hence the user could active its menu commands via the keyboard.

32.4.4 The DirectInput Object

The DirectInput object in an application represents the DirectInput subsystem. The DirectInput subsystem is all the input devices that the computer has installed, for example the mouse, the keyboard and a joystick. It is used to enumerate and manage these input devices.

32.4.5 The DirectInputDevice Object

Each DirectInputDevice object, as mentioned before, represents one input device such as a mouse, keyboard, or joystick. The methods of the DirectInputDevice object are used to gather information about the device, set its properties, and get data from it.

32.4.6 *DirectInputDevice Object Instances*

The DirectInputDevice object also has objects of its own, sometimes called object instances. These objects represent the controls available on an input device. For example the axes and buttons on a joystick.

32.4.7 *The DirectInputEffect Object*

The DirectInputEffect object is not used in the current code, so it is included for the sake of completeness. A DirectInputEffect object represents a force feedback effect that you have defined. It is used to manipulate the effect on the input/output device. Therefore it would be used if you wished to generate the force feedback result of the ROV and pass this information back to the user so that the control of the ROV would be even more intuitive.

32.4.8 *Integration with Windows*

DirectInput works directly with the device drivers, therefore it suppresses or ignores mouse and keyboard messages. It also ignores mouse and keyboard settings made by the user in Control Panel.

In DirectInput when using buffered data on a keyboard, DirectInput interprets each press and release as a single event, with no repetition. When using immediate data, DirectInput is concerned only with the present physical state of the keys, not with keyboard events as interpreted by Windows.

For the mouse, DirectInput ignores Control Panel settings such as acceleration and swapped buttons. Again, DirectInput works directly with the mouse driver, bypassing the subsystem of Windows that interprets mouse data for windowed applications.

As DirectInput works directly with the driver of the device it will recognise settings within the driver itself.

For a joystick, DirectInput uses the calibration data set by the user in the Control Panel. However if a joystick is not installed properly or not calibrated properly then the calibration data will be incorrect and invalid, thereby making the ROV almost impossible to control. Therefore the software as written also includes a set up section for the calibration of the joystick so that it can be fine tuned by the user for the control of the ROV.

32.4.9 Use of DirectInput

DirectInput was used to create non-exclusive access to the keyboard and joystick when either simulating or controlling the ROV so that it didn't matter what window if any was selected of the program, as long as the application was running.

32.5 ActiveX – An Overview

32.5.1 Goals

There are thousands of prebuilt components that can be plugged into your application to extend its functionality instantaneously – these are ActiveX controls. An ActiveX control is a software component that can be plugged into many different programs and used as if it was a native part of the program.

More technically an ActiveX control is a set of functionality packaged in a COM (Component Object Model) object. This COM object is self-contained, though it does not have the ability to run by itself.

ActiveX controls are intended to simplify the development process by increasing the ease by which the developer adds functionality to his application. In addition ActiveX components also standardise the way in which applications and controls appear to a user thereby increasing the user's familiarity with the controls' behaviour and hence the ease of use of the application.

For example drop down list boxes always look similar and behave in the same way.

32.5.2 Common ActiveX Controls

The most basic of ActiveX controls are commonplace. These include text boxes, drop down lists, radio buttons and check boxes to name a few and are used in most applications.

This software program uses some of these common ActiveX controls for the set-up of the ROV-User interface.

32.5.3 Specialised ActiveX Controls

The application also uses two specialised ActiveX Controls to extend the application's functionality. These are the controls for communication with the ROV (mscomm32.ocx) and for displaying the camera input in a window on the computer

screen (hew_WinTV.ocx). Mscomm32.ocx is a standard ActiveX control included with Visual C++ by Microsoft. Hauppauge however provides hew_WinTV.ocx so that developer's can write their own software using WinTV cards.

These ActiveX controls allow the developer to very easily attach a component for communicating with a serial port and for displaying the TV card signal. The hew_WINTV.ocx control also allows you to add some additional functionality. For example you can capture camera images simply, this is described in **Error! Reference source not found..**

32.6 PC Software Overview

32.6.1 Introduction

The PC code was written in Visual C++, using Microsoft Visual C++ version 6. The requirements of the software also made it necessary to use OpenGL and DirectInput, as already mentioned. Visual C++ uses a different structure to C and it is more similar to the OpenGL program structure. Visual C++ is an event driven language. It waits for the Windows Operating System to send messages and if any of those messages are present in the message map of the selected window then the code within that function is executed.

However you can use independent threads, which once they are started operate independently of the rest of the program. In other words they can be considered to have a similar relationship as the application does to the operating system. The independent thread was required for the switching manoeuvres, which meant that the signals sent to the PIC, had to occur independent of the user input until the variables were updated.

32.6.2 System Requirements

The software is designed for use on Windows 95/98 operating systems.

The software requirements are governed by the requirements for Windows 95 16Mb RAM and a Pentium 200MHz processor (recommended minimum). Though Windows 95 will run on a 486 but very slowly.

Higher processor speed is recommended and / or a graphics card that OpenGL routines can take advantage of since once you are controlling the ROV updating of four OpenGL windows takes place.

To take advantage of the joystick control capabilities of the software a joystick is required.

Also a Hauppauge WinTV Card (with a S-Video in-socket) and appropriately installed software is required to display the camera output on screen. In addition, according to Hauppauge, you need their OCX control installed. This OCX control file is installed via the use of the install program. If it doesn't already exist then it is installed to the windows\system folder and if it does exist then it is installed into the application folder where it is solely used by the application. This is to avoid conflicts with other programs and other problems.

The file "glut32.dll" is also required and is included in the installation in a similar manner as the OCX file.

DirectX 7.0a or later is also required to be installed. DirectX 7.0a is included in the application folder under "directx".

32.6.3 Installation

To install the program run the "ROV.msi" file and specify the install folder. This will create a shortcut file for the ROV executable on your desktop and in the start menu ROV program group. In addition a Camera Display shortcut in the program group is created, which runs the stand-alone application, displaying the camera output.

A copy of the user manual and the "pictures" folder are also included and shortcuts to them exist in the ROV program group.

If there is problem with installing the software and the error message says that it requires an upgraded windows installer a version of windows installer can be found on the CD, called "instmsia.exe".

32.6.4 Running the Software

The software is made up of two executables, ROV.exe and cppOCX.exe. The cppOCX.exe executable is a stand-alone program that displays the output of the S-Video socket from the TV Card, in our case the camera. ROV.exe calls cppOCX.exe

from within itself, therefore do not change the name of `cppOCX.exe` nor move it in relation to `ROV.exe`. Both the executables must be in the same directory.

After installation, the program can be run either directly from its executable or from one of the two shortcuts.

To test the camera in Windows, run the program `cppOXC.exe` either directly or via its shortcut.

32.6.5 Set-up Menu Window

Once the program has loaded the user setup interface will be displayed as shown in Figure 91. The window contains multiple options. There are two methods of enabling the “Simulate ROV” and “ROV” buttons:

1. First select primary controller for the ROV and then proceed to configure that controller.
2. Configure the controls first and then select the primary controller.

32.6.6 Control

If the keyboard is selected then any joystick or joystick specific inputs, such as sensitivity, will not have any effect on the signals sent to the ROV and there will be no changes to any of the displays.

If the joystick is selected as the primary control then the user still has to tell the application to detect the joystick so that it can be calibrated and configured the joystick. The keyboard will still be functional. This is because the some of the user inputs can be configured to be keyboard inputs rather than joystick ones. This depends on the functionality of the joystick and / or user preferences for control.

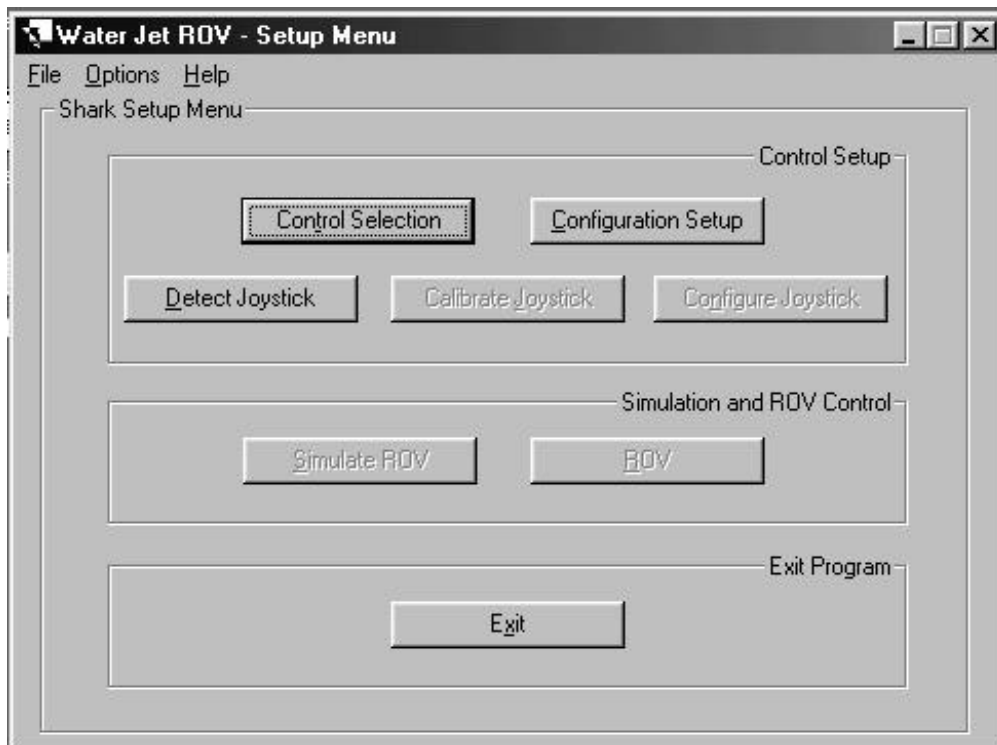


Figure 91 – The User Setup Interface

The keys allowed for configuring the keyboard are the standard alphabetical ones. However as yet there is no support in the main program for differences between lower and upper case. Nor is there support for integers as controls. This option could exist in later versions of the software and would depend on customer requirements.

The inputs are only allowed to be of one character length and are also validated (checked against each other to ensure no duplicates) when the cursor changes its focus. This character is validated to be one character long and different from all the others.

The joystick on the other hand has to be calibrated initially so that the program knows the zero values when the joystick is in its neutral position and its maximum deflection in all directions from the neutral point.

For the calibration of a successfully detected joystick, the user is asked to perform a standard joystick calibration. For example leave the joystick at rest and move it to its extremes. If a joystick calibration file already exists there is an option to skip the calibration of the joystick and move on to configuring the joystick.

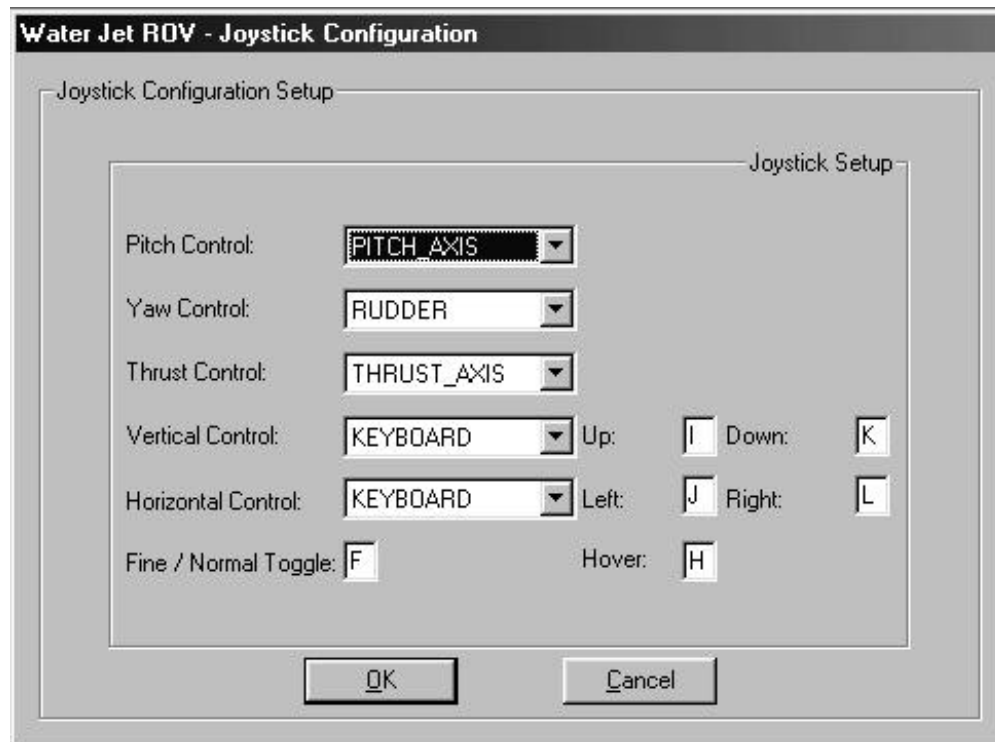


Figure 92 - Configure Joystick

The calibration of the joystick detects whether the joystick has rudder and / or thrust axes in addition to the standard pitch and roll axis. If either or both are present then whichever are present are calibrated.

To configure the joystick select the control on the joystick that is going to control a specific response on the ROV.

Using a mixture of keyboard and joystick controls is also possible. Referring to Figure 92, if “KEYBOARD” control is selected for one of the motions of the ROV then text boxes are shown so that keys can be added.

For the joystick it is also possible to vary the sensitivity. In normal operation the pumps can operate at 100% with the full motion of the joystick whereas in fine control the pumps can operate at 20% with the full motion of the joystick per manoeuvre (up to 100%).

Once the controls are set up and configured correctly then the main section of the program can be run to either simulate the ROV’s response or actually control the ROV.

32.6.7 Calibrating the Sensors

If the user wishes to communicate with the ROV, the sensor on board the ROV must be calibrated. This does not need to be performed by the software since the sensor can be calibrated for its environment and it will then store the calibration data. The software supplied with the sensor can perform the calibration. For the calibration of the sensors of the ROV, the program needs to run the multipoint calibration process that is included within the sensor. This means that the ROV must be turned slowly and tilted as much as possible, so that as many data points as possible can be stored so that the sensor can perform accurately.

32.6.8 Simulating The ROV Or Controlling The ROV

Using the application to either simulate the control of the ROV or to actually control it, the same user interface is displayed as shown in Figure 93.

The controls will respond in the same way in both modes of operation, but in the simulated control the ROV's rotational transformations are calculated depending on the desired attitude of the ROV, whereas they are normally calculated by the ROV’s actual response from the sensor input.



Figure 93 – The ROV User Interface

The translational transformations (up, down, port, starboard, forward and backward) are based on desired power input since there is no way on the current ROV to measure translational speed. This would obviously be a further development for a release version of an ROV, since for the user it would be easier to understand speed than desired pump power output. This is more useful if a variable power/speed setting is used.

The pitch window displays the pitch of the ROV and its roll, if any. The feedback should maintain the roll of the ROV at zero.

The feedback should also maintain the attitude of the ROV at the desired user attitude of pitch and yaw.

32.6.9 Camera Window

In all modes the camera window is displayed. If the camera is working correctly then you will get an image displayed in the window of what the ROV is “seeing”. The camera window has a menu (refer to **Error! Reference source not found.** for further details).

32.6.10 The Application's Menus

This program contains three menus. One menu is in the setup of the control system window, one menu is on the camera window and the third is on the telemetry window.

The functions on the setup menu are included in the 'File' menu, the 'Help' menu, the 'Mode' menu and the 'Options' menu.

They are described in more detail in this section.

The 'File' menu contains the functions:

- The 'Delete' function deletes all the text files currently used by the application.
- The 'Exit' function exits the ROV application.

The 'Options' menu contains the function:

The 'Splash' function has the ability to enable or disable the Splash Screen. If there is a check mark next to the menu option then the splash screen is enabled else it is not.

The Mode menu contains the options where you can select which mode of operation you wish to use. Simulate and ROV only become enabled when the "Simulate ROV" and "ROV" buttons become enabled on the main screen. Test is performed independent of user input and is therefore always enabled.

Test performs a series of tests including all the translational motions possible to the ROV and the rotational ones.

The 'Help' menu contains the about function, which displays the "About ROV" window.

There are only three functions in the camera menu and they are all in the 'File' menu. Every time the program is started, the images will restart from 001.

When the 'Capture...' function is clicked it captures the current camera input and saves it to a .jpg file. The file will be saved in the 'pictures' directory. The name of the file will be cameraxxx.jpg, where xxx stands for 001, 010 or 100 for example. Pressing 'Alt' and 'C' simultaneously can also activate the capture function.

This is a drop down menu that leads to a list of options: a '1 Second Delay Capture', a '2 Second Delay Capture', a '5 Second Delay Capture' and an 'End Capture' function.

Basically the Timer Delay Captures once initialised capture the camera image and save it the same way as described previously, however they do it continuously with the specified delay between images.

'End Multiple Capture' stops the continuous capture of images.

There are only two menus on this menu bar.

The only function on the File menu is the Reset function. This sends a command to the ROV to reset itself.

The control menu allows the user to switch between controllers – i.e. keyboard and joystick.

32.6.11 Testing

The application also has a testing sequence, which does not require the user to calibrate the controls as the application sends the desired information, based on the testing routine, to the ROV. (Refer to 34.1.5 or details)

32.6.12 Communication

The PC software generally only has to send information about what pumps to turn on to the PIC. This is done by effectively assigning jets 1 to 8, the following values: 1, 2, 4, 8,16, 32, 64, 128. Then the combination of the four jets for the 12 possible manoeuvres (typically ten except for testing) gives a unique 8-bit word of the format 01010101. The '1's correspond to which pumps to turn on.

Other hexadecimal codes that are not used in these manoeuvre combinations can be used for specific functions. For example turning hover on and off.

The port must be initially opened at 9600 baud rate, no parity, and capable of sending 1 start bit, 1 stop bit and 8 bits of data. This is the default setting for the sensor and the PIC hence it is simpler to maintain the default settings. However with future higher performance ROV's this may be restrictive and a slightly different approach in the software must be taken. In that the sensor must be configured first by using its default settings then the PIC to match and lastly the port of the computer.

The MSCOMM control used sets up and opens a port as follows:

```
m_CommROVCtrl.SetCommPort(1);  
m_CommROVCtrl.SetSettings("9600, N, 8, 1");  
m_CommROVCtrl.SetSThreshold(1);  
m_CommROVCtrl.SetRThreshold(1);  
m_CommROVCtrl.SetPortOpen(TRUE);
```

The SetCommPort method sets the communication port that the program is going to use in this case COM1. In a commercially viable piece of software it would be required that the user could specify which port to use.

The SetSettings method then sets up the settings of the port in this case 9600 baud, with no parity, 8bits of data and one stop bit.

The following two methods SetSThreshold and SetRThreshold set the send and receive thresholds therefore telling the program when to process the onComm function, which processes all the received data. In this case the received threshold is set at 1 byte, so that when the program receives at least one byte of information then the onComm function is called.

This method of communication is event-driven and allows greater flexibility than polling the input buffer for data.

32.6.12.1 Sending Binary Data

To send the commands to the PIC it is required that they are sent in binary format. This is done as follows:

```
CByteArray Byte;  
Byte.InsertAt(0, COMMAND);  
m_CommROVCtrl.SetOutput(COleVariant(Byte));
```

Firstly create a CByteArray, called Byte, and into that at the first and only location the command that you wish to send to the PIC is placed. Then with the SetOutput method the Byte is converted to a VARIANT and sent.

32.6.12.2 Receiving Binary Data

Receiving binary data is slightly more complex and the code is as follows:

```

if(m_CommROVWait.GetCommEvent() == 2)
{
    COleVariant vVar(m_CommROVWait.GetInput());
    hr = SafeArrayGetUBound(vVar.parray, 1, &ILen);
    if(hr == S_OK)
    {
        ILen++; //upperbound function is zero based index
        hr = SafeArrayAccessData(vVar.parray, (void**)&pAccess);
        if (hr == S_OK)
        {
            for(int i = 0 ; i <= ILen ; i++)
            {
                if(pAccess[i] == ACKNOWLEDGE)
                {
                    received = ACKNOWLEDGE;
                }
            }
            SafeArrayUnaccessData(vVar.parray);
        }
    }
}

```

GetCommEvent method is used to get the last event or error code, the receive event is coded as 2. Initially the input is taken from the input buffer via the GetInput method and then stored in a VARIANT called vVar. For receiving binary data it is required to use SAFEARRAYS. The command SafeArrayGetUBound gets the number of bytes, starting from zero, in the input buffer and stores that size in ILen. Then the command SafeArrayAccessData gets the data and stores it in the array pAccess, which can then

be searched for data and acknowledgements of commands. `SafeArrayUnaccessData` clears the input buffer.

32.6.12.3 Updating The Displays Due To Sensor Data

A limitation with the software is that the pitch, roll and yaw values are only requested each time the manoeuvre loop starts. The manoeuvre loop is for the switching on and off of the pumps when multiple manoeuvres are being performed or for simulated pulse width modulation. Hence the more manoeuvres that are being performed the longer the delay between requests.

A solution to this problem is to create another independent thread that continually loops round sending requests for pitch, roll and yaw. However this may require synchronisation with the other communication thread.

32.6.13 Simulated Pulse Width Modulation

The ROV's Control Software has two modes of operation:

1. Variable thrust mode.
2. ON-OFF mode.

Due to the switching manoeuvres it was required that the state of the jets, on or off, be updated almost independent of user input. Hence an independent thread was used which told the ROV what jets to turn on and which to turn off and when.

This then led to a slight modification in the code where the total manoeuvre time was kept constant however the pumps were not always on in this period. The time that the pumps were on was proportional to the user input for that particular manoeuvre. A simplified pseudo example of the code is as follows:

Consider for example that the user wishes the ROV to travel forward at 20%.

```
// turn aft pumps on, send signal to ROV
handle_to_port.send_character(FWD);

//keep pumps on for a period of time
Sleep(TOTAL_PERIOD*user_input/100);

//turn aft pumps off, pause for a period
Sleep(TOTAL_PERIOD - TOTAL_PERIOD*user_input/100);
```

32.6.14 Summary

This software is easy to use and allows a fully configurable control system. It displays all the available information about the ROV's motion in a user-friendly format.

32.6.15 Source Code

The source code for the software is extensive and as such is stored on the CD.

32.7 Future Developments of the Software

The software could be expanded as already mentioned to include the ability to load in a specified configuration file so that the software could control multiple ROV configurations. This could easily be done by removing the actual values of the variables that are specific to a ROV such as BUOYANCY, MASS and so on, then having in the initialisation of the Telemetry dialog the opening of the configuration file and assigning the values to the variables.

You could also configure the ROV to send back a specific code to tell the software program that firstly the ROV is attached and switched on and secondly which of the configuration files to use instead of having one specified by the user. This would require that the user had the correct configuration file stored on their computer in the correct place.

In addition it might also be beneficial and perhaps necessary to have the calibration of the sensors either every time the program was used to control the ROV or when specified by the user via some menu option. This would involve the sending of a start calibration code to the PIC, which would then either wait for the ASCII commands required to calibrate the sensor or send them itself.

A more elegant user interface for the display of the ROV's telemetry and graphical representation of this would be to have the camera input full screen and the graphical displays as overlays. This would then have the advantages of having a large as possible view screen for the camera and being a *true* head up display interface.

There could be a remote access requirement for the software so that, for instance, a diver could control the ROV in either a business environment or recreational environment. The diver would be able to control the ROV either via the computer or directly using a simple wrist-attached controller. This could be used to record video

input on the computer's hard drive. Alternatively, it could be used to override the local user's input, which might be of use in an industrial application.

32.8 PIC Software

32.8.1 Requirements

The software for the PIC16C73A needed to be able to perform a number of tasks. These fell into three main areas:

- Communicating with the sensor
- Communicating with the PC
- Operation of the water jets based on the results of communications including the ability for the ROV to maintain an orientation ('hover') by use of sensor feedback.

It was thought that the best order of events would be to first read sensor data and transmit it to the PC before reading a command from the PC. This command would then be acted on before returning to the start of the program. The PIC software is programmed in assembler using Microchip's MPLAB software.

32.8.2 Sensor communications

Communicating with the sensor required the setting up of a software USART. This was done by the production of two subroutines - RXBYTE and XMIT. RXBYTE receives the 8-bit serial byte from the sensor and gets rid of the start and stop bit that accompany it. The start and stop bit are used to indicate the beginning and end of a byte.

RXBYTE therefore looks for the start bit and once received stores the next eight bits in the byte file called SERIAL and dumps the stop bit. XMIT can be used to transmit bytes and, with more time, would have been implemented to allow calibration of the sensor via the PIC. It could also be used to request data rather than receive it continuously. XMIT takes the data in SERIAL and moves it serially to a digital I/O pin with the correct timing for 9600 baud. It also sends a start and stop bit.

The RXBYTE routine is used in the main program to receive the continuously transmitted sensor data. The sensor data is in ASCII format. Before it sends the value it sends a letter – P for pitch, R for roll, Y for yaw. After that it sends the ASCII

format of the value. For example if sending a pitch of 32.4 degrees and a roll of -12.5 degrees it would transmit:

P 3 2 . 4 R - 1 2 . 5

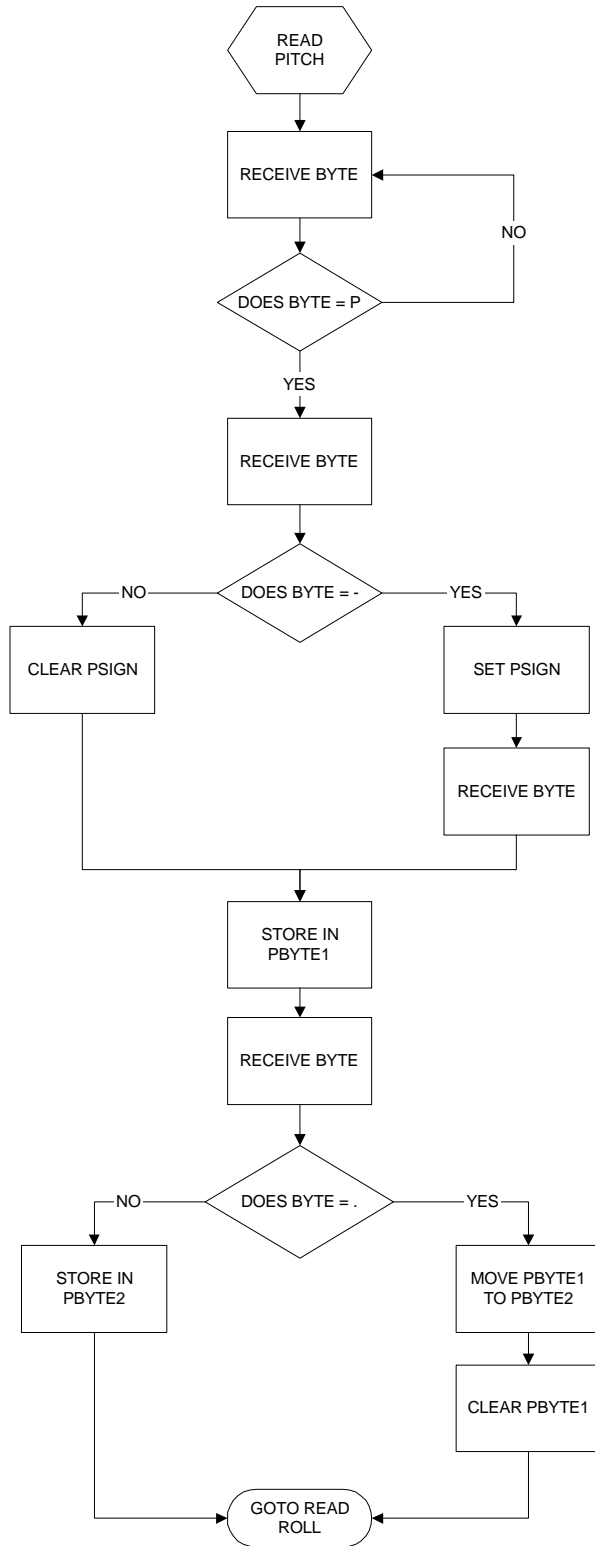


Figure 94 - Receive Pitch Flow Chart

Each number, letter, minus sign and decimal point is transmitted as a separate ASCII byte. The sensor transmits a number of other bytes of information but these are ignored by the PIC. The PIC software looks for the ASCII P (50 in hexadecimal). Once this is received it gets the next byte. If this is the ASCII code for a minus sign, it sets the register PSIGN to one and stores the next two bytes in PBYTE1 and PBYTE2 (see Figure 94). If it isn't a minus sign, it stores that byte in PBYTE1 and the next in PBYTE2 and clears PSIGN. The software then waits to receive an R and does the same for roll, storing the values in registers RSIGN, RBYTE1 and RBYTE2. All values after byte two are ignored, as this degree of accuracy is not necessary.

Once the roll and pitch are received, the analogue to digital conversion of the yaw is processed and stored in YBYTE.

32.8.3 PC communications

The PC communications use the PIC's inbuilt hardware USART and so require only one extra subroutine to be written. The TX_232 subroutine checks the USART control register TXSTA to see if transmission is complete and if not, waits until it is.

The first PC communications transmit the sensor data received. The format is a truncated version of what the sensor outputs. First an identifying byte is sent (ASCII P for pitch, R for Roll, Y for Yaw), then the sign register (1 for negative, 0 for positive) followed by the two ASCII bytes of the number. For yaw the number is only one byte representing 0 to 360 degrees from North. The command sequence for transmission is as follows:

- Load the byte to be sent into the USART transmit register TXREG
- Call TX_232 to wait for the end of transmission before sending the next byte.

After the transmission of all the sensor data is complete the PIC looks to receive a command from the PC. The GET_CHAR routine tests the PIR1 register bit RCIF that is set by the PIC hardware when a byte is received. This byte is then stored in the file COMMAND before it is checked to see what it represents.

32.8.4 Commands and actions

Since the PIC and standard RS232 communications work on eight bits and the configuration of the ROV uses eight water jets it seemed sensible to assign each bit to

a jet so that setting a bit would represent turning on a certain jet. For example, to go forwards the command would be 00001111 (see Figure 95).

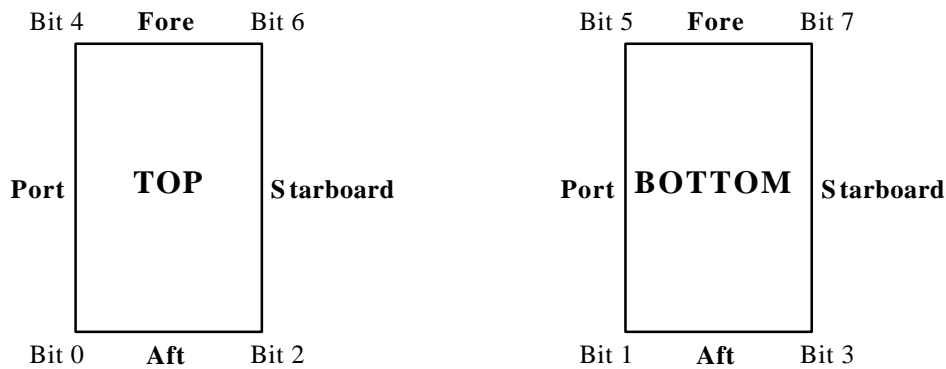


Figure 95 - Command word bits representing different ROV water jet positions

This would make the PIC software easy as the value of the command could simply be transferred directly to the PORTB register to set the outputs of port B to which the MOSFETs controlling the pumps would be attached.

The water jets are limited to a maximum of four on at a time. This leaves many 8-bit combinations that could be used for other purposes. At the moment the additional command list consists of handshake (decimal 7), reset (decimal 6), set wait time (decimal 4), hover on (decimal 2) and hover off (decimal 3). This could easily be expanded to include others in the future.

In order to determine the command, the received value is compared to a stored hexadecimal value of a command using the eXclusive OR command. If they match, the result will be zero, which sets the z bit of the status register, and the appropriate action is taken. If they don't match, the program checks it against other hexadecimal values until a match is found. If all the additional commands are ruled out then the software simply transfers the command to port B to set the outputs (see Figure 96).

32.8.4.1 Handshake command

The first command to be checked for is the handshake command. As detailed earlier the PC initially sends decimal value seven continuously until it receives the same command back, indicating that the ROV is attached. If the PIC sees a seven it immediately transmits a seven to the PC and then checks for a new command.

32.8.4.2 Reset command

The next command looked for is reset. This clears the error flags of the hardware USART, clears all registers and then returns to the main program setup routine. This was included mainly to reset communications if a problem arises. The SETUP routine is only called when the PIC first starts up or when a reset command is received. It clears all the I/O pins and then sets which will be inputs and which will be outputs. It also sets up which of the analogue to digital converter pins will be active and the format and speed of serial communications. In this case the USART is set to asynchronous communication at 9600 baud and the data format is eight data bits with one start and one stop bit.

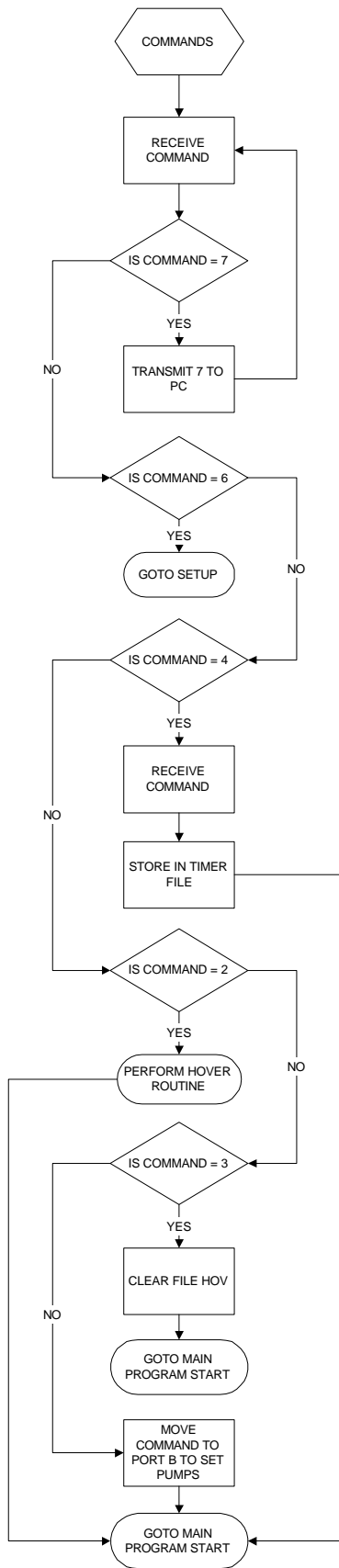


Figure 96 - Command Analysis Flowchart

32.8.4.3 Set wait command

If the program sees a number four, then this is the “set wait” command. The number transmitted immediately after this command will be stored in the TIMER register which is used in the HOVER function to set the time delay between each orientation correction (see section Hover command). The set up of the WAIT subroutine means that the delay it creates is 0.104856 seconds times the value in TIMER. The WAIT command uses the built in timer TIMER1 (TIMER0 is used by the software USART). This timer uses two 8 bit registers to create a 16-bit timer. The timer runs at a quarter of the PIC clock frequency, which in this case is 20MHz. The WAIT subroutine starts TIMER1 and when it overflows (i.e. it reaches binary 1111111111111111 or decimal 65535) it decreases the value in register TIMER by one and starts TIMER1 again (see Figure 97).

This continues until the value in TIMER is zero. The length of the delay is therefore roughly the value in TIMER multiplied by the time it takes TIMER1 to overflow.

Since TIMER1 is given a pre-scale of 1:8 in the SETUP routine and it increments after the time for one instruction we have:

$$\text{Frequency} = F_{\text{PIC}} / 4 = 20 / 4 = 5\text{MHz}$$

$$= 5000000\text{Hz}$$

$$\text{Time for one increment of TIMER1} = 8 / 5000000$$

$$= 0.0000016 \text{ seconds}$$

$$\text{Time from timer start to overflow} = 0.0000016 * 65535$$

$$= \underline{0.104856 \text{ seconds}}$$

So for example to get a two-second delay TIMER should be set to a value of 19.

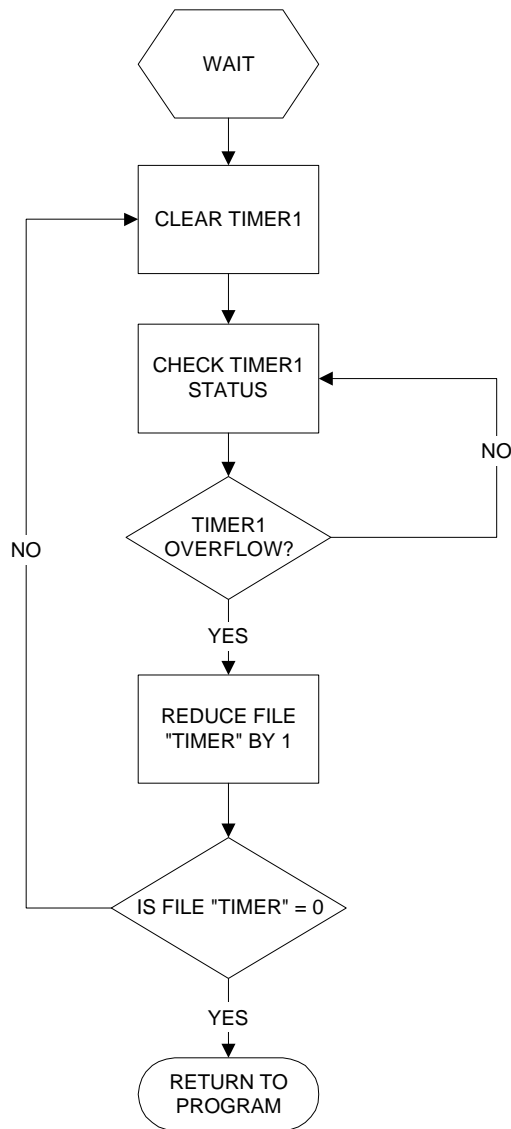


Figure 97 – Set Wait Command Flowchart

32.8.4.4 Hover command

If the command sent by the PC is two then this is the “hover on” command. Hover is a routine designed to keep the ROV at the same orientation as when it is first called. In order to do this, it first of all records the current ROV orientation in files used only by the hover routine and sets a file that prevents them from being overwritten until the “hover off” command is sent. On the next pass through the program, if the “hover on” command is still being sent, then it skips recording the current orientation and goes straight to comparing the current position with that recorded. In assembler, an easy way of finding the magnitude of the difference between current and stored values could not be found. This prevented the implementation of proportional control, where the difference could be transferred to the length of time for which a correction

manoeuvre would occur. Instead feedback simply relied on knowing if the difference was zero, positive or negative and moving in the correct direction. As it had been decided that no more than four water jets at a time would be operated, and for ease of programming, each orientation is dealt with in turn. Firstly pitch is compared and corrected, then roll and finally yaw. The yaw comparison is relatively straight forward as there is only one byte to deal with. Using the subtraction function SUBWF, the current position is subtracted from the stored position. If the z bit of the STATUS register is set, then the result is zero and no movement is required. If not, then the c bit of the STATUS register is checked as this indicates a positive or negative result, and port B is set to switch on the water jets that will move the ROV back towards the stored yaw. At this point the WAIT command is called to allow this move to continue for a set length of time, determined by testing. Too long will result in oscillations about the stored position and too short will result in a slow response.

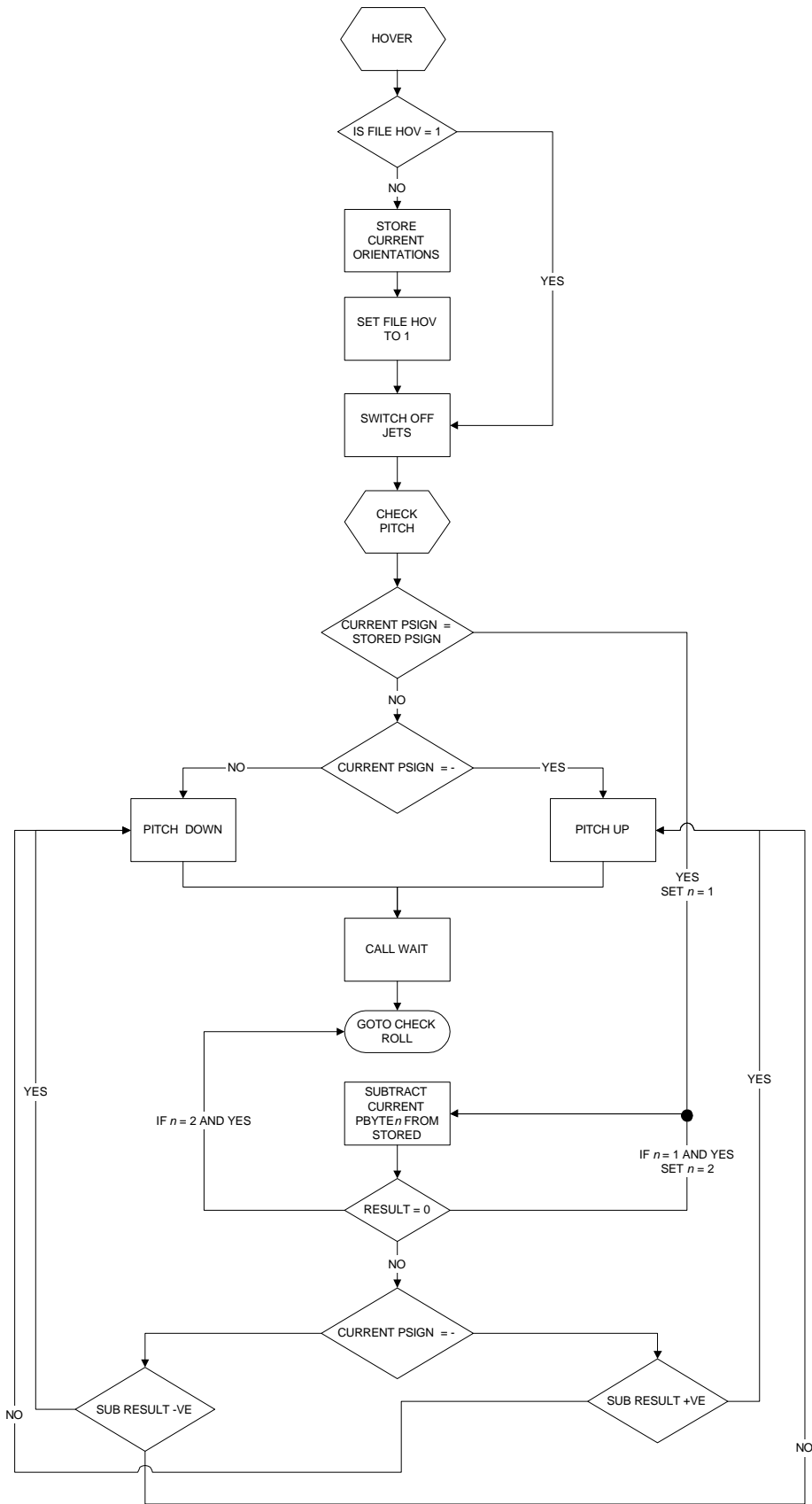


Figure 98 - Hover Command Flowchart

The roll and pitch are more complicated to compare as they involve looking at three bytes – the sign and the ASCII values of the most and least significant decimal digits. Firstly the sign is checked. If the current sign is different to the stored sign then it is immediately known that a move is required. The direction of that move is determined in the software by the sign of the current position. If the signs are the same then the most significant decimal digits are compared in the same way as yaw. The ASCII format has no effect on the subtraction, as decimal 0 to 9 is 30 to 39 in ASCII code. Subtraction gets rid of the common thirty and so the results are the same. If the most significant number is the same then the least significant number is checked. If this is also the same then no moves are made and the program moves on.

Hovering continues as long as the “hover on” command is being sent. The “hover off” command simply clears the bit that prevents the hover routine from storing the current position as its reference. It is therefore necessary for the PC to send the “hover off” command before sending a command to directly set the pumps. If this is not done, then the next time the “hover on” command is sent the ROV will move to the orientation stored from the previous hover. A flow diagram of the hover routine is given in Figure 98. Due to the long time that could be taken to finish this routine and others, it was necessary to leave the PIC watchdog timer off as it could time out unnecessarily.

32.8.4.5 Set pumps command

If none of the above commands occur, then it is assumed that the command is one to directly set the pumps. In this case the value of the command is directly transferred to port B, setting the relevant outputs on and off to control the MOSFETs that control the pumps. This is the last command in the software and at this point the program returns to the beginning.

32.8.5 Possible future modifications

Although the software for the PIC is good enough for this project’s purposes, there a number of additional features that could be implemented:

- Calibration of the sensor – with full implementation of the software USART, calibration commands could be sent from the PC to the sensor via the PIC to remove the need for access to the sensor/camera box. This would greatly ease on location calibration of the ROV.

- Improved feedback – the hover routine has been successfully implemented but uses a very basic algorithm. It would be much better if the size of a change in orientation could be measured and used to give the time for which the jets should be activated. These times could be altered using adaptive feedback to get the optimal time required per degree of difference as it may be dependent on operating conditions. The implementation of such an algorithm would require much work and could be used as the basis of an individual project.
- It has also been realised that the hover routine creates a delay in the system due to the time delays to allow moves to take place. This could be removed by using interrupts that would stop the routine if a command other than “hover on” were received, or perhaps by checking the command within the routine after every move. The problem mainly results from the limitation of having only four jets on at a time. If more were allowed then the roll, pitch and yaw could be corrected all at once and no delay between moves would be required.
- Error Messages – to simplify communications, only orientation data is read from the sensor. The sensor also outputs error information and this could be transmitted via the PIC to the PC for the user’s information.
- PC positional requests – for simplicity the ROV is mainly user controlled. The user analyses the camera and sensor data and decides where to move next. The only feedback occurs in the hover routine to keep the ROV stationary. If the speed of the ROV is known or measured then a routine similar to HOVER could be implemented to send the ROV to a specific position away from its origin. Once arriving at a destination, the original manual control could be used for precise location of the ROV to examine the area.

33 Construction Phase

Initial concepts for the nozzle mounting have already been discussed. The pipe diameter and jubilee clips used to secure the pipes to the nozzles, and clearance, around the chassis had to be taken into consideration when designing the mounting system. This, combined with the required location and orientation of the nozzle determined through the 3D modelling, as described earlier, specified the path that the pipes had to take and in which no mounting components could be present. The components were built out of aluminium, which will not bend more than 45°. The relative locations of the nozzles and the chassis combined with the pipe path required 90° angles in the design. For this reason L-sections and channels were investigated, and a 50mm width channel was found that was suitable. As accurate orientation of the nozzles is required, it was decided to use pairs of bolts to secure the nozzle mounting components together. This was considered the best solution that did not require permanent fixing of the components, so adjustments can be made to the ROV. The final design is given in Appendix AC. This shows the channel section and 30° angle piece used to secure the nozzles. There are two different designs reflecting the symmetry required to achieve the nozzle orientation. However, on assembly, it was found that this design was not stiff enough, as the forces exerted by the pipes and pumps changed the nozzle angles. As a result, it was very difficult to achieve accurate location of the nozzles. This will probably affect the trim of the ROV as the forces will not be as balanced as intended.

With the nozzles mounted on the chassis and the shell present, accurate positioning of the holes through the shell was possible. The initial holes in the chassis were filled with epoxy putty and then ground out to give correct clearance and direction for each nozzle.

During the assembly of the propulsion system, it was found that the original planned locations of the pump was not the most compact and optimum. By positioning twelve pumps in the bottom of the shell and four in the sides, it was possible to reduce the pipe bending radii, improving flow, and lower the centre of mass. This increased the static stability of the ROV.

33.1 Manufacture and Construction of the Shell

The shells were manufactured jointly by the University of Southampton EDMC and GF Jones Pattern Makers Ltd, based in Hedge End, Hants. There are four main stages in the manufacture and construction of the shells.

33.1.1 Stage One

The first is the design and manufacture of a pattern or plug as a parent to the mould. The accuracy and the quality of the pattern will determine the accuracy and quality of the shells. Of the four processes this is the most costly portion. Quotes for the pattern were in the region of £800. It was also found that to turn the revolution on a lathe, by hand might take up to 10 working days, which for the purposes of the project is too long. Due to the time delay and cost it was decided this would not be possible and an alternative solution is required, else there would be no complex shell.

After scouring local machine shops and model/pattern makers it was found that any company in Hampshire, Dorset or Sussex could not quickly turn the plug.

A rethink of the plug manufacture strategy found that the pattern could be machined at the EDMC. The 3D shell design was drawn in AutoCAD and the EDMC converted the file into computerised milling software and a surface model was generated. It was found that due to the size of the plug it would need to be made from laminated pieces of timber and milled in three sections, the ends and then the mid body. First the two ends are roughed and the outline cut, next the section shape is bull nosed with a cut length of 1mm. This process was achieved in two and a half working days. A machine time of roughly 14 hours, not including software conversion and programming, eight days faster than by hand and the only cost is in materials, as the plug is made in house. However, if it had been done commercially at a rough cost of £35 per machine hour alone the cost would have been £573.30 including VAT, still lower cost than by hand.

The wood used is builders' pine, which is not the best choice for a good finish as it has a wide grain and is quite waxy/sappy. A better choice although more expensive, would have been yellow pine or modellers wood: jelutong, but these were not available in the time scale.

Alternately painting and sanding the plug with 1200 grade wet and dry sand paper finishes off the plug. Once the desired finish is obtained stage two of manufacture can begin.

33.1.2 Stage Two

Stage two is to make the mould. The mould is made by encasing the plug in a wooden frame, painting it with gel coat and then hand laying over it with chopped strand matt (CSM) glass fibre and resin. For speed this resin mix also contained filler material. Once the mould has set and gone off the plug is removed and the mould is ready for use.

33.1.3 Stage Three

Stage three is the manufacture of the shells, and the joggle to join the two halves together. Ideally these would be made layer by layer with a relatively tough resin mix. By manufacturing in this way the shell thickness can be made to be thinner and still be stable and not warp. It will also have better impact and fracture toughness. Due to time constraints however the two shells were made using multiple layers, all in one fabrication and left to set. The resin and gel are also not that of pattern makers' preferred choice, because it is hard and more brittle when set than desired for this application. As a result there is more material, and a less uniform and greater thickness than desired or thus greater mass of material than required to keep the shell stable than if done layer by layer.

In the lay up process the GFRP overlaps the mould, and this overlap is trimmed off when set.

The second shell, which in this case was the bottom half has the joining mechanism attached to it. Once the main half shell has been laid up, set and trimmed, the joggle is attached. It is made from four 15mm thick sheets of wood cut in the same profile of the section but offset inwards by the material thickness, as an overlap over the four quarters of the mould. The laying up process then begins and the lip to join the two halves is made. Due to the excessive thickness of the top shell (8mm thick) it is then ground down to remove excess material thickness (3-4mm) and make it easier to flex the mould back into its desired shape. Before grinding of the top shell the mass of

resin put into the shells is 12kg in total. When weighed on scales the completed shells with fittings (not frame, electronics boxes etc.) weigh in at about 10kg, the bottom shell being the heavier at 6kg.

33.1.4 Stage Four

Stage four is the fitting out and finishing the shells ready for the rest of the internal components to be fitted in. Firstly an aluminium rail is bonded along the inside edge of the lip. The top shell is attached and fourteen 5mm holes are drilled through the top shell into the lip and aluminium strip. The aluminium is then tapped with M6 screw threads for M6 countersunk hexagonal key bolts.

The camera lens hole is cut into the mould with both halves screwed together.

The tether hole is not done in the designed manner, as there is the possibility that taking away both ends of the mould in such a manner would make the warp/distortion worse and the halves not fit. However, this should not be a problem with a layer-by-layer manufacture. Instead an eighteen-millimetre hole is drilled through above mid-plane, on the centreline of the top shell.

Structural support rails are fitted next. This is done using aluminium strip 500mm in length, which is bonded and glass fibred over the ends to impart strength to hold the ROV weight when picked up from the internal frame. Again, holes are drilled in the internal structure and the aluminium is drilled and tapped with six M6 screw threads, the bolts are short as longer ones will penetrate the hull and/or increase the risk of pulling the rail from the shell. The top of the rail is 90mm down from the centreline, and the rails are set in at level trim, ensuring that the nozzles attached to the frame will be equidistant from the shell (if there was a constant material thickness) and hence provide even thrust in all planes of motion.

The profile hole for the drag test strut is machined into the top shell. Due to the aforementioned resin properties, there is some chipping and a few hairline cracks in the gel coat, although being GFRP these can be patched with little effort.

The nozzle holes are a compound angle of 30° rotation and 30° elevation, making them not easily manufactured. However, a method was devised to attach wooden blocks to the outside of the mould with the bottom shell and the frame and nozzles secured in the operating condition. An insert with a hollowed out hole in its centre is

turned such that a long (300mm) drill bit can be fed up through the nozzle from the inside and into the blocks of wood, these holes then become guide holes to drill back through the secured top shell for nozzles with the correct orientation. This is not an ideal method and there is some flex of the drill bit, giving some inaccuracy of the holes. The bottom holes are quite simple, drilled straight through the bottom shell using the insert, with no need for guide blocks.

With the holes cut the next task is to create the nozzle jet tunnel to ensure the jet escapes the shell and is not sprayed inside of it. This is achieved by inserting guides through the hole at the correct orientation, and up to the face of the nozzle. Waxing both the guide and nozzle and then filling around the guide and end of the nozzle ensures a direct channel for the jet. Once the filler has set the orientation guide can be removed and any excess filler removed. This can then be painted with a waterproof sealer (resin or lacquer) to stop water ingress.

This need only be done once, after which the shell can be used to make a new mould with the holes preformed.

The camera box support, an aluminium plate, is attached to the frame on the front middle transverse L section. The aluminium plate is drilled and tapped to M6 standard and two spacers keep it in position. There are two M5 tapped holes in the plate for the camera box to be bolted to if required.

The holes to be drilled or machined out of the shell are the water intakes slots. To have zero net force these are required to be equal and opposite in orientation such that there is no suction or unwanted translation of the ROV when underway.

The bottom shell is machined with two longitudinal slots either side of amidships, such that there is still a cross piece of material to help preserve the shell shape and to withstand any residual stresses. Having the shell thicker is advantageous for this process. At first there are only the two bottom intakes at 150x30mm each, with a combine area of 0.009m². The top shell is not machined out, at this stage of design it only has a profile hole for the strut to assess the hull drag in full scale towing tank tests.

34 ROV Testing

Unfortunately, due to delays in the project, notably delays in the design and supply of components, the construction of the ROV was completed behind schedule. As a result, only drag testing and preliminary wet testing of the ROV could be conducted. Further testing could have been possible but the test tank was required for other uses at a critical point and full wet testing was not completed before the publication of this report.

It is still intended to measure the forces developed by the ROV in the other axes. These will then be compared to the forces predicted through the propulsion system tests. Overall efficiency tests will be conducted. The input power shall be compared to the forces generated and the speeds achieved.

Due to problems with the electronics, in order to conduct wet testing, the pumps were hard wired to the power supply. Due to time constraints only forward movement was tested. For this the eight rear pumps were attached directly to the power supply. This allowed the full speed potential of the ROV to be seen.

Static force testing was conducted and a maximum forward force of 12N achieved. This is less than the prediction of 14.6N produced from the pumps tests. This still enabled a significant forward speed to be achieved. Unfortunately due to a lack of time, this speed was not measured but was estimated to be at least 0.5m/s.

There are several reasons for the lower than expected force. Firstly the force was measured using the dynamometer in the test tank, as the force generated was too large for the spring balances available. This measures the force directly forwards and as the line attached to the ROV had to be attached approximately 0.5m above the ROV the force was vectored. The line used was approximately 3m long, which through simple trigonometry increases the force to 12.2N. Secondly the voltage drop along the tether was not taken in to account. The top of the tether was provided with 24VDC. Therefore, the pumps will see a lower voltage and will run below their operating speed and will therefore produce a lower force. Further testing will be conducted to eliminate this. Finally, it realised that the pump force experiments conducted were inaccurate. This was because the force measured was not solely the force generated by the water jet. It also included the force of the water entering the pump. This force is not present when the pumps are mounted in the ROV as they are enclosed in the shell. From these results it is estimated that 0.6N of the individual water jet forces

measured is accounted for by the intake force. This increases the difference between the analytical predictions and the measured forces. This difference explains why the results from the free discharge nozzle tests are greater than the predicted values. Taking this into account increases the percentage difference between the analytical predictions and the measured results from 2.73% to 16%. In order to confirm this difference, it is intended to conduct further experiments using only one water jet.

During the tests the ROV experienced an erratic path as a result of the tether. Due to the tether being both too stiff and stored coiled, there was a residual bend present that resisted being straightened. This produced a force on the ROV that varied with the length of tether in the water and affected the ROV's direction.

34.1 Test Programme

In order to ensure that the ROV meets its requirements, its performance must be assessed and documented in such a way as to verify that it does so. To achieve this, a formalised test programme was used. Some of the stages of the testing are dependent on successful operation of the ROV. However some of these are not and so the tests were broken down into stages; these included drag tests, buoyancy tests, performance tests, electronics tests and control software tests.

34.1.1 PC Control Software Testing

The control software was extensively tested throughout its entire development. This was done to ensure correct and reliable operation of the software. This would then ensure that any problems that resulted would be due to either the PIC or the communication between the PIC and the PC. Therefore these problems would be more easily identified and corrected within the project timescale.

34.1.2 Control System Testing

34.1.2.1 Sensor Testing

The first test in this process was to see if the purchased sensor operated correctly. The sensor was connected directly to a PC's serial communications port in the way described in the sensors manual, and tested using the evaluation software provided with it. Initial testing on a laptop resulted in failure, but testing on a desktop PC allowed the sensor to be calibrated and orientation readings to be made.

34.1.2.2 PIC to PC interface

Initially it appeared that the PIC was transmitting some data to the PC but would then stop. However, the data received did not relate to what the PIC software should be sending. In order to work out if the problem was with the PC software or the control circuit, a shareware serial communications program (called *LookRS232*) was used to see if the PC was receiving any data. This program showed that the problem did not lie with the PC. A number of checks to the circuit proved fruitless. All board connections were checked for breaks and shorts and a capacitor was added between ground and supply of the MAX233 chip to smooth the supply. The voltage levels were once again checked. The 12V regulator was working well, but the 5V regulator was only giving 4.5V. At this stage this was not felt to be a problem, and so it was felt that the fault must be with the PIC code, in particular the serial communications part of the program. On initial examination of the program no reason for failure could be found. However, a search of relevant Internet sites gave a number of hints as to areas in which the USART may fail that are not mentioned clearly in the microchip documentation.

The first suggestion we tried was to connect up the handshaking lines of the PC's communication port at the PC end of the RS232 cable. This is required so that they "fake" one another into seeing valid handshake signals, as the PIC does not generate them. With the changes to the cable we again tested the circuit using the serial communications software with no improvement. Occasionally values would be received, but they seemed to bear no relevance to what should be sent.

It was therefore necessary to once again look at the PIC program. It may have been the case that the data being received at turn on was sensor data and that transmission stopped because the buffers on the PIC overflowed from the constant stream of data. In the current program there was no form of communication error handling. Therefore if an error such as overflow was occurring the program had no facility to clear it and try again. For this reason error handling routines were added. The Internet site <http://redrival.com/mcgahee> highlighted many quirks on the PIC that would stop USART communications. This included the need to send a dummy transmission before sending your data to initialise the port. If this is not done the USART will not operate. It was also found that it is necessary to do three reads of the USART to clear the buffers or the receiver may come up with an error on start-up. Lastly, the transmit

and receive pins of the USART both need to be initialised as digital inputs, despite the fact that transmit is an output.

Taking these facts into account the PIC program was heavily modified. In order to test the hardware a serial communications program, called *picuart.asm*, guaranteed to work, from the same website mentioned above, was used in conjunction with *LookRS232*.

This program simply mirrors what is sent to the PIC back to the PC, and was found to work on our PIC proving that the serial communications part of the circuit was working. The heavily modified program was then tested and the alterations allowed the PIC to successfully respond to the PC's commands. This was shown through an alteration to make the PIC send back to the PC the command it had just received. The program had also been changed to make the PIC only send sensor data when requested. Pitch is requested by sending the value of ASCII P, roll by ASCII R and yaw by ASCII Y. This showed that the Yaw was being read correctly by the PIC, but the Roll and Pitch were not as when requested the data received was always zero. Since the roll and pitch are received serially this implied that the software UART was not working. A number of methods were tried to change the software UART without success. It was felt that it might work if the data was not input continuously but requested. The software was therefore set up to send ASCII characters to the sensor that matched the sensor command to check inclinometer readings. The returned input would then be completely read before formatting. However with these changes the hardware USART appeared to cease functioning. Returning to the original program it still ceased to function. Therefore it was impossible to determine whether problems had been software based or hardware based.

Once the hardware USART was working again, it was decided to test whether the output from the PIC was turning on the correct MOSFETs. This test found that although the commands were being recognised the pins being set did not correspond to the software. A pattern was looked for and not found, hence it was concluded that the PIC was functioning incorrectly and temperamental in its operation. In addition the PIC Programmer was used to verify the PIC and this produced an error, this confirmed suspicions of a problem with the PIC hardware. Therefore a new PIC will be purchased and testing will continue.

34.1.3 Camera Testing

The signal line and ground line from the camera can be easily attached to a SCART plug, making it extremely simple to connect to a television, while it was found that the pair of lines can also be attached to an S-Video connector. If there is a need, it can also be converted to a standard coaxial cable signal via an RF converter that changes the 1V peak-peak signal into a high frequency signal. Through the additional use of an external TV card, the image can also be viewed on the computer screen, thereby easing the operator's task of controlling the ROV.

Due to the small size of the camera and the fact that the IR LEDs were slightly movable, the window to be set in the box only needed to be approximately 4cm wide by 2cm high. When the box is placed at the front of the ROV, and no obstructions are placed in front of it, the camera has a viewable angle of 92°. This should be sufficient for control of the ROV and underwater inspection, while the adjustable focus on the lens means that its depth of vision can be changed to optimise the image received on the shore.

The only noticeable disadvantage was the fractional time lag between the camera itself and the shore side image, but when the overall response time of the ROV is considered, the camera lag is insignificant.

One slight hitch was that the IR LED's reflected on the window's surface when being tested, and so the camera could not see clearly. However, placing a baffle between the camera lens and the LEDs can very easily solve this. In the end, it was found that a baffle was not required since the reflection could be removed by positioning the camera lens very close to the window.

34.1.4 Enclosure Testing

After the enclosures had been equipped with all the relevant connectors, the whole system had to be tested to ensure that their IP ratings were intact. Therefore, the enclosures were filled with moisture indicating materials, closed and sealing caps were attached to their respective connectors. Then the enclosure was immersed for a few minutes, and then removed from the water and opened. The moisture indicating material indicated any places where water had leaked in. These places were mostly where connector caps had been over tightened, and the sealing gland displaced from

its correct location. After these leakages had been remedied, the enclosures were tested again to ensure that the leakages had been properly stopped.

To further ensure that the enclosures were sealed to the IP68 requirement of immersion for long periods of time, the main enclosure was immersed for 9 hours. After this time, it was found that the enclosure had retained its watertight seal.

34.1.5 Acceptance Testing

Dry acceptance testing was used to confirm correct operation of as much of the control system as possible without having the inconvenience of trying to rectify any errors tank side. Other parts of the acceptance testing had to be performed in the test tank. The testing included the following tasks:

Test No.	Test	Pass (P), Fail (F) or No Test (NT)
1.	Switch on	P
2.	Check voltage levels	P
3.	Check not overheating	P
4.	Test Software reads pitch	
5.	Test Software reads roll	
6.	Test Software reads yaw	P
7.	Wait for PC Control Software to Confirm ROV Presence	P
8.	Confirm Camera Output to TV	P
9.	Confirm Camera Output to PC	P
10.	Test Pitch Down (Automatic in Test Mode)	
11.	Test Pitch Up (Automatic in Test Mode)	
12.	Test Yaw Port (Automatic in Test Mode)	
13.	Test Yaw Starboard (Automatic in Test Mode)	
14.	Test Roll Starboard (Automatic in Test Mode)	
15.	Test Roll Port (Automatic in Test Mode)	
16.	Test Forward Motion (Automatic in Test Mode)	
17.	Test Backward Motion (Automatic in Test Mode)	
18.	Test Port Motion (Automatic in Test Mode)	

19.	Test Starboard Motion (Automatic in Test Mode)	
20.	Test Down Motion (Automatic in Test Mode)	
21.	Test Up Motion (Automatic in Test Mode)	
22.	Pitch ROV $\pm 45^\circ$, check sensor readings	
23.	Roll ROV $\pm 45^\circ$, check sensor readings	
24.	Yaw ROV $\pm 180^\circ$, check sensor readings	
25.	Switch off	P

Table 13 - Table of Testing Procedures

35 Budget

In Appendix AD a complete breakdown of the production costs is available. This includes the suppliers and items provided free of charge. An initial budget of £3,780 was given. This consisted of £780 from the University, £1,000 from Halliburton and £2,000 from Perry Slingsby. The project spent in total £2928.06. This is below the initial budget by £851.94. Had the services of the EDMC and Penske Cars not been available, then the project costs would have been significantly higher.

36 Conclusions

- The group succeeded in building a small, low cost ROV.
- The cost is comparable to similar observation ROVs and, considering this is a prototype stage, the possibility for reduced costs in mass production is considerable.
- Though the wet testing of the ROV was not completed, the experimental results suggest that a water jet powered ROV is a viable alternative to thrusters. Water jets are capable of producing high enough forces to power a small ROV.
- Unfortunately due to time constraints the group has been unable to finish the testing of the ROV prior to the publication of this report and therefore confirm if it has a comparable performance to other ROV's in its target market.
- There was a lack of suitable pumps available on the market, and no suitable bi-directional pumps were found.
- The pump performance calculations proved to be reasonably accurate from the tests conducted.
- The LVM Congo pump was selected as the most suitable pump found and an eight water jet solution adopted.
- Bi-directional pumps would be a better option as they reduce the number of pumps required to achieve the same number of degrees of freedom.
- It was found to be difficult to accurately mount the nozzles. Though not tested yet, this probably will affect the trim of the ROV.

- Due to the decision to use a structural shell, the necessity for an internal framework is removed. The nozzles and so on could be mounted on the shell, thereby reducing the overall weight of the ROV.
- It is possible to tow a large amount of tether from the ROV.
- As the initial thrust has been improved and the hydrodynamics optimised, these two factors combined have improved the ROV operational capabilities.
- If viewing an object in the water is impractically slow side ways then perhaps extra cameras could be placed on the beam of the ROV, or a retracting camera, which could be extended outside the hull and rotated after transit to the required destination. These are just a few considerations for further work.
- A full set of open water tests will be required to finalise the ROV performance.
- The non-dimensional total drag coefficient of the ROV is 0.08, from full-scale tests.

37 Recommendations for Further Work

- Further testing of the ROV's manoeuvrability and speed capabilities should be conducted.
- Further pump searches should be conducted for other more suitable pumps available on the market.
- Further pump experiments should be conducted for the remaining exit tube, and possibly free discharge nozzle sizes, to confirm the predicted force curve shape and the location of the maximum. Also, measure flow rate for different nozzle sizes to confirm the location of the force predictions on the force/flow rate pressure loss graphs.
- Possibly develop a bi-directional pump using a flexible impeller. This would enable a reduction in ROV size and an increase in the force generated.
- Further nozzle research to optimise design for the situation and to maximise the forces generated. Also investigation into more accurate nozzle loss coefficients could be conducted.

- Investigation into the possibility of using a hybrid system, thrusters for main propulsion, fore and aft, and water jets for the other degrees of freedom. This combination could provide the greatest manoeuvrability and tether length for size of ROV.
- The software could be expanded to be more portable and more configurable so that alternative configurations of ROVs could be supported.
- In addition, it might also be beneficial and perhaps necessary to have the calibration of the sensors performed every time the user requested it to increase accuracy of the sensor.
- A fully integrated Head Up Display would allow for a larger viewing area and a more elegant user interface.
- There could be a remote access requirement for the software so that, for instance, a diver could control the ROV in either a business environment or recreational environment. The diver would be able to control the ROV by using a simple wrist-attached controller.
- PC positional requests – for simplicity the ROV is mainly user controlled. The user analyses the camera and sensor data and decides where to move next. If the speed of the ROV is known or measured then it would be possible to send the ROV to a specific position away from its origin. Once arriving at a destination the original manual control could be used for precise location of the ROV to examine the area.
- A more accurate nozzle mounting method is required. Less flexibility and more dimensional accuracy between the nozzles is needed.
- The tether is too large for the ROV and could be reduced in diameter, and therefore drag. As a result an increase in the length of cable the ROV could tow would be achieved.
- To improve the performance of the nozzles, a more efficient, ideal design formula could be used to improve nozzles performance.
- The size and the weight of the ROV can be optimised further, enabling faster operation and reduced costs.

- The in-service stability and manoeuvrability of the ROV needs to be assessed with regards to having such a hydrodynamic shape.

38 References

38.1 Bibliography

1. Bell M, Driscoll N, Goodman A, Price J, Tam E, “*Water Jet Powered Remotely Operated Underwater Vehicle*” MEng GDP Report. April 1999
2. Chapman “*Sams Teach Yourself Visual C++ in 21 Days*”, Edition 4, Published by Sams Publishing 1998
3. Miller DS “*Internal Flow*” BHRA Fluid Engineering 1978
4. Douglas J, Gasiorek J, Swaffield J, “*Fluid Mechanics*” 3rd Edition Longman Group Limited, Reprinted 1996
5. Munday A, Farrar R, “*An Engineering Data Book*” University of Southampton 1979
6. Given, D. “*ROV Review*” (5th Edition) 1993-1994 ISBN 0-9623145-3-6
7. Frederik E. Lange-Nielson, “*The sailors handbook*”, 1993, Marshall Editions Ltd.
8. B.S. Massey, “*Mechanics of Fluids*” sixth edition, 1998, Chapman and Hall
9. Hoerner S. F. Dr. -Ing. “*Fluid-Dynamic Drag. Theoretical, experimental and statistical information*”, 1965, Hoerner.
10. Grigg J.S et AL, “*A Design Study For The Elimination Of Divers In Submarine Model Tests At DERA Haslar*”, 1997, MEng GDP Report Ship Science, University of Southampton.
11. Turnock S.R Dr. “*Technical Manual and User guide for surface panel code Palisupan*”, October 1997, University of Southampton Ship Science report 100
12. Bursnall and Loftin. “*Pressure Distribution on Yawed circular cylinder in the critical Reynolds number range NACA T. Note 2463 (1951).*”
13. Sayer P, “*Research and Development in ROV Hydrodynamics*”, ISOPE 1993 conference proceedings

14. IRA H. Abbot and Albert E Von Doenoff, "*Theory of wing sections*", Dover 1959
15. Jacquet-Lagrange T, "*OPTIMISATION OF A LONG RANGE AUTONOMOUS UNDERWATER VEHICLE USING COMPUTATIONAL FLUID DYNAMICS*", Department of Ship Science 2000, University of Southampton
16. Putaman K, "*PhD Thesis, Ship Science 2000*", University of Southampton
17. "Engineering Sciences Data Unit (EDSU)" Item number 74036, 1974
18. P.J. Gregson, "*Advanced Materials 1 lecture notes*", Southampton University, 2000

38.2 Web Site References

1. <http://www.bulgin.co.uk/> Bulgin Components PLC (Connectors)
2. <http://www.weidmueller.de/uk/> Weidmüller (Enclosures)
3. <http://www.kvaser.se/> Kvaser AB (CANbus Systems)
4. <http://rswww.com/> RS Components Ltd.
5. <http://www.maplin.co.uk/> Maplin Electronics
6. <http://msdn.microsoft.com/> Microsoft's Developer Network Library
7. <http://www.codeguru.com/> Visual C++ code tutorials
8. <http://www.rov.net/>
9. <http://www.resourceregistry.com/>